RHEOLOGICAL COMPARISON OF THREE POLYETHYLENE FILM RESINS

A RHEOLOGICAL COMPARISON OF THREE LOW DENSITY POLYETHYLENE FILM RESINS

by

Andres Garcia Rejon G.

Submitted to the Faculty of Graduate Studies and Research
of McGill University
in Partial Fulfillment
of the Requirements for the
Degree of Master of Engineering

Thesis Supervisor: Professor John M. Dealy

Department of Chemical Engineering
McGill University
Montreal, Canada

December 1976

ACKNOWLEDGMENTS.

I would like to express my gratitude to:

my research director, Professor J.M. Dealy, for his advice, guidance and encouragement throughout the facets of the project.

the machinists and technical personnel of the Department of Chemical Engineering, for their valuable service and advice.

Dr. J.M. Starita and the personnel of Rheometrics, Union N.J., for their kind assistance.

my colleague J. Rhi-Sausi, for his help and advice in some aspects of this project.

the Universidad Nacional Autonoma de Mexico (UNAM) and the Banco de Mexico for their financial support.

A ti Maricruz

mi ilusion, mi fuerza y alegria de mi vida

ABSTRACT

The rheological characterization of a molten resin is an important element of Polymer Science and Engineering. In the present work three low density polyethylene film resins manufactured by three different companies were studied, and three rheological properties were measured: first normal stress difference, die swell and extensional viscosity.

Methods for determining the first normal stress difference are presented and the possible sources of error discussed. The experimental equipment and technique used in this study are described. Experimental data for the first normal stress coefficient are compared with the predictions obtained by use of a method proposed by Abdel-Khalik, Hassager and Bird.

The die swell phenomenon is briefly reviewed and the experimental equipment and technique are presented. The experimental die swell data are used to calculate the first normal stress coefficient using a theory proposed by Tanner.

Steady uniaxial extensional flow is reviewed and the previous work on the measurement of extensional viscosity is discussed. The experimental equipment is described and some of the modifications made to it are discussed. Experimental results for the strain rate and stress as a function of time for a stress growth experiment are presented and recommendations for further improvement of the apparatus are presented.

RESUME

La charactérisation rhéologique d'une résine fondue est un élément important de la Science polymérique et du Génie.

Dans le travail présent on a étudié trois résines de polyéthylène à faible densité fabriquées par trois différentes compagnies et trois propriétés rhéologiques ont éte mesurées: Différence des contraintes normales principales, gonflement du filament et viscosité extensionnelle.

Les méthodes pour déterminer la différence des contraintes normales principales est présentée et les sources possibles d'erreur discutées. Les résultats expérimentaux pour le coefficient des contraintes normales principales sont comparés avec les prédictions obtenues par l'emploi d'une méthode proposée par Abdel-Khalik, Hassager et Bird.

Le phénomène du gonflement du filament est repassé brièvement, l'appareillage expérimental et la technique sont presentés. Les résultats expérimentaux du gonflement du filament sont employés pour calculer le coefficient des contraintes normales principales employant une théorie proposée par Tanner.

L'écoulement en extension uniaxiale en régime permanent est passé en revue brièvement et les travaux faits auparavant sur la mesure de la viscosité extensionnelle sont discutées. L'appareillage expérimental est décrit et quelques unes des modifications faits à ce dernier son discutées. Les résultats expérimentaux pour la vitesse de déformation et de contrainte comme une fonction de temps pour une expérience de croissance de contraintes sont présentés et des recommendations pour l'amélioration de l'appareillage sont données.

RESUMEN

La caracterización reológica de una resina fundida es de gran importancia para una mejor comprensión de los procesos poliméricos.

El presente trabajo estudia tres propiedades reológicas de tres polietilenos de baja densidad producidos por diferentes compañias. Las propiedades estudiadas son: Diferencia Primaria de Esfuerzos Normales, Die Swell y Viscosidad Extensional.

Una breve revisión de los métodos empleados para determinar la Diferencia Primaria de Esfuerzos Normales es presentada enfatizando los problemas experimentales existentes al llevar a cabo estas mediciones. Los datos experimentales de la Diferencia Primaria de Esfuerzos Normales son comparados con las predicciones obtenidas a partir del método propuesto por Abdel-Khalik, Hassager y Bird.

El fenomeno de Die Swell es discutido y el equipo experimental es presentado. Los datos experimentales de Die Swell son empleados para calcular la Diferencia Primaria de Esfuerzos Normales por medio de una teoria propuesta por Tanner.

El Flujo Extensional Uniaxial y los estudios anteriores sobre este tema son revisados brevemente. El equipo experimental es descrito y varias modificaciones al mismo son propuestas para obtener datos experimentales de mejor calidad.

TABLE OF CONTENTS.

LIST OF FIGURES

LIST OF TABLES

CHAPTER 1. INTRODUCTION

1.1) Overview of the Study.

The rheological characterization of a resin has several important aspects in the field of Polymer Science.

It is essential to test the applicability of the theories developed to explain the behavior of different polymeric materials under different flow patterns and to point out their relevant and weak points.

It is very important in the design of new equipment for polymer processing operations.

It is important in the better understanding of the polymer processing operations since it helps to separate the effects of the parameters of the process from those of the material.

Rheological properties are also useful tools in the comparison and characterization of resins. The material functions measured can be used as a basis for empirical correlations or quality control procedures.

The purpose of this work is to study three rheological properties of three LDPE film resins, manufactured by different companies. The rheological properties studied are:

First Normal Stress Difference

Die Swell

Extensional Viscosity.

Chapter 2 discusses the methods and possible sources of error in the measurement of normal stresses. Chapter 3 presents the experimental equipment and experimental technique used for the normal stress measurements. The first normal stress coefficient is calculated and compared with the prediction of the theory proposed by Abdel-Khalik, Hassager and Bird,[1] based on the Goddard-Miller equation of state. This model is introduced briefly in the last section of this chapter. Chapter 4 reviews the concept of Die Swell and the methods used to measure it. Chapter 5 presents the experimental equipment and technique used in this work to measure the die swell. The die swell data were used to test the predictions of the theory proposed by Tanner.[1,2] Chapter 6 is concerned with steady uniaxial elongational flow and the work done previously to measure elongational viscosity. Chapter 7 describes the experimental equipment and techniques used. Experimental results and recommendations for the improvement of the present equipment are given.

1.2) Description of the materials studied.

Three LDPE resins were studied. For convenience, they will be referred to by use of their inventory numbers at the McGill Polymer Engineering Laboratories.

Resin 1

Resin 1 is a film grade LDPE resin made by means of a low pressure copolimerization process by Dupont of Canada Ltd. The trade name is Sclair 15-11E. Some of the characteristics of

the resin are listed below:

Density: 0.9197 g/cm^3

Melt Index: 1.6 g/10min (190° C)

Narrow Molecular Weight Distribution.

Rod climbing studies were performed on this resin by T.K.P. Vu[3]. It was found that the height is proportional to the square of the angular velocity.

Resin 9

Resin 9 is a film grade LDPE resin made in a two stage autoclave by CIL. The trade name is Polythene 560D. Some of the characteristics of the resin are listed below:

Density: 0.925 g/cm^3

Melt Index: 2.0 g/10 min (190° C)

Medium Molecular Weight-High branching.

Resin 10

Resin 10 is a film grade LDPE resin made in a tubular reactor by Union Carbide of Canada Ltd. The trade name is DFDQ 4400 Some of the properties of the material are given below:

Density: 0.918 g/cm^3

Melt Index: 2 g/10min (190° C)

Low Molecular Weight and High long chain branching.

Unmodified.

Rod climbing studies were performed on this resin by T.K.P. Vu[3]. It was found that the height was larger than for Resin 1. No satisfactory correlation between height and angular velocity was found.

Large amplitude oscillatory shearing studies were done on this material by T.T.Tee[4]. It was found that this material exhibited highly non linear viscoelastic behavior.

1.3) Goddard-Miller Model.

The results of the viscosity, normal stress difference and die swell experiments were compared by use of the Goddard-Miller rheological model. There is given below a brief review of the model.

The central problem in describing the fluid dynamics of non-newtonian fluids is the quest for an analytical expression for the stress tensor $\underline{\underline{T}}$. Obtaining an appropriate expression for $\underline{\underline{T}}$ is extremely difficult as non-newtonian fluids are known to differ qualitatively in many ways from newtonian fluids. A complete expression for the stress tensor $\underline{\underline{T}}$ has to be able to account for all the phenomena exhibited by this type of fluid. Among these effects we can mention:Shear rate dependent viscosity; normal stress effects in steady shear flows; transient response in unsteady shear flows; die swell and rod climbing.

The quest for constitutive equations or rheological equations of state, as the expressions for the stress tensor $\underline{\tau}$ are often called, has been going on for some time. Over a century ago, Maxwell observed that for incompressible materials, Newton's law of viscosity and Hooke's law of elasticity can be combined to give:

$$\underline{\tau} + \lambda_o \frac{\partial \underline{\tau}}{\partial t} = \eta_o \dot{\underline{\gamma}} \qquad (1)$$

This is the simplest equation for a linear viscoelastic fluid. We know that viscoelastic materials are very complex and we would expect to have several time constants (λ_k) and viscosities (η_k). This can be done by superposing equations of the form of equation (1) as shown in equations (2):

$$\underline{\tau} = \sum_{k=1}^{\infty} \underline{\tau}_k$$

$$\underline{\tau}_k + \lambda_k \frac{\partial \underline{\tau}_k}{\partial t} = \eta_k \dot{\underline{\gamma}} \qquad (2)$$

Alternative forms of equation (2) are obtained by performing succesive differentiations to give equation (3), by integrating to get equation (4) or by integrating the latter by parts to get equation (5).

$$\left(1 + \sum_{n=1}^{\infty} a_n \frac{\partial^n}{\partial t^n}\right) \underline{\tau} = \eta_o \left(1 + \sum_{n=1}^{\infty} b_n \frac{\partial^n}{\partial t^n}\right) \underline{\dot{\gamma}} \quad (3)$$

$$\underline{\tau} = \int_{-\infty}^{t} \left\{ \sum_{k=1}^{\infty} \frac{\eta_k}{\lambda_k} \exp\left(-\frac{t-t'}{\lambda_k}\right)\right\} \dot{\gamma}(t')dt' \quad (4)$$

$$\underline{\tau} = -\int_{-\infty}^{t} \left\{ \sum_{k=1}^{\infty} \frac{\eta_k}{\lambda_k^2} \exp\left(-\frac{t-t'}{\lambda_k}\right)\right\} \dot{\gamma}(t')dt' \quad (5)$$

To develop non linear viscoelastic constitutive equations many investigators have chosen to begin with one of the above linear viscoelastic expressions but formulated in terms of a special coordinate system which moves with the fluid element.

A number of rheological equations of state have been formulated by use of a convected coordinate system, as originally proposed by Oldroyd [5]. In such a coordinate system the coordinate axes translate, rotate and deform with the fluid element.

An alternative procedure is to use a co-rotational coordinate system. In this coordinate system the coordinate axes translate and rotate with the fluid element. This approach yields different models more attractive in some respects, as covariant and contravariant tensors in a co-rotational coordinate system both reduce to same result when

referred to fixed coordinates.

If we consider the co-rotational analogs of equations (2) and (4) we obtain alternative expressions for what is called the generalized ZFD (Zaremba, Fromm, DeWitt) model.

$$\underline{\tau} = \sum_{k=1}^{\infty} \underline{\tau}_k \quad ; \quad \underline{\tau}_k + \lambda_k \frac{D}{Dt} \underline{\tau}_k = \eta_k \dot{\underline{\gamma}} \tag{6}$$

$$\underline{\tau} = \int_{-\infty}^{t} \{ \sum_{k=1}^{\infty} \frac{\eta_k}{\lambda_k} \exp \left(- \frac{t-t'}{\lambda_k} \right) \} \dot{\underline{\Gamma}}' (t')dt' \tag{7}$$

where D/Dt is the co-rotational or Jaumann derivative and $\dot{\underline{\Gamma}}'$ is the co-rotating rate of deformation tensor.

Goddard and Miller[6] went one step beyond equation (7) and replaced the quantity in braces by an arbitrary function of (t-t').

$$\underline{\tau} = \int_{-\infty}^{t} G_I (t-t') \dot{\underline{\Gamma}}' (t')dt' \tag{8}$$

or

$$\underline{\tau} = \int_{0}^{\infty} G_I (s) \dot{\underline{\Gamma}} (t-s)ds \tag{9}$$

Equation (8) or (9) is known as the Goddard-Miller Model. Goddard[7] has demostrated that the simple integral in equation (8) is the first term of an integral expansion for the simple fluid of Colemann and Noll. Bird, et al.,[8] have

shown that the first term of this expansion predicts behavior more consistent with experimental observations than the first terms of other integral expansions.

The Goddard-Miller model can be used to derive many relations among measurable rheological properties. For example, it has been shown[8] that non-newtonian viscosity data can be used to predict normal stresses using an empiricism based on an analytical relation obtained from the Goddard-Miller model. These relations are:

$$\theta(\dot{\gamma}) = \frac{4}{\pi}\int_0^\infty \frac{\eta(\dot{\gamma}) - \eta(\dot{\gamma}')}{(\dot{\gamma})^2 - \dot{\gamma}^2}\, d\dot{\gamma}' \qquad \dot{\gamma} > 0 \qquad (10)$$

$$\eta(\dot{\gamma}) - \eta_\infty = \frac{1}{\pi}\int_0^\infty \frac{(\dot{\gamma}')^2\,\theta(\dot{\gamma}')}{(\dot{\gamma}')^2 - \dot{\gamma}^2}\, d\dot{\gamma}' \qquad \dot{\gamma} \geq 0 \qquad (11)$$

CHAPTER 2. METHODS FOR MEASURING NORMAL STRESSES.

2.1) Introduction.

A viscometric flow is a flow in which the deformation, as seen in a co-rotating frame, is indistinguishable from simple shear. Simple shear is a unidirectional flow with a linear velocity gradient. If the velocity is constant with time, the motion is called steady simple shear. The flow kinematics are described by:

$$u_1 = \dot{\gamma} x_2$$
$$u_2 = u_3 = 0 \qquad (12)$$

where $\dot{\gamma}$ is a constant called the shear rate and 1 denotes the direction of flow and 2 the direction of the velocity gradient. In steady simple shear the general form of the stress tensor is:

$$\underline{\tau} = \begin{vmatrix} \tau_{11} & \tau_{12} & 0 \\ \tau_{21} & \tau_{22} & 0 \\ 0 & 0 & \tau_{33} \end{vmatrix} \qquad (13)$$

Since the deviatoric stress tensor is symmetric we can rewrite it as:

$$\underline{\tau} = \begin{vmatrix} \tau_{11} & \tau_{12} & 0 \\ \tau_{12} & \tau_{22} & 0 \\ 0 & 0 & \tau_{33} \end{vmatrix} \qquad (14)$$

It would appear that there are four quantities which we could measure in a steady simple shear experiment. But we cannot actually measure the deviatoric stress tensor $\underline{\tau}$ but only the total stress tensor $\underline{\sigma}$. The deviatoric stress tensor differs from the total stress tensor by an undefined isotropic contribution.

$$\underline{\sigma} = \underline{\tau} - p\underline{I} \tag{15}$$

We can eliminate the isotropic contribution by taking differences.

$$\begin{aligned} \tau_{11} - \tau_{22} &= \sigma_{11} - \sigma_{22} \\ \tau_{11} - \tau_{33} &= \sigma_{11} - \sigma_{33} \\ \tau_{22} - \tau_{33} &= \sigma_{22} - \sigma_{33} \end{aligned} \tag{16}$$

It is obvious that only two of these three differences are independent. So we choose two of these quantities and we call them

$$\begin{aligned} N_1 &= \tau_{11} - \tau_{22} \quad \text{First Normal Stress Difference} \\ N_2 &= \tau_{22} - \tau_{33} \quad \text{Second Normal Stress Difference} \end{aligned} \tag{17}$$

Now we have identified three measurable quantities in viscometric flows

$$\tau_{12}, \quad N_1, \quad N_2$$

These quantities are functions of the shear rate, and these functions are called the viscometric functions. They depend also on the material subjected to the viscometric flow.

It is common practice to report values of these material functions in terms of the following ratios:

$$\eta(\dot{\gamma}) = \frac{\tau_{12}}{\dot{\gamma}} \qquad \text{Shear Viscosity}$$

$$\theta_1(\dot{\gamma}) = \frac{N_1}{\dot{\gamma}^2} \qquad \text{First Normal Stress Coefficient} \quad (18)$$

$$\theta_2(\dot{\gamma}) = \frac{N_2}{\dot{\gamma}^2} \qquad \text{Second Normal Stress Coefficient}$$

Many flows of practical interest fall into the category of viscometric flows. Among them the more relevant are: Poiseuille flow, Couette flow, cone and plate flow and torsional flow.

In the late 60's and early 70's much work was done to study the normal stress differences exhibited in viscometric flow by polymeric materials both in solution and melt form.

The purpose of this chapter is to give a brief review of the methods and equipment used to measure the first normal stress difference and to comment about the conditions required for a meaningful measurement and the problems and sources of error encountered in each method.

A very good reference on this subject of rheometry is the book by Walters[9].

2.2) Cone and Plate Flow.

Cone and plate flow is obtained in the region bounded by a flat plate and a convex cone whose apex touches the plate. A diagram of the cone and plate geometry is shown in Figure 1. The cone rotates with a rotational speed Ω and the plate is held stationary.

Cone and plate flow can be considered as viscometric flow if the inertia terms in the Cauchy's equation are neglected. The kinematic description of the flow is given by

$$u_\phi = \Omega r \qquad (19)$$
$$u_\theta = u_r = 0$$

using a spherical coordinate system.

A detailed analysis of the flow in a cone and plate geometry based on the following assumptions is given in the Appendix I.

Assumptions:

a) Inertial effects are negligible.

b) The cone angle is very small. This enables us to assume that the shear rate is constant throughout the gap.

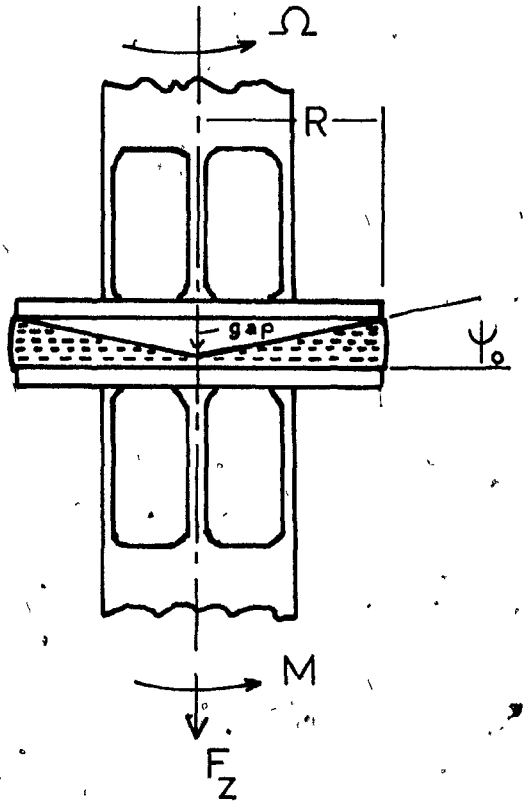

Fig.1

Cone and Plate Geometry.

c) The cone and plate have infinite dimensions.

d) Steady simple shear flow is the flow regime up to the free surface.

e) Surface tension forces are negligible.

In this section we present a summary of the equations for the material functions in cone and plate flow.

$$\dot{\gamma} = \frac{\Omega}{\Psi_0} \qquad \text{Shear rate} \qquad (20)$$

$$\tau_{12} = \frac{3M}{2\pi R^3} \qquad \text{Shear stress} \qquad (21)$$

$$\eta(\dot{\gamma}) = \frac{\tau_{12}}{\dot{\gamma}} \qquad \text{Shear viscosity} \qquad (22)$$

$$\eta(\dot{\gamma}) = \frac{3M\Psi_0}{2\pi\Omega R^3}$$

$$N_1(\dot{\gamma}) = \tau_{11} - \tau_{22} = \frac{2F}{\pi R^2} \qquad \text{First Normal Stress Difference} \qquad (23)$$

$$\frac{d\sigma_{\theta\theta}}{d \ln r} = \{ N_1(\dot{\gamma}) + 2N_2(\dot{\gamma}) \} \qquad \text{Second Normal Stress Difference.} \qquad (24)$$

where 1 denotes the ϕ coordinate, 2 the θ coordinate and 3 the r coordinate of a spherical coordinate system.

It can be seen that the viscosity and the first normal stress difference can be computed directly from the geometrical factors of the cone and plate, the rotational speed of the cone or plate and the measurement of the torque and normal force. This is not the case for the se--

cond normal stress difference because we have to know the distribution of $\sigma_{\theta\theta}$ as a function of the radius of the plate in order to use equation (24) to calculate N_2.

Experimentally, this is done by placing pressure transducers at different radial positions on the plate. This method introduces an important source of error in the measurement, the so called pressure hole error, unless flush-mounted transducers are used. We will not discuss this effect in further detail since the present work is only concerned with first normal stress measurements.

The equations summarized above are based on certain assumptions made concerning the flow field. If this flow field is not reproduced in the experimental instrument these equations are not valid. Therefore, the following discussion is designed to point out the sources of error of the apparatus, their cause and elimination.

Sources of Error in Cone - Plate Rheometers.

Cone Angle.

In order to get meaningful experimental results in the cone and plate flow a constant shear rate must exist throughout the fluid and therefore a constant state of stress. This assumption is dependent on the cone angle. The cone angle has to be small in order for the assumption of

constant shear rate to hold.

Lodge[10] made experiments with different cone angles varying from 1 to 10^0 and found that the error involved for cone angles employed in commercial equipment can be tolerated since they are within experimental error. Table 1 shows these results.

Cone Angle (^{0} , rad)	Variation of Shear Rate across Gap(%)	Error in using formula $\dot{\gamma} = \Omega/\Psi_o$ (%)
1, 0.017	0.03	0.02
2, 0.034	0.21	0.08
3, 0.052	0.28	0.18
4, 0.069	0.49	0.32
5, 0.087	0.77	0.50
7, 0.122	1.50	0.98
10, 0.174	3.10	2.00

Table 1. Variation of Shear Rate across Gap.

Inertia Effects.

Another possible source of error is the assumption that the inertia terms of the equations of motion can be neglected. It can be shown that the simple shear flow proposed for cone and plate geometry is not compatible with the governing equations of motion when the inertia effects are not ne

gligible. If these equations are to be made compatible we must take into account the ocurrence of secondary flows. This effect can be critical for the case of low viscosity materials or materials being sheared at high speeds. The distortion of the flow field consists of a slow circulatory flow radially inwards along the stationary element and radially outwards on the rotating element. This flow pattern gives rise to a radial variation of the normal stress on both elements with a minimum at the axis of rotation.

A qualitative measure of the importance of this effect can be obtained by using the definition of the Reynolds number for cone and plate flow

$$Re_{cp} = \frac{r^2 \Psi_0 \Omega}{\nu} \qquad (25)$$

Since the Reynolds number represents the ratio of inertial to viscous forces, a small Reynolds number would mean that the inertial forces are small compared to the viscous ones. For the experimental conditions encountered in the case of polymer melts, the Reynolds number is, in fact, a small number. For example, with a cone and plate 50 mm. in diameter and 0.1 rad cone angle and assuming a rotational speed of 1.0 rad/sec, the Reynolds number for a LDPE resin at 180^0C is of the order of 10^{-6} .

Finite Size of the Fixtures.

The assumption that the cone and plate have infinite dimensions leads to another possible source of error. The finite size of the fixtures can cause an edge effect known as shear fracture instability. Most of the work done on this particular effect has been carried out by Hutton[11]. It is observed that an instability occurs in the cone and plate flow when a certain critical stress is reached. This instability causes the stress to fall rapidly and the higher the shear rate the shorter the time before the fall occurs. When the stress falls it tends to oscillate considerably. The fall of the stress is due to a fracture that starts at the periphery of the sample and grows inward. This fracture tends to decrease the effective radius of shearing. Some recent experiments done by Gleissle[12] indicate that these instabilities may be the cause of the phenomenon of stress overshoot. Hutton also suggests that this fracture depends strongly on the elasticity of the material.

Also related to the finite size of the fixtures are the surface tension and free surface shape effects. The surface tension effect depends to some degree on the characteristics of the test fluid and the instrument members and to a large extent on the relative total normal force values arising from the true normal stress effects. It can be considered that for highly elastic materials that genarate normal stress effects the surface tension

can be neglected as a possible source of error.

Ginn and Metzner[13] have shown that normal force data are not dependent on the configuration on the boundary but mainly on the changes of contact angles between the fixtures and the test material. This effect appears only during the starting and stopping of the rotation.

Viscous Heating.

In any real situation where there is viscous shear flow of some materials, there is viscous dissipation of energy. The work expended in shearing the fluid is transformed to internal energy which causes the temperature of the fluid to rise. If the flow boundaries are maintained at constant temperature, temperature gradients will develop in the system. These gradients must be minimized or corrections should be applied since the viscosity of most polymeric materials is highly temperature dependent.

The rate of energy generation by shearing work per unit volume of fluid in simple shear flow is given by

$$\frac{\text{Rate of energy generation}}{\text{Unit volume}} = \underline{\tau} : \nabla \underline{u} = \tau_{12}\dot{\gamma} = \eta\dot{\gamma}^2 \qquad (26)$$

From this expression it is clear that an increase in either viscosity or shear rate will give rise to an increase in the rate of energy generation and therefore to temperature gra-- dients. Considering the flux of energy going out of the system suggests that low thermal conductivity and large distances for heat flow to the isothermal boundary will give rise to large temperature gradients.

Polymer melts generally have low thermal conductivity. Therefore in order to minimize the effects caused by viscous heating it is important to employ well thermostatted test fixtures with a small gap and to work at low shear rates.

Error Sources due to Apparatus Imperfections.

The points discussed above were concerned mainly with the validity of the assumptions in the development of the equations governing cone and plate flow. Some other problems can occur due to imperfections in the apparatus.

Axis of Rotation not perpendicular to the Stationary Plate.

If the surface of the rotating element is perpendicular to the axis of rotation but the stationary element is not, the resulting non-parallelism of the two elements results

in a converging flow in one half of the gap and a diverging flow in the other half. For the case of a viscous liquid in a narrow gap this non-parallelism can give rise to a large pressure maximum in the region of converging flow and an equally large pressure minimum in the region of diverging flow. This is sometimes called the wedge effect. This effect can be eliminated if an average is taken of the normal forces recorded with two directions of rotation.

Axial Movement of Rotating Member.

If the bearing is not perfect the rotation of the shaft gives rise to a very small periodic axial movement of the shaft and its attached element. This gives rise to a small periodic movement of the fluid in the gap between rotating and stationary elements. Because the gap is small and the area of the rotating element is large this small movement can give rise to large periodic stresses. It has been proposed that the equation[10]

$$\tau_{jj} = -\frac{6\eta u}{\Psi_0^3}\left\{\frac{1}{r}-\frac{1}{R}\right\} + \tau_R \qquad (27)$$

where τ_{jj} is the stress contribution from the axial movement, u is the instantaneous speed that separates the ele-

ments and τ_R is the stress at the rim, can give a good approximation to this effect.

This effect will cause a flow that will be superimposed on the simple shear flow arising from the rotation and therefore will make the assumption of simple shear flow invalid. Since this flow is of a periodic nature and in most cases unsymmetric it has been shown that with the fluid in which the viscosity depends on shear rate the average value of $\tau_{jj} - \tau_R$ is different from zero. However, this variation is small compared with the amplitude of the stress variation and in most cases can be neglected. It is important to point out that since the stress τ_{jj} depends on the cube of the cone angle, the use of a very small angle could give rise to variations that are not negligible.

2.3) Other Methods.

Although cone-plate flow has been preferred as the method for measuring normal stress differences, several other flows have also been used. Several of these are described below.

Torsional Flow.

Torsional flow is obtained in the disc shaped region between two parallel plates, which rotate in their own

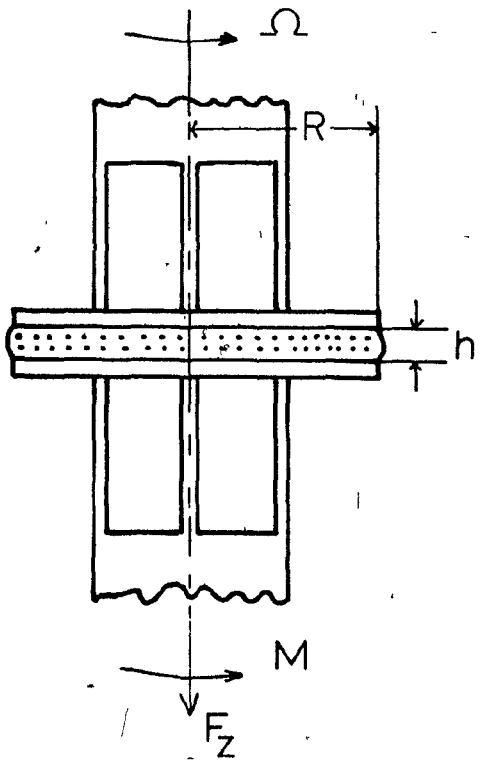

Fig. 2

Parallel Plates

Geometry.

plane with an angular velocity difference $\Delta\Omega$ and are separated a distance h. A schematic diagram of the parallel plates geometry is shown in Figure 2.

The kinematic description of the flow is given by

$$u_\theta = \Delta\Omega\left(\frac{z}{h}\right) + \text{const.}$$
$$u_r = u_z = 0 \qquad (28)$$

using a spherical coordinate system. A detailed analysis of this type of flow is given by Walters[9].

The basic equations relating the viscometric functions to measured quantities are:

$$\eta(\dot{\gamma}_R) = \frac{3M}{2\pi R^3 \dot{\gamma}_R}\left\{ 1 + 1/3 \frac{d\ln M}{d\ln \dot{\gamma}_R} \right\} \qquad (29)$$

$$\frac{2F}{\pi R^2}\left\{ 1 + \tfrac{1}{2} \frac{d\ln F}{d\ln \dot{\gamma}_R} \right\} = \{ N_1 - N_2 \}\Big|_{\dot{\gamma}_R} \qquad (30)$$

It can be seen from the above equations that the computation is not straightforward as in the case of cone and plate flow. The evaluation of the viscosity requires differentiation of the experimental data and for the normal stress differences, equation (30) has to be used in conjunction with, for example, data from cone and plate flow. This can be done since both flows are viscometric, therefore the viscometric functions are the same.

It can be said that the parallel plate flow suffers from the same sources of error (of course not on the cone angle) as the cone and plate flow. It is also known that inertial effects and edge effects can be critical in this type of flow and have a large influence in the analysis of the results.

Jet Thrust Measurements and Capillary Jet Swelling.

We have discussed in previous sections how rotational viscometers can be used to measure the material functions η, N_1 and N_2 taking care to minimize the possible sources of error. The applicability of rotational viscometers is restricted mainly by the shear rate range. These types of rheometers work best at low shear rates. Therefore if we are interested in higher shear rates, the capillary viscometer is the necessary choice.

The jet thrust method is analized in detail in reference[9]. The equations that relate the viscometric functions to measured quantities are:

$$(N_1)_w = P^{(RL)} + \tau_w \frac{\partial}{\partial \tau_w} P^{(RL)} \qquad (31)$$

$$(N_2)_w = -\tau_w \frac{\partial P^{(RL)}}{\partial \tau_w} \qquad (32)$$

Both of these equations involve the measurement of the wall pressure at the capillary exit $P^{(RL)}$. These measure

ments are often made by drilling pressure tappings along the capillary and extrapolating the pressure values to the capillary exit. This has given rise to questions as to the possibility of error resulting from the pressure hole effect. Although it has been suggested that this effect is not important for the case of polymer melts, the evidence is not strong enough to justify neglecting this source of error at the present time.

Another source of error is the surface tension effect. This effect causes a reduction in the jet thrust which is approximately equal to the product of the perimeter of the capillary and the dynamic surface tension of the liquid. It is found in general that this is a small effect.

Many attempts have been made to correlate normal stresses to die swell. Since the study of die swell is another part of this work we will talk about it in another chapter.

CHAPTER 3. FIRST NORMAL STRESS DIFFERENCE - EXP. RESULTS.

3.1) Experimental Equipment.

The first normal stress difference as well as the shear viscosity of three LDPE resins were measured in a Rheometrics Mechanical Spectrometer. This is a high precision instrument for measuring the flow behavior of materials as a function of time and temperature. It can operate with several geometries and in steady or dynamic models. A schematic diagram of the instrument is shown in Figure 3. The instrument has the facility to control the temperature of the sample environment from ambient to 325^{0}C by means of a forced convection air chamber. Rotary speeds may be varied from 0.001 to 250 radians per second in simple shear.

The transducer consists of a central, load receiving air bearing, supported by four cantilever beams. On all four sides of each cantilever beam silicon piezo resistive strain gauges are attached. By means of the appropiate circuit the transducer can simultaneously detect forces acting in the three spatial directions and a torque acting about the rotational axis. The X, Y and Z force range is from $5x10^2$ to 10^6 dynes and the torque range is from $5x10^3$ to 10^9 dyne cm The output signals from the transducer are amplified and recorded on a Honeywell Elektronik strip chart recorder.

Fig.3

Schematic Of Mechanical Spectrometer

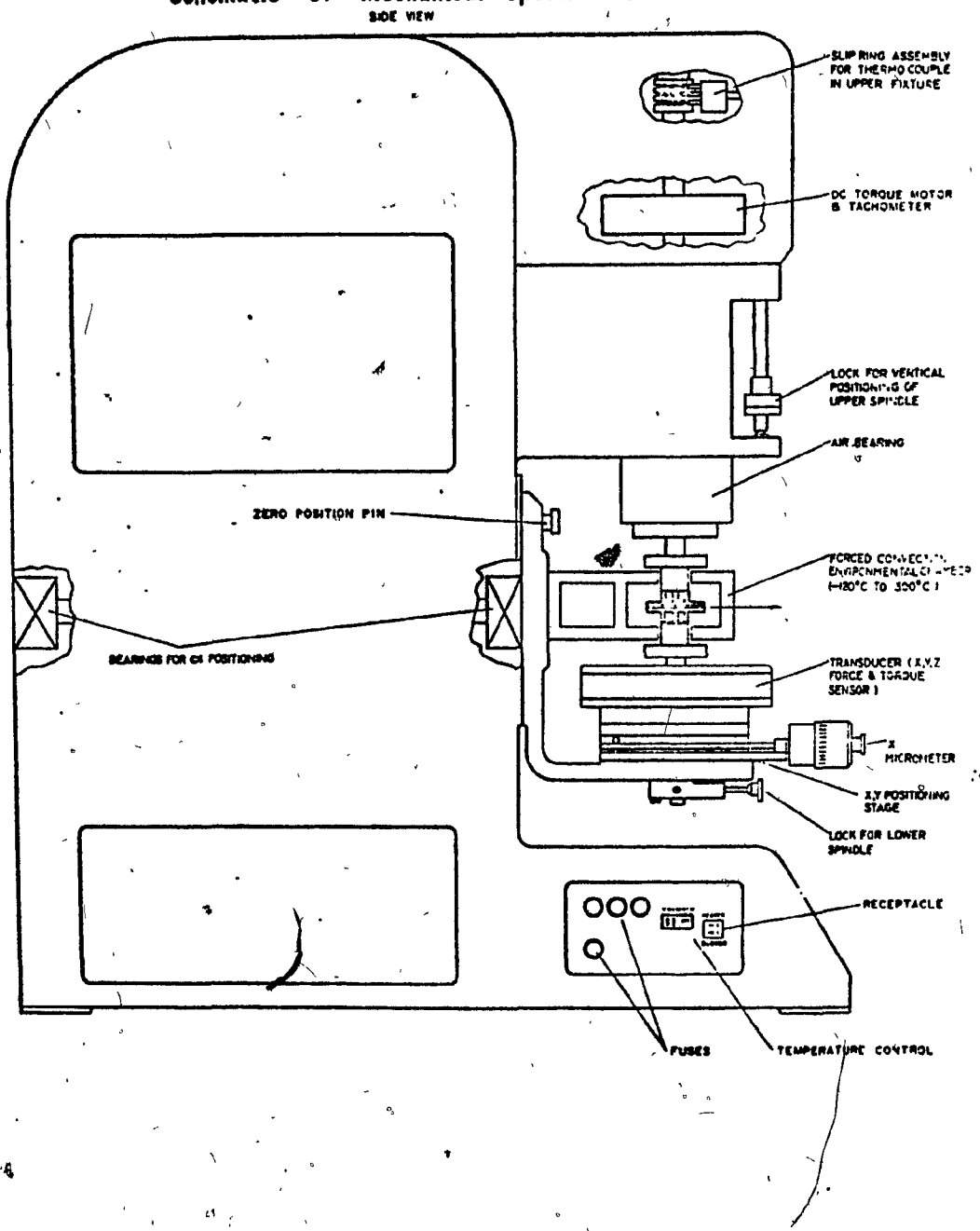

3.2) Experimental Technique.

The Rheometrics Mechanical Spectrometer was used with cone and plate fixtures since this geometry is convenient for the measurement of torque and normal forces and also because both viscosity and normal stress difference can be calculated directly from the experimental data.

The fixtures were heated to the desired temperature by means of the forced convection chamber. Since the apex of the cone is truncated to avoid damage of the fixtures, the cone and plate must be separated so that the position of the hypothetical apex of the cone would correspond to the point of contact between the cone and the plate. This separation is specified by the manufacturer. To set the cone in the correct vertical position, the truncated cone was lowered until it just made contact with the plate. This was determined by observing the output from the Z force channel. A dial indicator was used to set this point of incipient contact as the reference point. The cone was then raised to the position specified by the manufacturer. A vertical position stop and locking nut allowed the cone to be repositioned at the same location with respect to the plate.

The test samples were premolded by compression molding at 150^{0}C and 20000 psi. The samples were discs 50 mm in diameter and 2 mm thick.

The sample was placed on the lower plate, allowed to melt and then the cone was lowered to the proper position. A small amount of material was squeezed out from the fixtures and trimmed away with a spatula. In these experiments the lower plate was held stationary. A rotational speed was selected and the material sheared by rotating the cone.

A wide range of rotational speeds (shear rates) can be studied with only one sample. The limitations are degradation of the polymer due to high temperatures involved and, at high shear rates, material losses.

Experimental Conditions.

A cone and plate with the following dimensions was used:

Cone angle: 0.1 rad (5.76^0).

Diameter : 50 mm

Gap : 0.05 mm

This particular cone angle was used because it reduces the oscillations of the normal force due to the axial movement of the rotating member.

Shear rate range: 0.01 - 2.5 sec^{-1}

Temperature of the tests: 160 and 180^0C.

3.3) Experimental Results.

Figures 4 to 9 present the viscosity curves as a function of the shear rate for resins 1, 9 and 10 at 160 and 180°C. All the resins exhibit the expected variation of viscosity with shear rate and temperature. Reliable zero shear viscosity values can be estimated since the curves level off at low shear rate.

The normal stress data are presented in two different ways.

Figures 10 to 15 show the first normal stress difference as a function of shear rate for resins 1, 9 and 10 at 160 and 180°C.

The alternative way of presenting the normal stress data are the curves of the first normal stress coefficient, defined as

$$\theta = \frac{\tau_{11}-\tau_{22}}{\dot{\gamma}^2} \qquad (33)$$

as a function of shear rate.

Figures 16 to 21 show the curves of θ as a function of shear rate for resins 1, 9 and 10 at 160 and 180°C.

In all three resins the first normal stress difference increased with shear rate and the first normal stress coefficient decreased with shear rate.

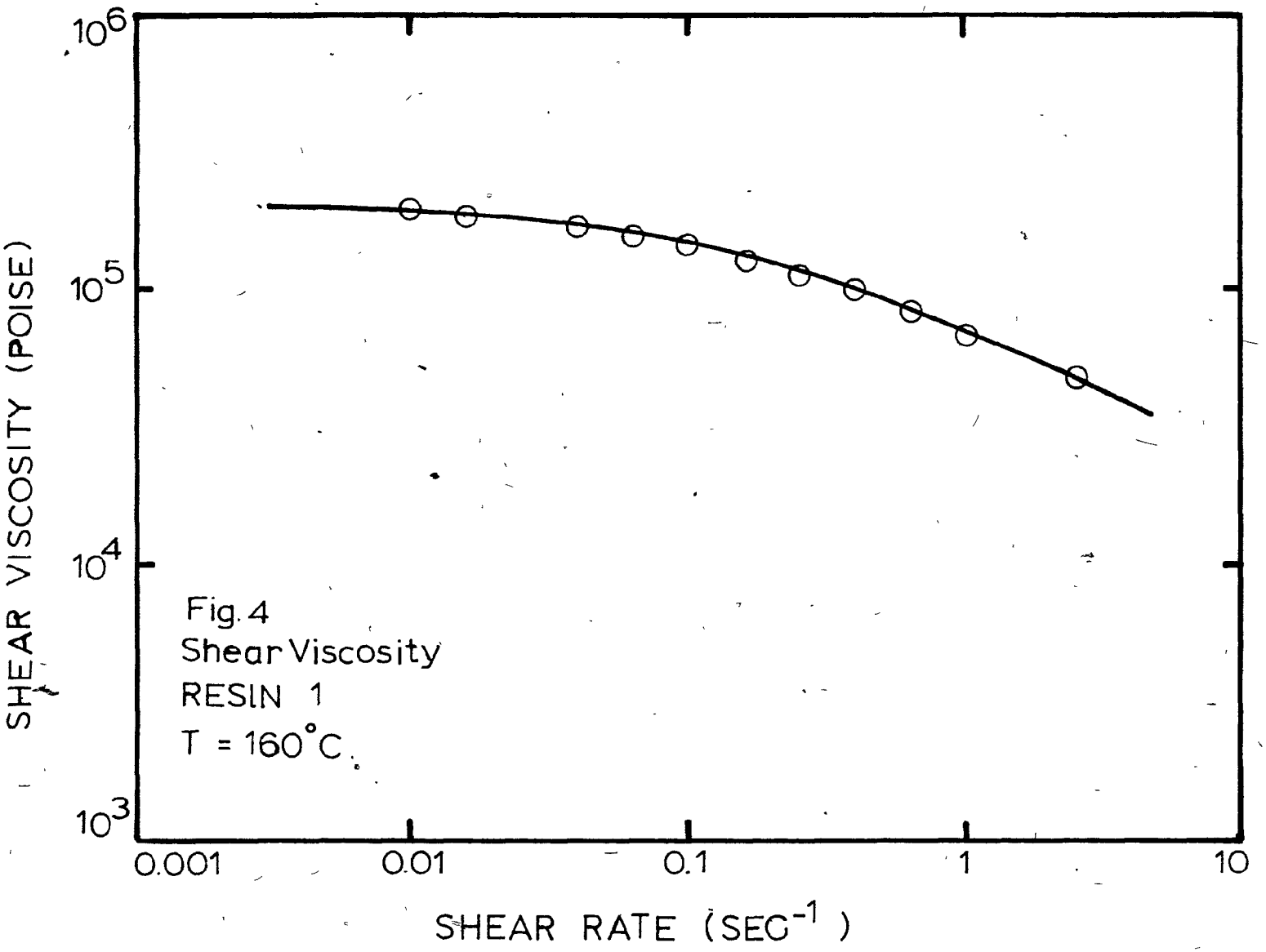

Fig. 4
Shear Viscosity
RESIN 1
T = 160°C

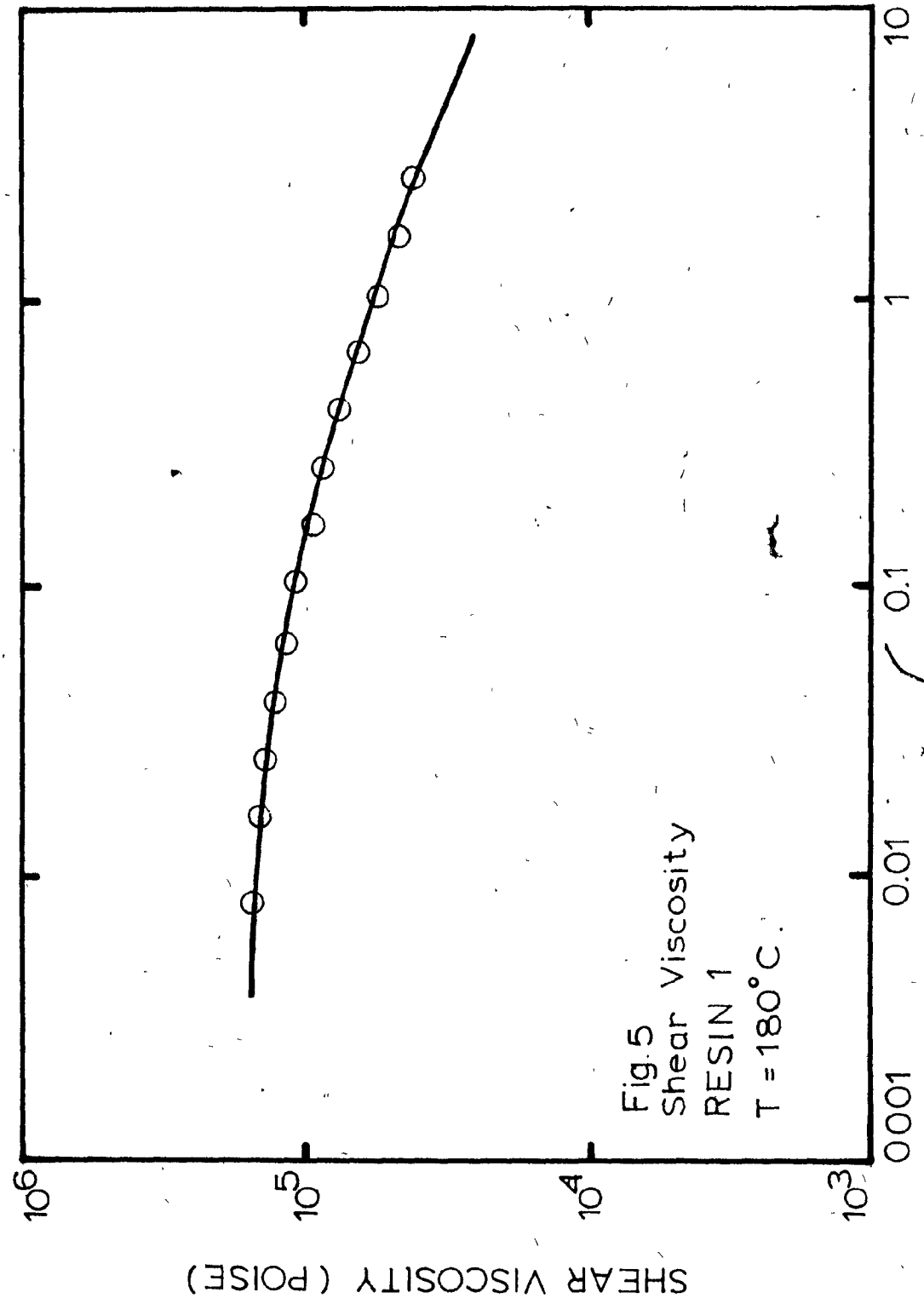
SHEAR VISCOSITY (POISE)
10^6
10^5
10^4
10^3
.0001
0.01
0.1
1
10
SHEAR RATE (SEC^{-1})
Fig.5
Shear Viscosity
RESIN 1
T = 180°C.

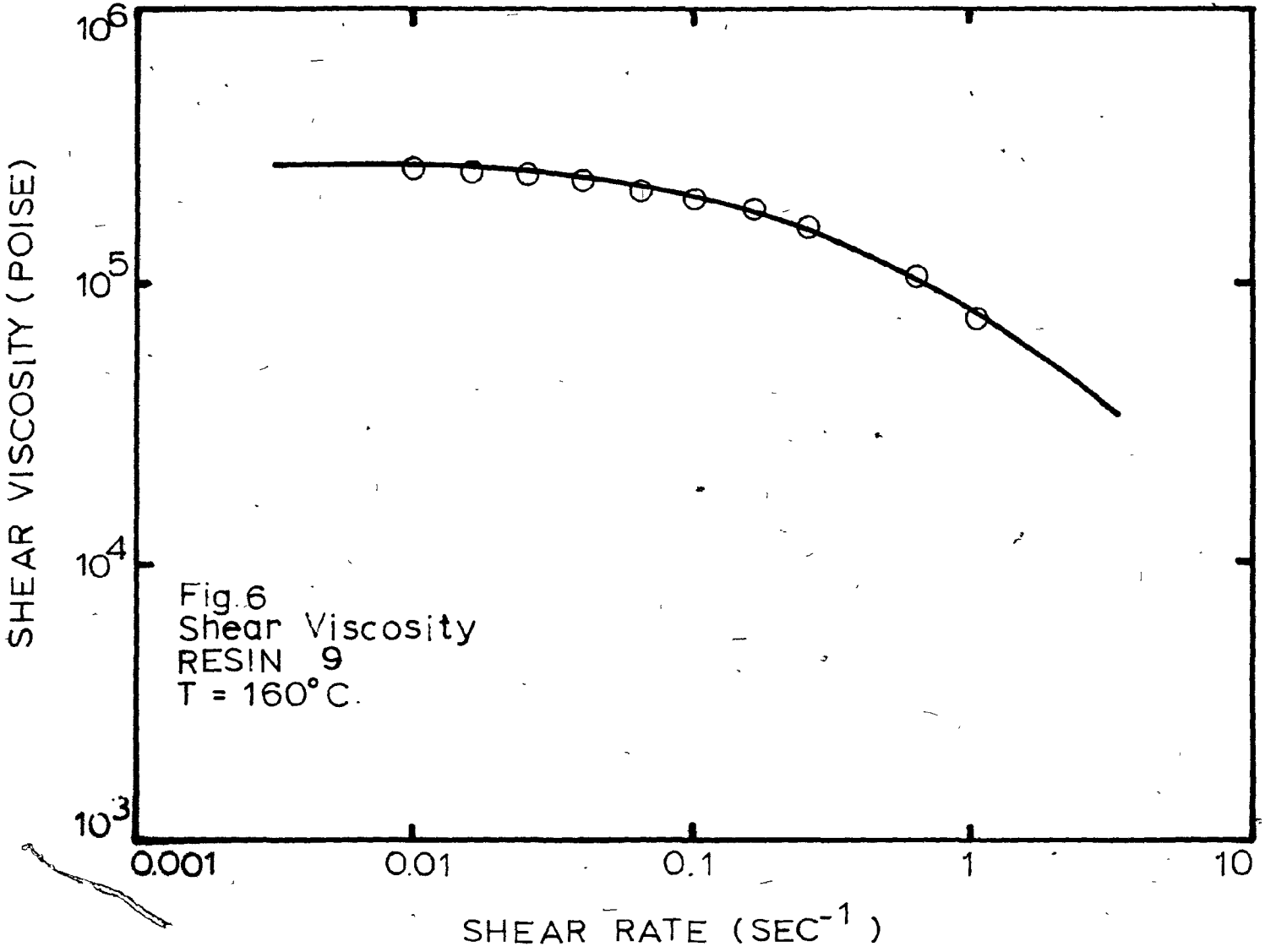

Fig.6
Shear Viscosity
RESIN 9
T = 160°C.

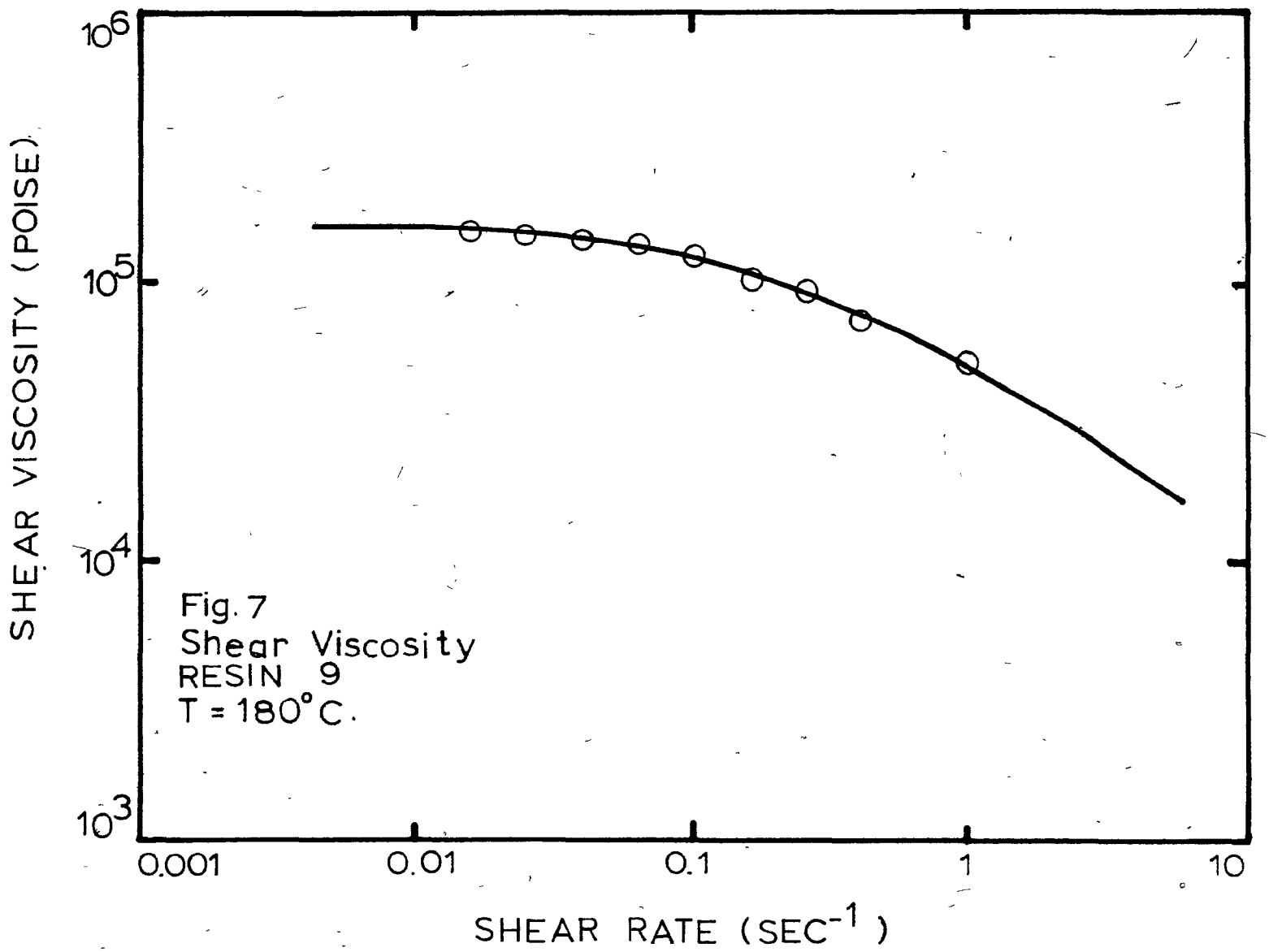

Fig. 7
Shear Viscosity
RESIN 9
T = 180°C.

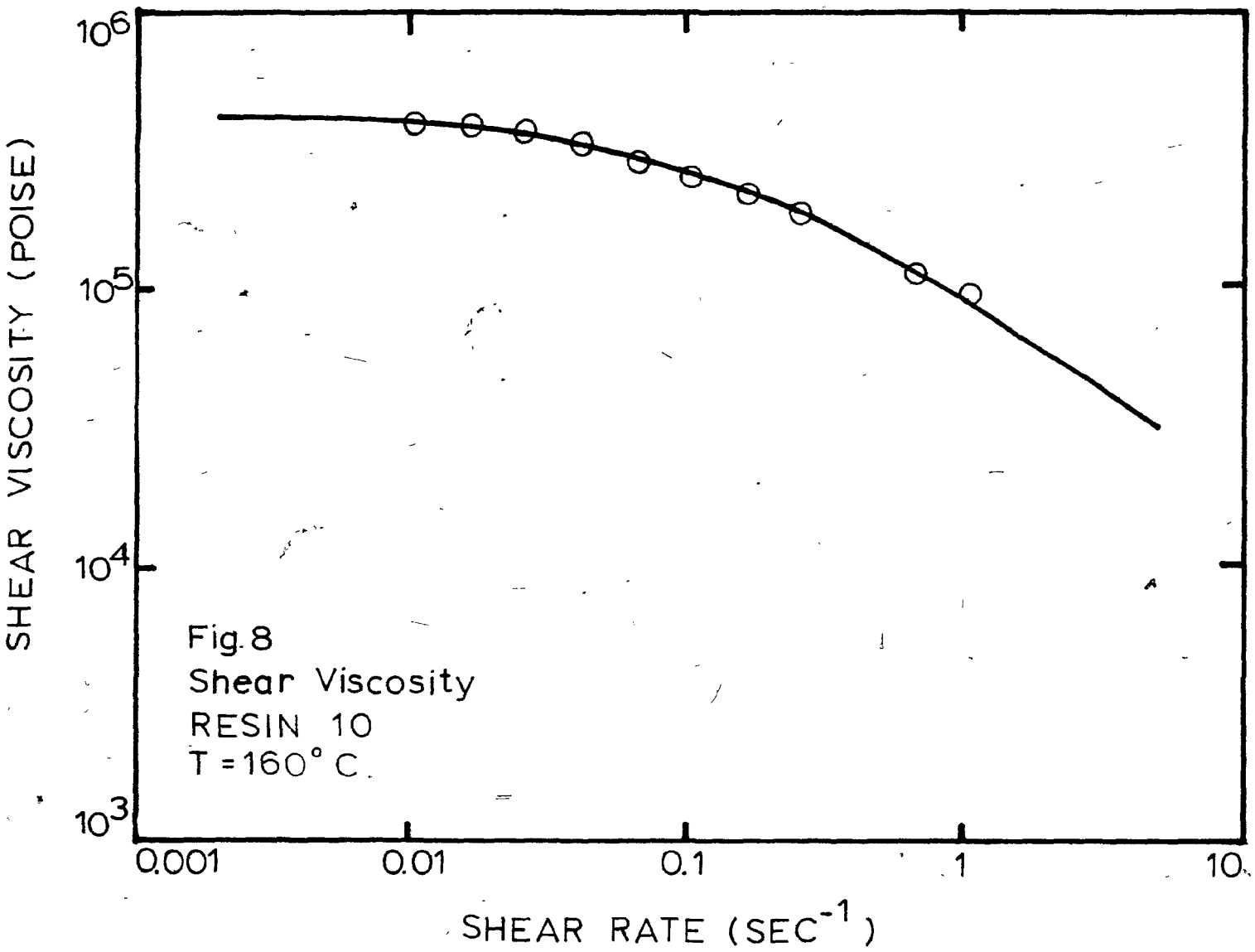

Fig. 8
Shear Viscosity
RESIN 10
T = 160° C.

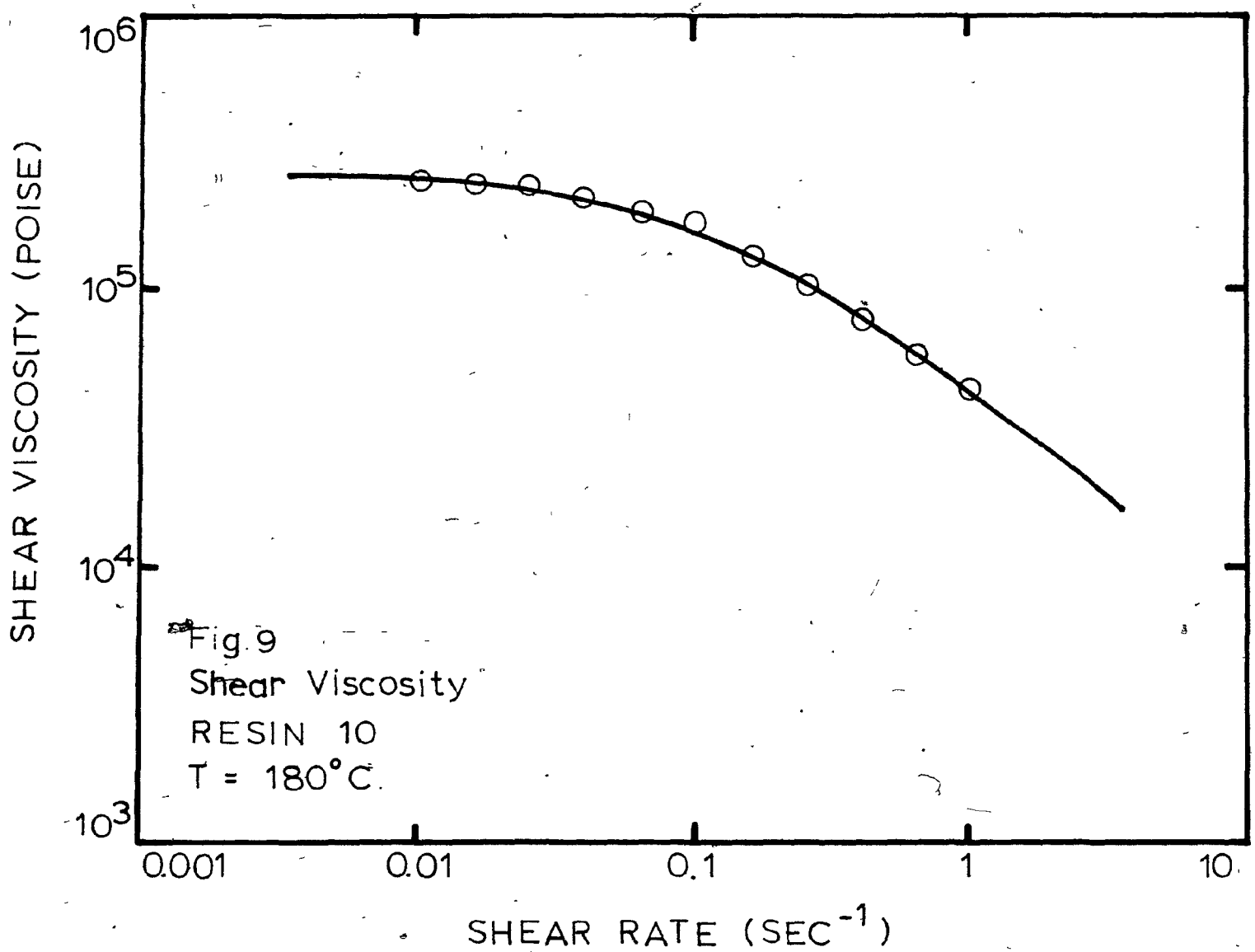

Fig. 9
Shear Viscosity
RESIN 10
T = 180°C.

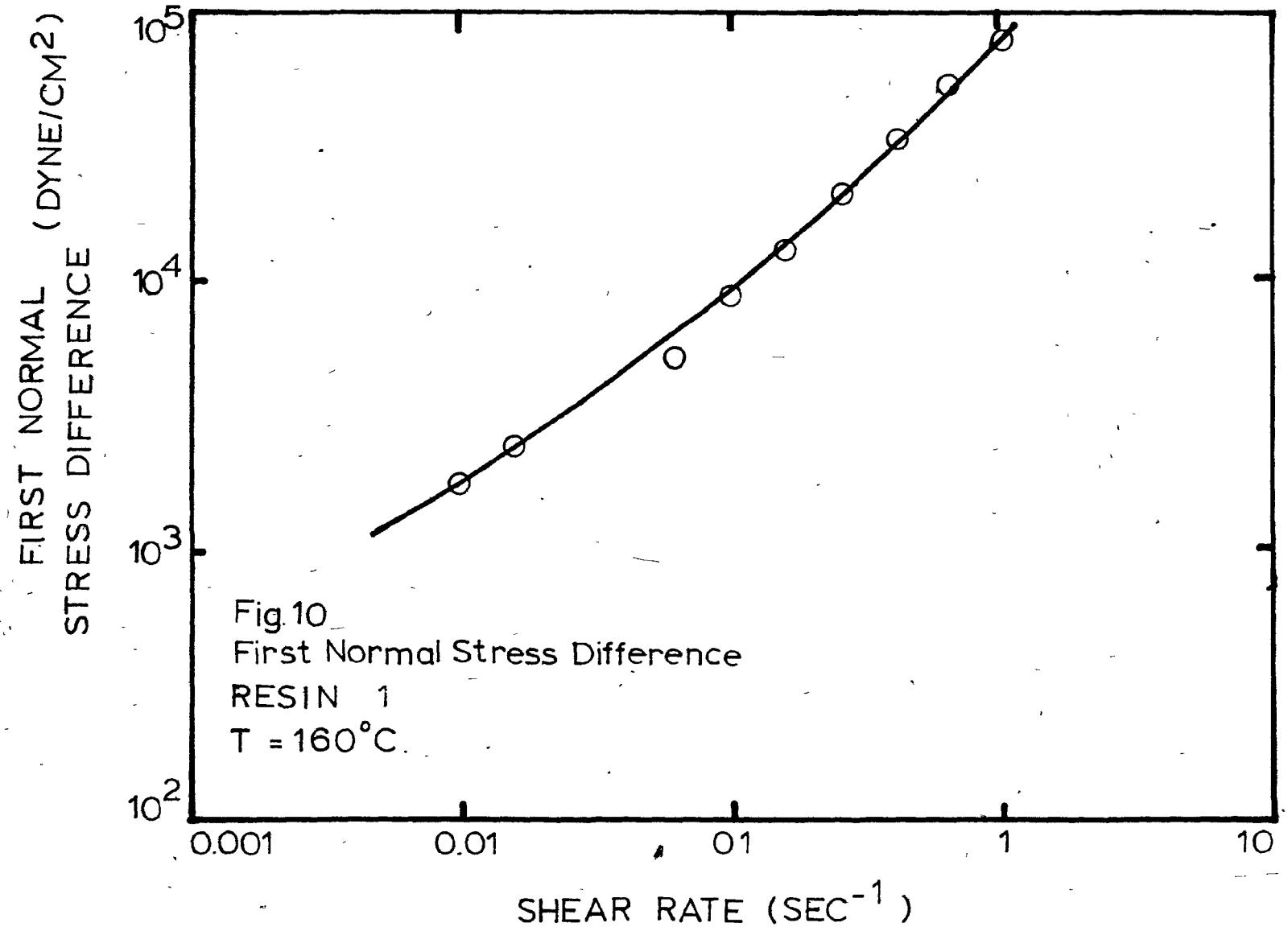

Fig. 10
First Normal Stress Difference
RESIN 1
T = 160°C.

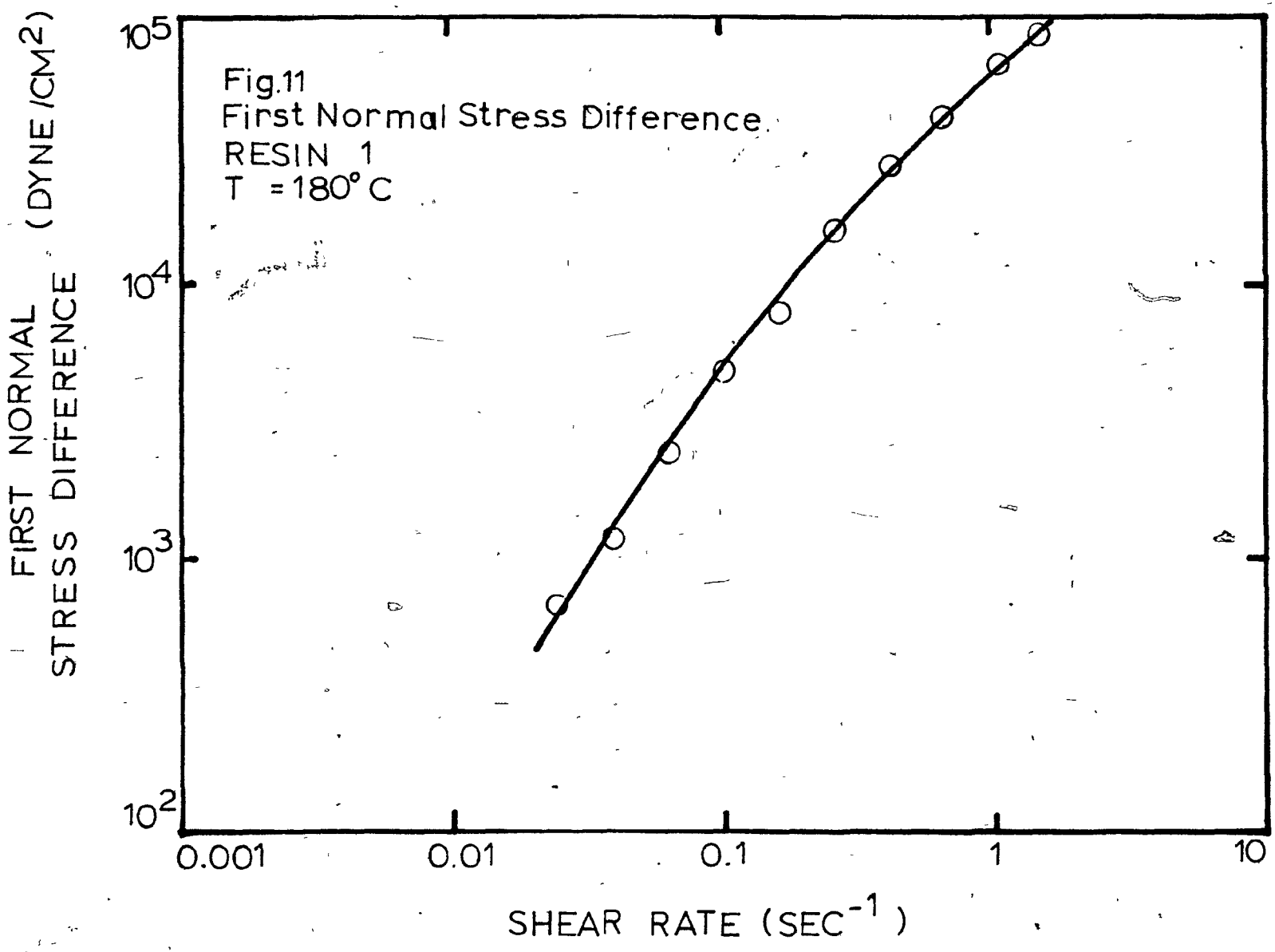
Fig.11
First Normal Stress Difference
RESIN 1
T = 180° C
FIRST NORMAL STRESS DIFFERENCE (DYNE/CM2)
10^5
10^4
10^3
10^2
0.001
0.01
0.1
1
10
SHEAR RATE (SEC^-1)

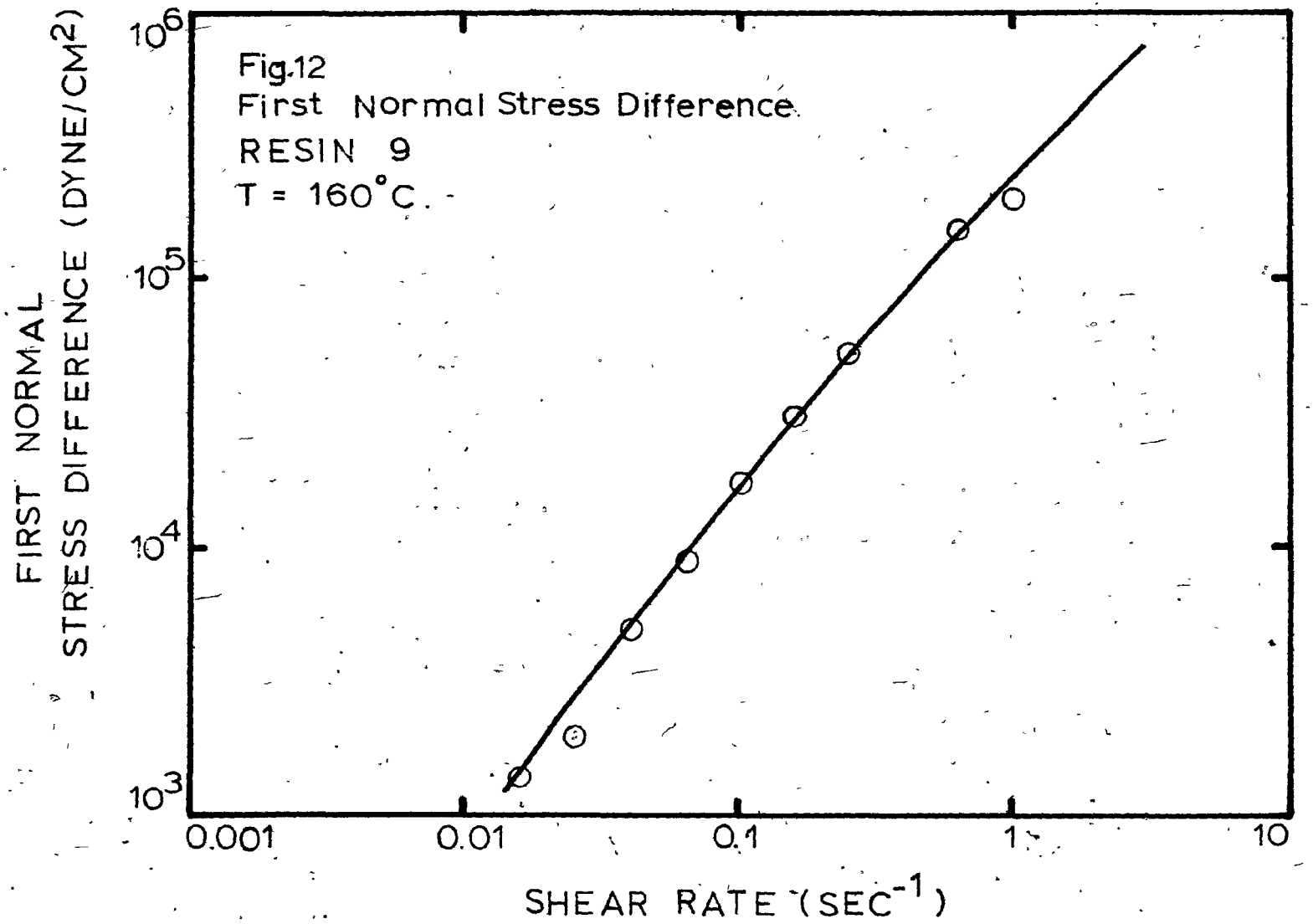
Fig.12
First Normal Stress Difference
RESIN 9
T = 160°C.
FIRST NORMAL STRESS DIFFERENCE (DYNE/CM2)
10^6
10^5
10^4
10^3
0.001
0.01
0.1
1
10
SHEAR RATE (SEC^-1)

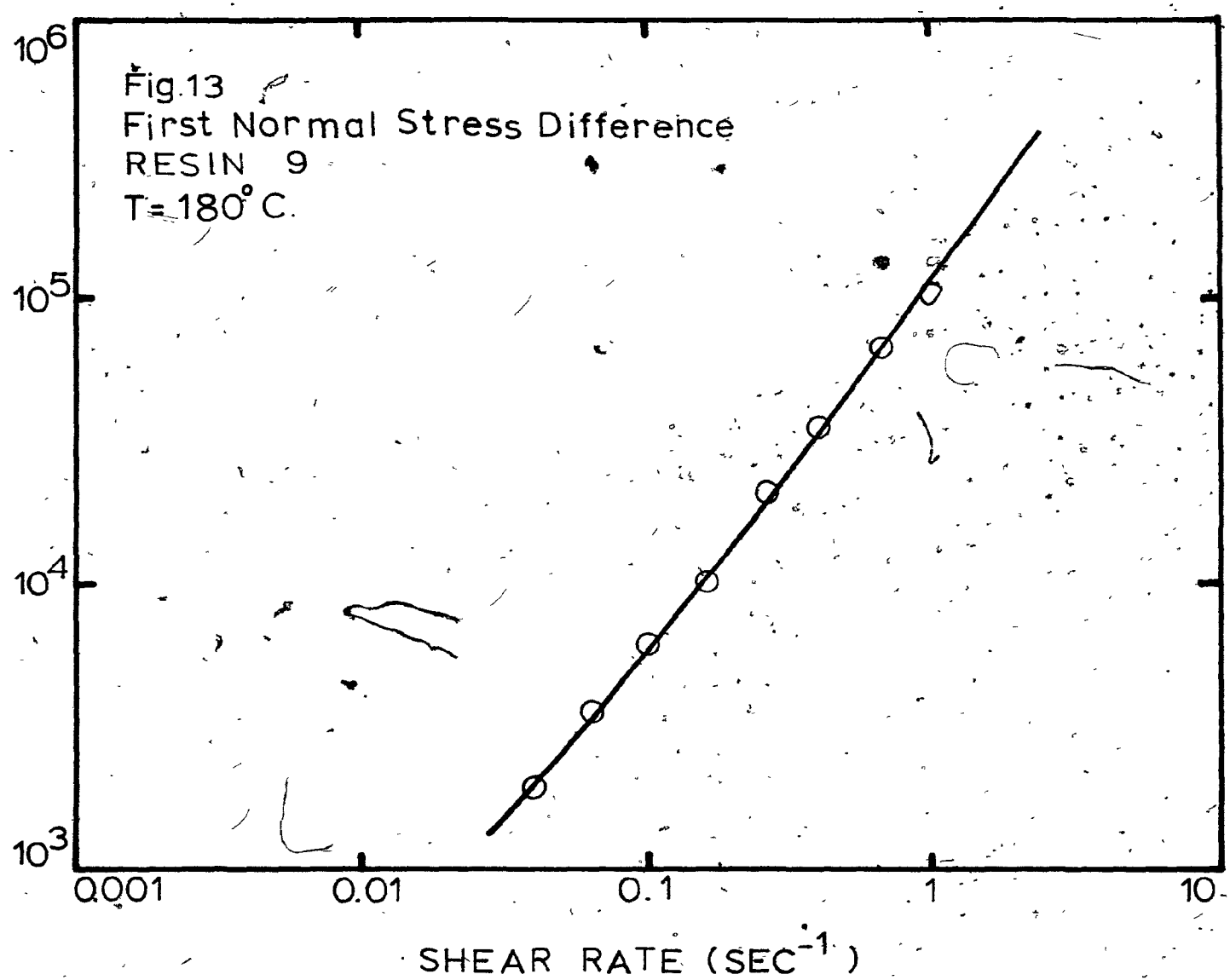
Fig.13
First Normal Stress Difference
RESIN 9
T=180°C.
FIRST NORMAL STRESS DIFFERENCE (DYNE/CM2)
10^6
10^5
10^4
10^3
0.001
0.01
0.1
1
10
SHEAR RATE (SEC^-1)

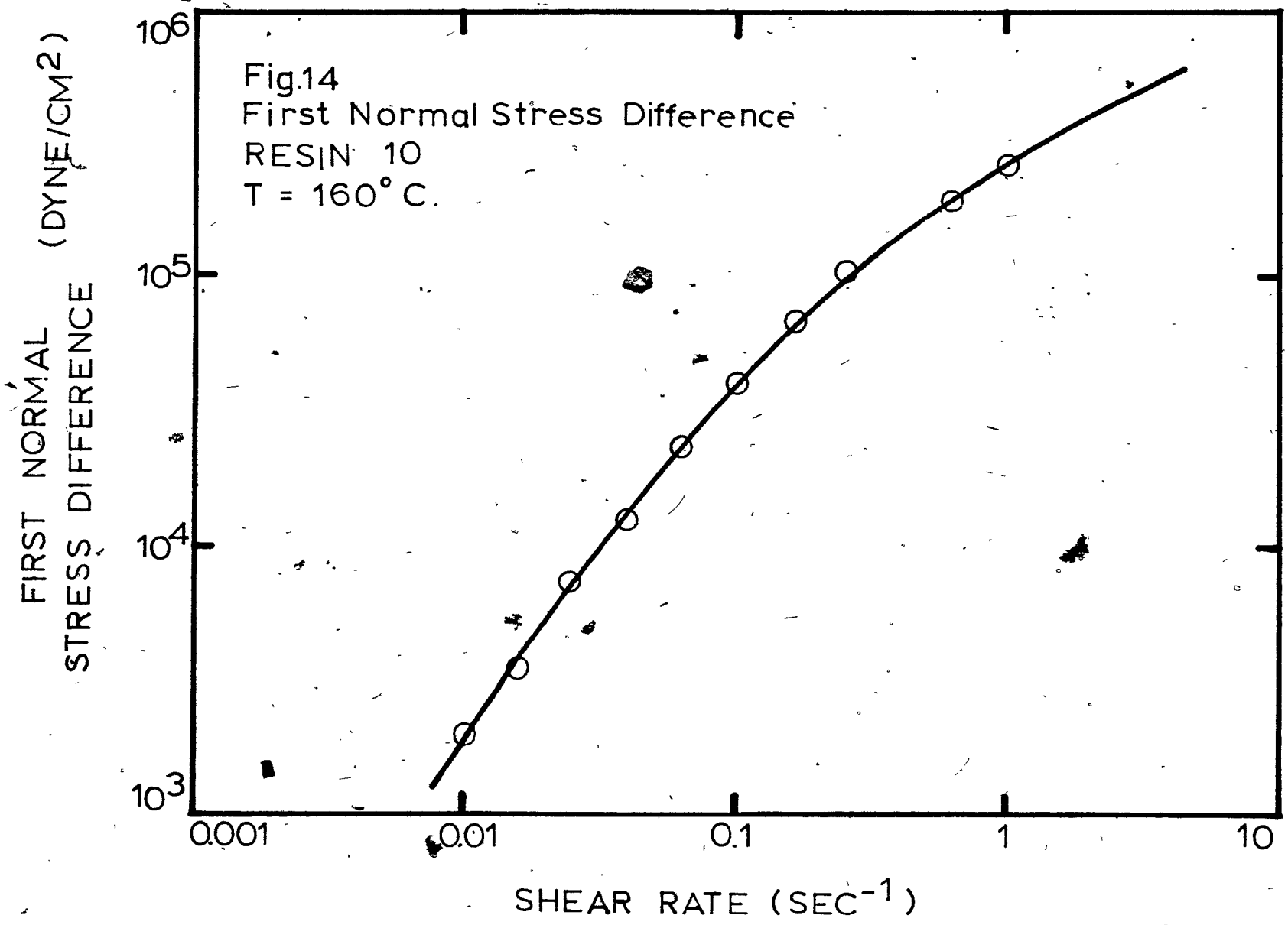
Fig.14
First Normal Stress Difference
RESIN 10
T = 160° C.
FIRST NORMAL STRESS DIFFERENCE (DYNE/CM2)
10^6
10^5
10^4
10^3
0.001
0.01
0.1
1
10
SHEAR RATE (SEC^-1)

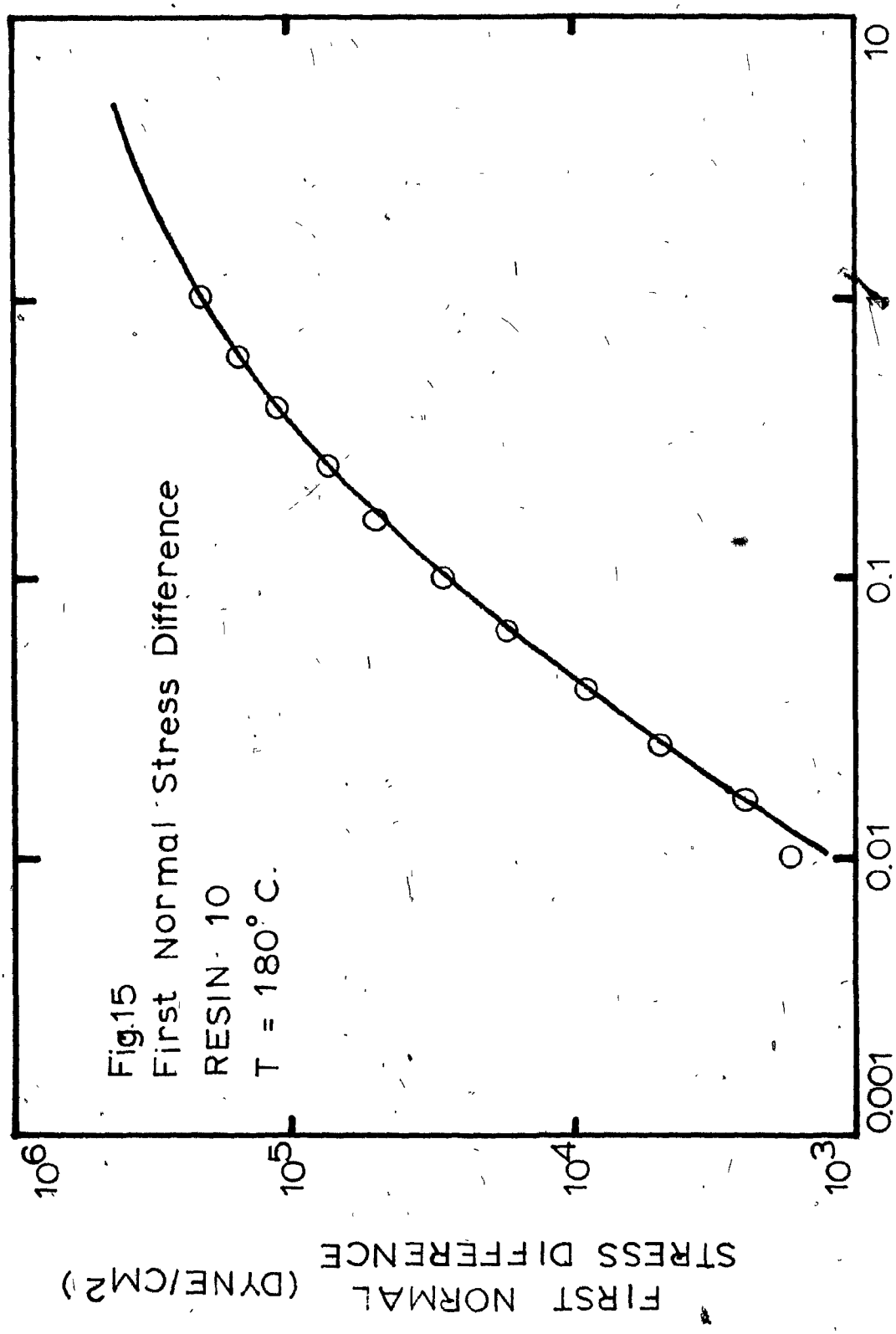
FIRST NORMAL STRESS DIFFERENCE (DYNE/CM2)
10^6
10^5
10^4
10^3
0.001
0.01
0.1
1
10
SHEAR RATE (SEC^{-1})
Fig.15
First Normal Stress Difference
RESIN 10
T = 180° C.

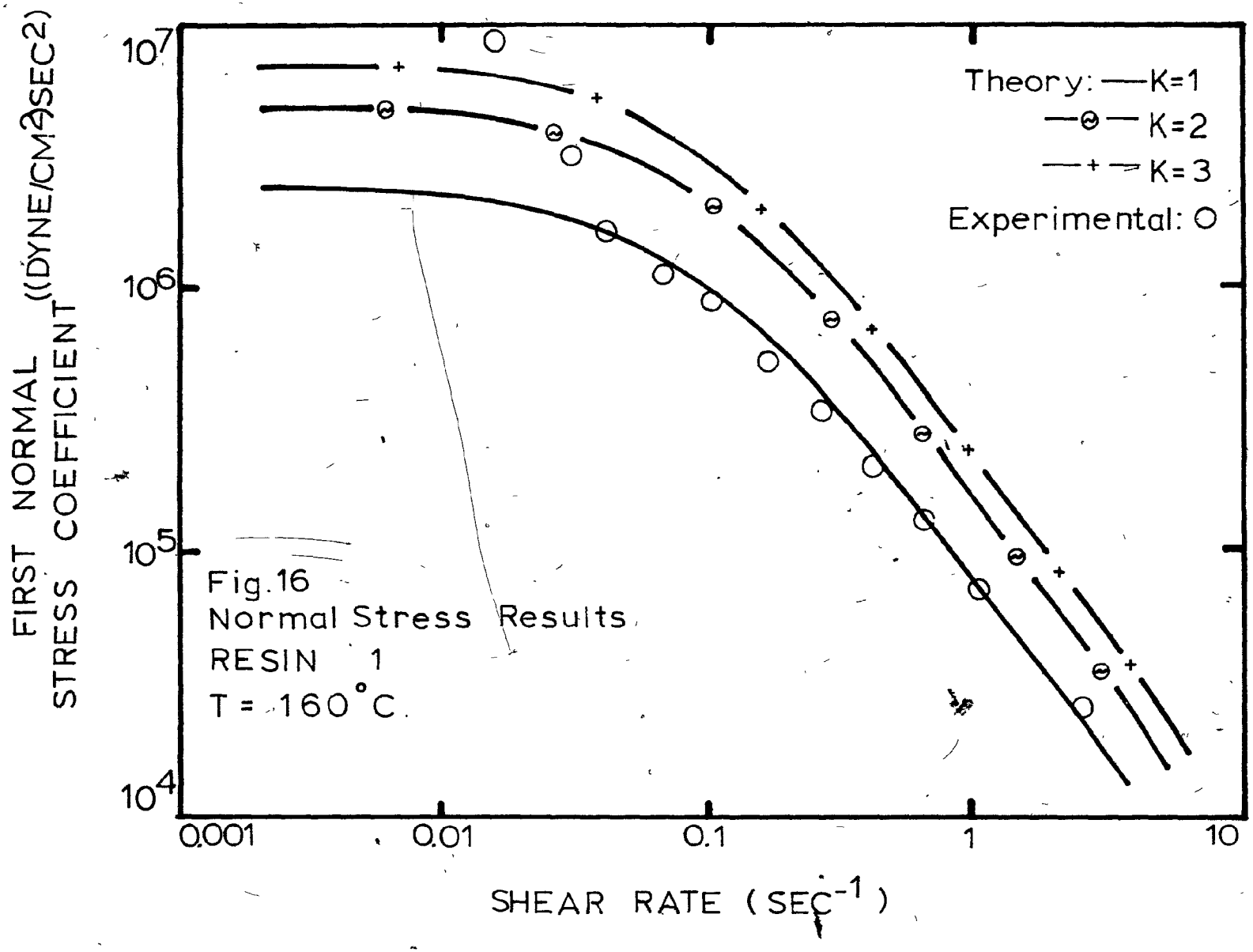

Fig.16
Normal Stress Results
RESIN 1
T = 160°C.

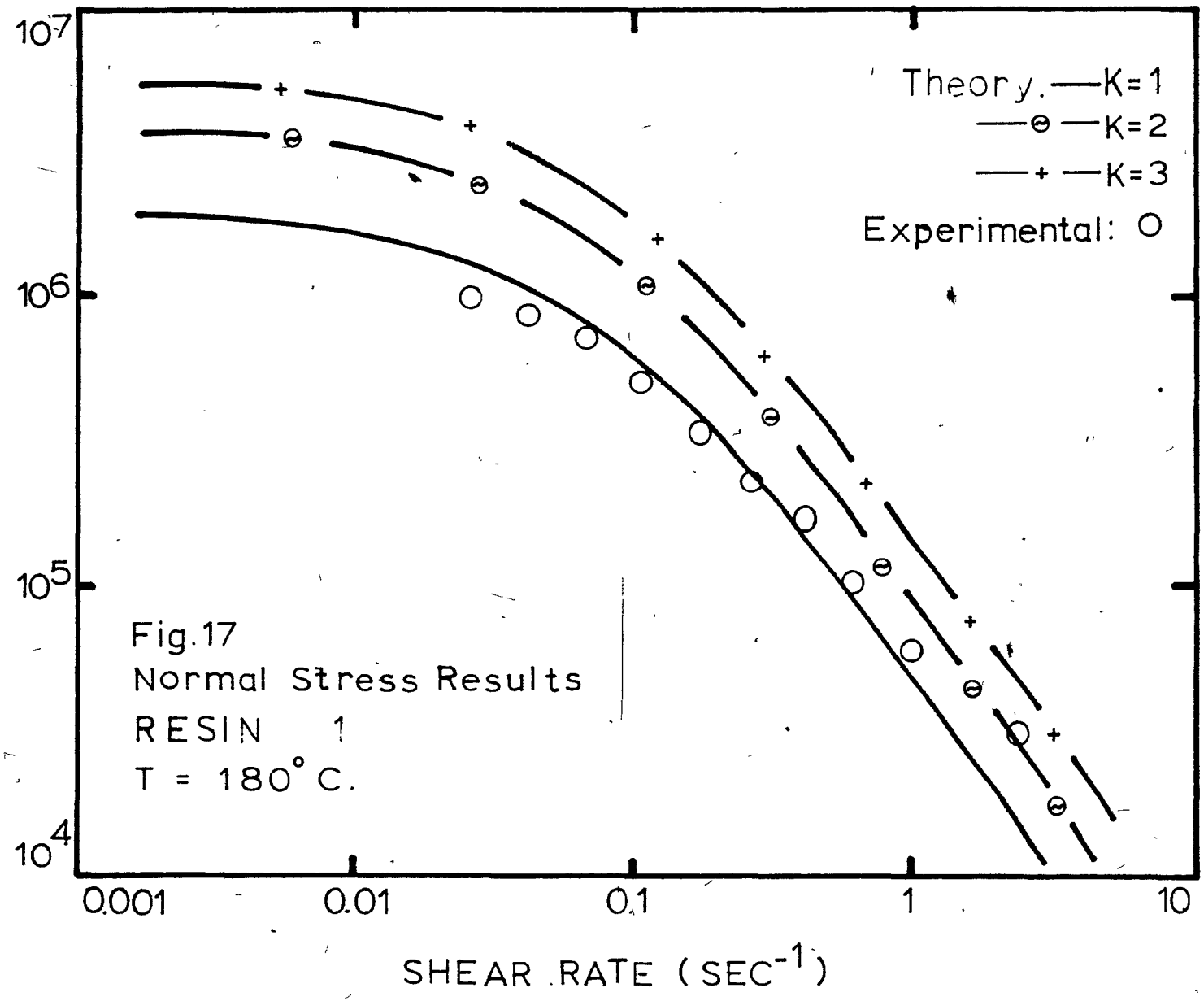

Fig.17
Normal Stress Results
RESIN 1
T = 180° C.

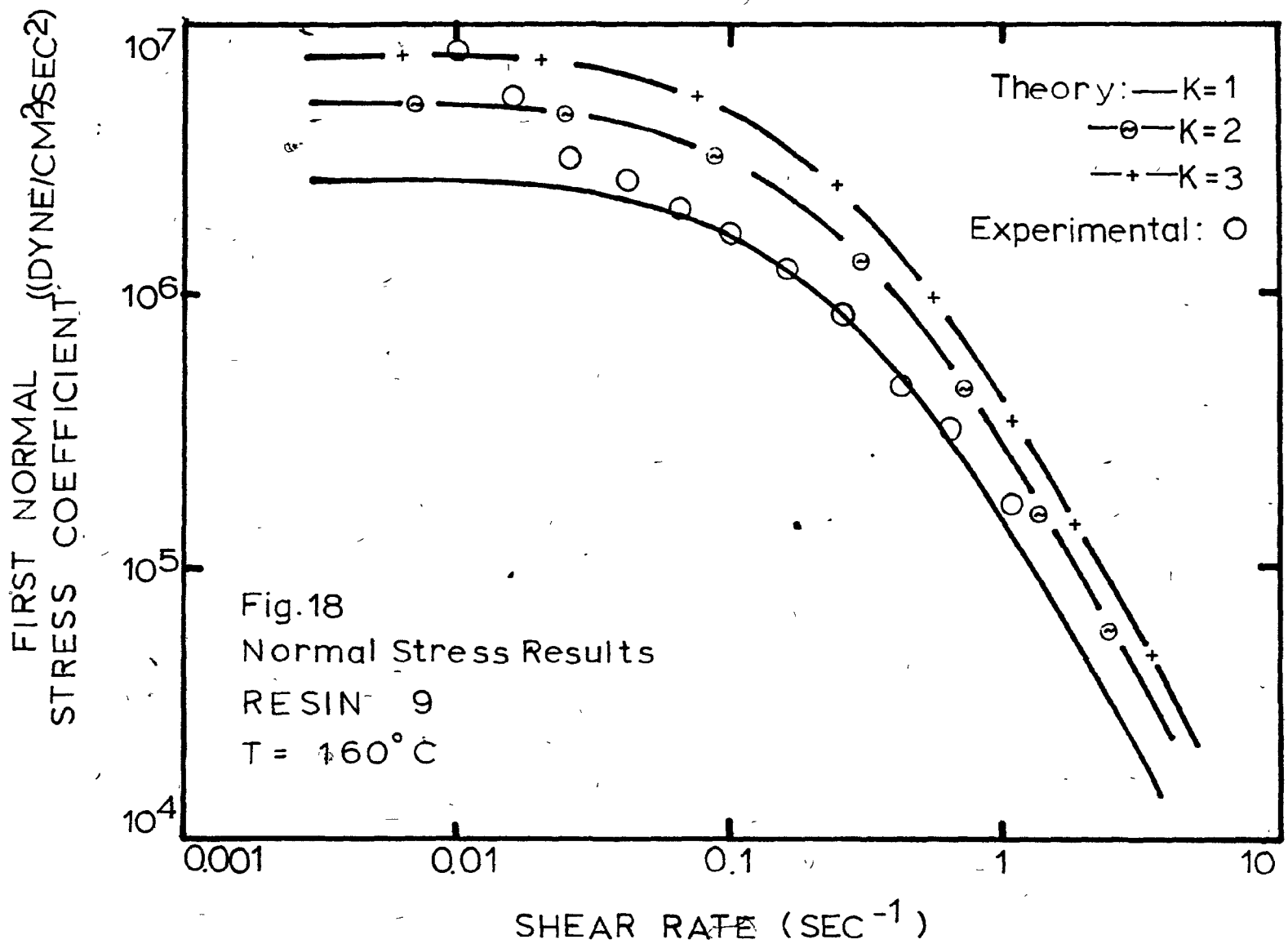

Fig.18
Normal Stress Results
RESIN 9
T = 160° C

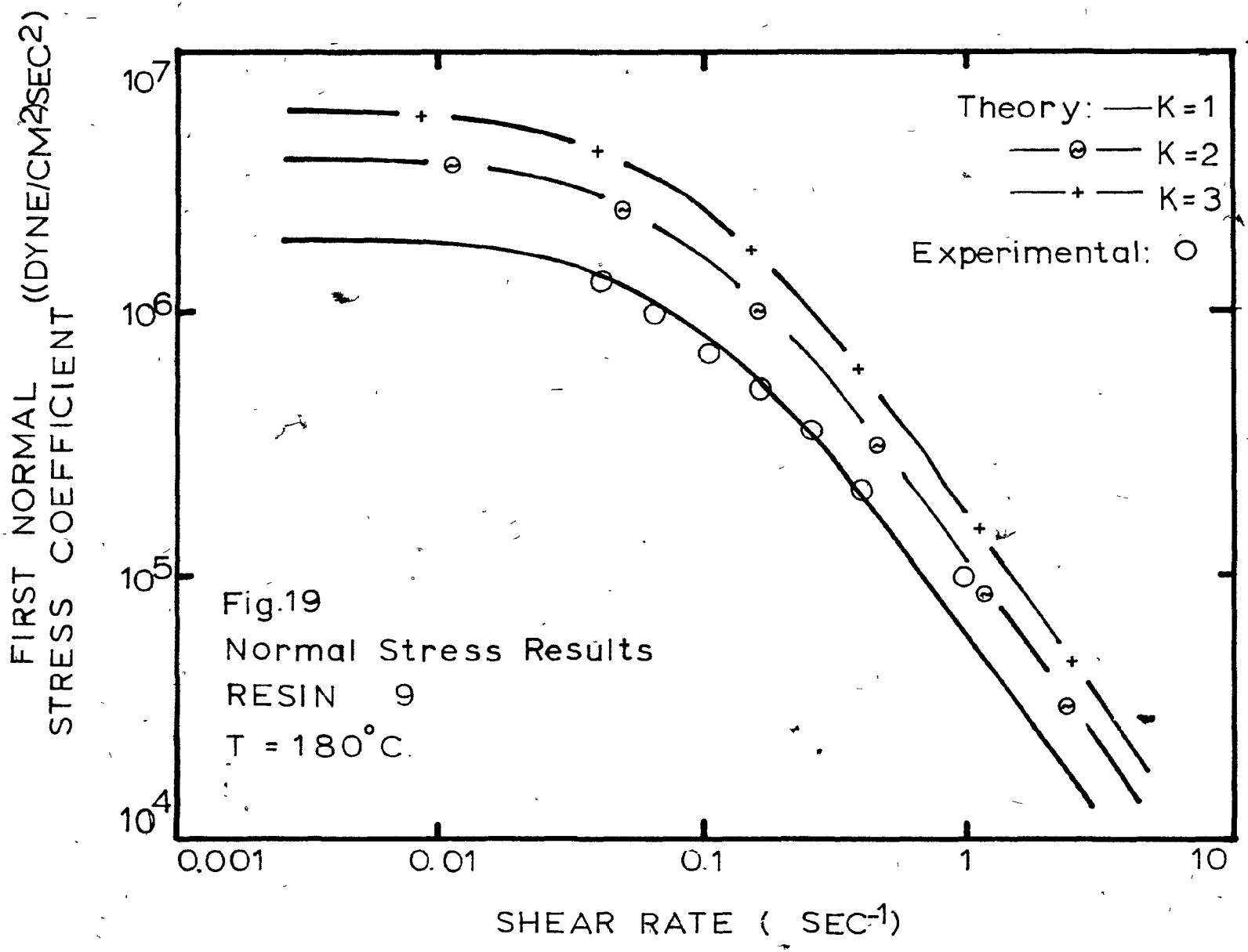

Fig.19
Normal Stress Results
RESIN 9
T = 180°C.

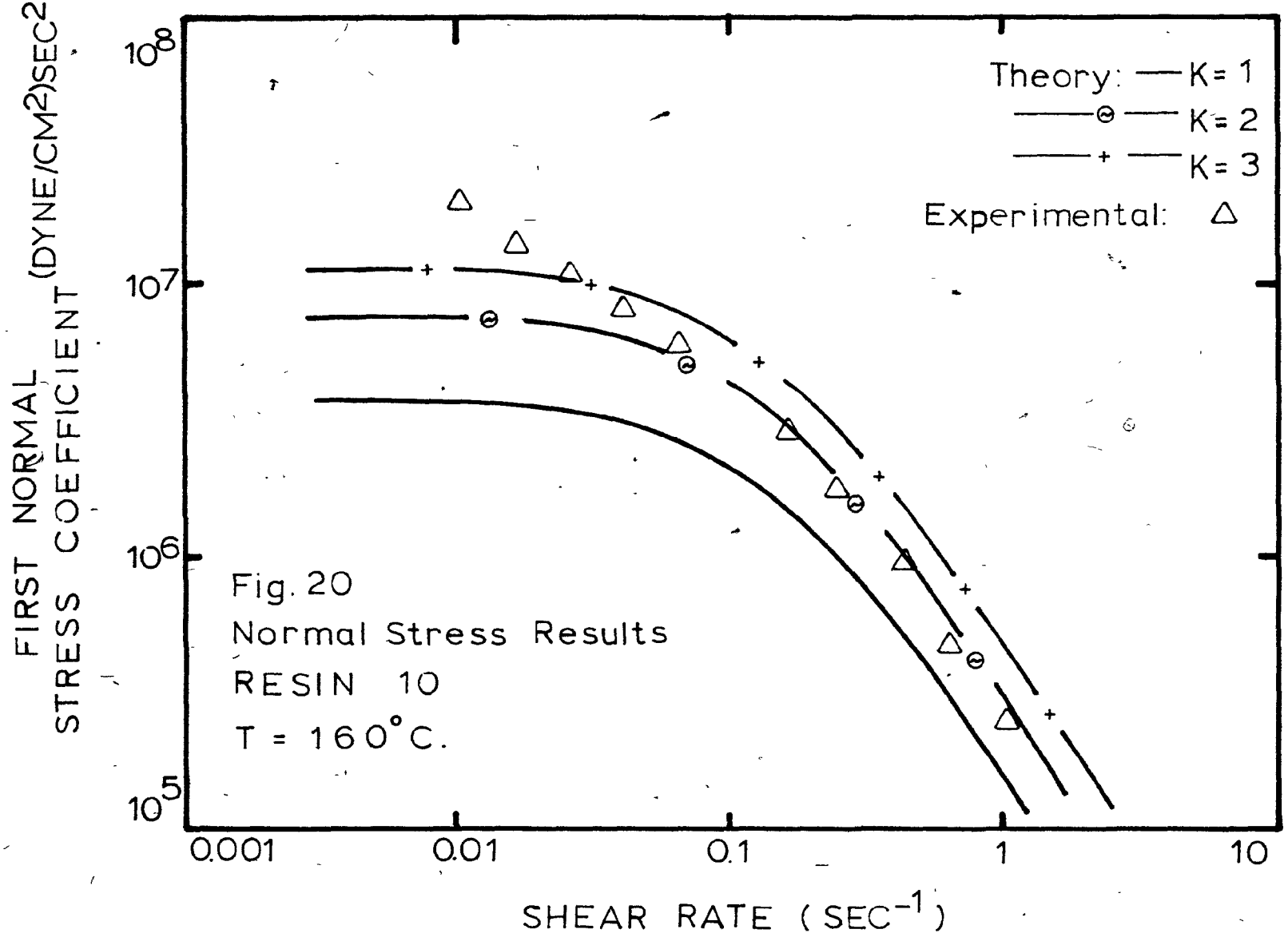

Fig. 20
Normal Stress Results
RESIN 10
T = 160°C.

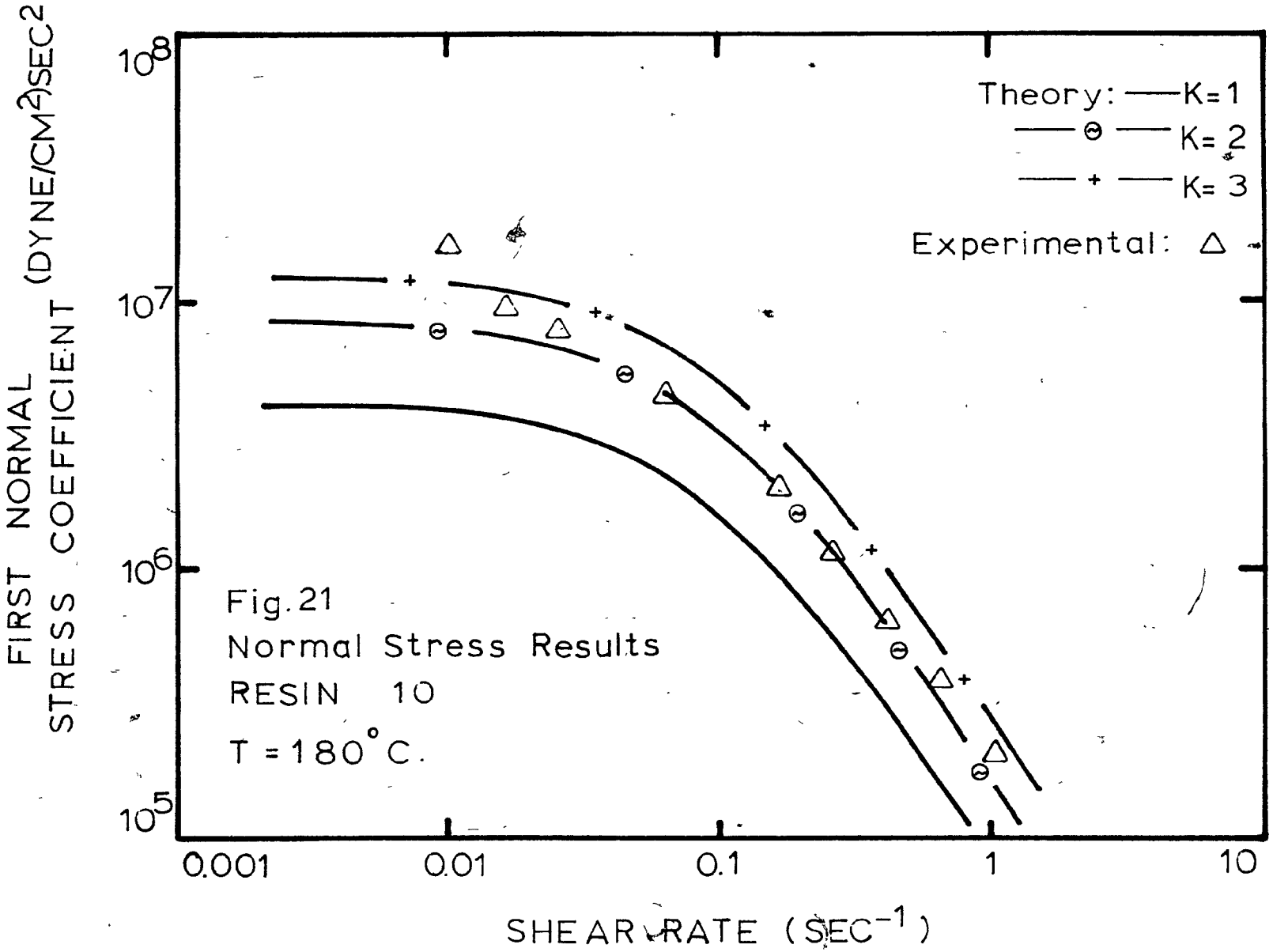

Fig. 21
Normal Stress Results
RESIN 10
T = 180°C.

3.4) Discussion.

The three resins studied although being LDPE of similar densities exhibited quite different viscosity and normal stress coefficient behaviors.

Resins 1 and 9 have similar values of zero shear viscosity. Resin 10 is more viscous than the other two.

Normal stress differences which are commonly accepted to be measures of elasticity in a material, were larger for Resin 10 than for Resins 1 and 9. Resin 9 had a larger first normal stress difference than Resin 1.

The normal stress data were analized according to the method outlined by Abdel-Khalik, Hassager and Bird[1]. This method is based on the Goddard-Miller constitutive equation described in Chapter 1, and it predicts the first normal stress coefficient from viscosity-shear rate data. The viscosity-shear rate data are used to compute the parameters in the Carreau viscosity equation[1]. The parameters λ and N for resins 1, 9 and 10 are given in Appendix II.

$$\frac{\eta - \eta_\infty}{\eta_o - \eta_\infty} = \{ 1 + (\lambda\dot{\gamma})^2 \}^{-N} \qquad (34)$$

With the parameters N and λ and using generalized charts for the first normal stress coefficient as a function of the dimensionless quantity $\lambda\dot{\gamma}$, the first normal stress coefficient can be predicted. The relation between the first normal stress coefficient and the viscosity is plotted in

generalized charts that show the quantity $\frac{\pi\theta}{4K\lambda(\eta_0-\eta_\infty)}$ vs. $\lambda\dot{\gamma}$ on a log-log graph. K is an empirical constant and on the basis of their experiments, Abdel-Khalik, Hassager and Bird[1] proposed that it takes the value of 2 for polymer solutions and 3 for polymer melts.

Figures 16 to 21 show the comparison between the values predicted by the method described above and the experimental results. The predicted curves were calculated for several values of the empirical factor K. K was varied from 1 to 3, 1 corresponding to the unmodified Goddard-Miller equation of state, 2 recommended for polymer solutions and 3 for polymer melts[1].

Resin 1 at both temperatures follows quite closely the curve predicted by the Goddard-Miller equation of state in the range of shear rates from 0.04 to 2.5 sec^{-1}. At shear rates lower than 0.04 sec^{-1} the first normal stress coefficient raises sharply. The predicted curves level off at low shear rates.

Resin 9 at both test temperatures follows closely the curve predicted by the Goddard-Miller equation also in the range of shear rates cited above. A departure is seen at the shear rate of 2.5 sec^{-1}. A leveling off at low shear rates is not observed.

Resin 10 at both temperatures followed the predicted curve with the empirical factor K equal to 2. The leveling off at low shear rates is not observed.

It can be said that the agreement of the experimental data with a predicted curve starts at a shear rate of 0.04 sec^{-1}. This behavior is observed also in the literature[1] for different polymeric systems.

Resins 1 and 9 are less elastic than resin 10 and have the tendency to follow more closely the curve predicted by the Goddard-Miller equation. Resin 10 is more elastic and presents the largest departure from the curve predicted by the Goddard-Miller equation. It may be possible that the need for an empirical factor K to fit the data for resin 10 (a highly branched resin) becomes more necessary when the elasticity of the material increases.

The steep rise of the first normal stress coefficient at low shear rates could be due to experimental error both from the apparatus and interpretation of the data. The first normal stress coefficient is a function of the reciprocal of the square of the shear rate. At low shear rate values this quantity becomes very sensitive to shear rate and if the measurement of total normal force is not accurate enough this can produce a higher normal force than expected.

From the analysis of the experimental data obtained in this work it can be concluded that further experimental work has to be done on different polymers to accept or reject the validity of the values of the empirical constant K proposed by Abdel-Khalik, Hassager and Bird[1].

CHAPTER 4. THE PHENOMENON OF DIE SWELL.

4.1) Introduction.

The phenomenon of expansion or increase in diameter of jets of viscoelastic liquids emerging from capillaries is well known; this phenomenon is called die swell. Reasons for increased interest in this behavior are numerous, ranging from the desire to determine the viscoelastic properties of polymeric systems, for example to predict first normal stress difference at high shear rates, to the need to obtain direct relations between die swell and such polymer processing characteristics as parison swell in blow molding and thickness and surface texture in extruded wire and cable.

Many interpretations of this phenomenon have been suggested. Also several techniques have been used to measure die swell. It is our purpose in this chapter to give a brief review of both theoretical treatments and experimental techniques related to the die swell effect.

4.2) Theoretical Treatment of the Die Swell Phenomenon.

Die swell (B), is defined as the ratio of the diameter of a polymer extrudate (D) to that of the capillary from which it is extruded (D_o). The causes of this phenomenon are not

clearly understood.

Two main approaches have been taken to explain it and correlate it with the normal stresses exhibited in viscometric flow. The first one, developed by Metzner[14], is based on fluid mechanics considerations. It is mainly concerned with the distortion of the velocity profile as the jet of material exits the capillary. This approach considers that the distortion of the velocity profile due to the change of boundary conditions can give rise to normal stresses that will cause the jet to expand. This assumption fits newtonian and non-newtonian purely viscous fluids, where an enlargement of the jet is observed, although these fluids do not exhibit normal stress effects in a viscometric flow. In the case of viscoelastic fluids, it is difficult to separate the effect of distortion of the velocity profile from the normal stress effect inherent in these materials.

More recent work is based on the assumption that die swell arises from an elastic recovery from the shear flow in the capillary. This elastic recovery is related to the normal stresses developed by the material during the flow in the capillary. Several mechanisms have been proposed for the type of elastic recovery that the material exhibits and how the elastic energy is stored during flow in the tube. A detailed discussion of this topic can be found in the papers of Mendelson[15] and Vlachopoulos[16].

At this point we will discuss a model proposed

by Tanner[2] since we use this model in the next chapter to analize the die swell results and correlate them to the first normal stress coefficient. Tanner postulates that the die swell effect is due to elastic recovery of the material and that this expansion occurs in two steps: The first is very rapid, relatively large and close to the die exit; the secondary expansion occurs slowly and is much smaller. The expression obtained is derived from a rational mechanics point of view and the main assumptions made are:

a) The flow is isothermal and incompressible.

b) $L/D \rightarrow \infty$

c) Inertial effects are neglected.

d) Gravity and surface tension are ignored so that the final extruded rod is load free.

e) The small slow recovery far from the die is ignored.

f) The constitutive equation for a KBKZ fluid is used.

The final expression is

$$S_w^2 = 2 \{ (B-0.1)^6 - 1 \} \qquad (35)$$

where S_w is the recoverable shear strain at the wall defined as

$$S_w = \frac{\sigma_{11}-\sigma_{22}}{2\tau_{12}} \qquad (36)$$

Equation (35) can be modified to yield:

$$B = 0.1 + \left\{ \frac{\theta^2 \dot{\gamma}^2}{8 \eta^2} + 1 \right\}^{1/6} \qquad (37)$$

4.3) Experimental Methods for Measuring Die Swell.

A survey of the existing techniques for determining the die swell for polymer melts indicates that there are many discrepancies in the experimental data reported. This is because different methods were used to collect the extrudate flowing from the capillary viscometer. The principal methods are described below.

a) Method used for polymeric solutions[17].

This method involves photographing the polymer stream as it exits from a horizontal capillary. This method is not good for polymer melts since gravity affects the extrudate dimensions and to be sure that the polymer has relaxed to the equilibrium die swell the photographs should not be taken at the very exit of the capillary.

b) Method for polymer melts.

In this method the vertical extrusion of a short length of polymer is frozen when contacting the air and then measured with a micrometer[18]. There are two important problems with this method. First, the uncontrolled cooling of the extrudate can cause stresses to be frozen in and thus prevent the extrudate from reaching its equilibrium swell dimensions.

This effect can be more severe in the case of crystallizing polymers. Second, gravity will promote the sagging of the polymer extrudate. This problem can be avoided by taking the measurements near the end of the extrudate where gravity effects can be neglected. This method also utilizes a density correction to express the die swell at the extrusion temperature from the experimental measurements at ambient temperature.

A variation of this method is also used in which the extrudates are collected at room temperature and then annealed in an oven or within a silicon oil bath for a period of time to allow all the stresses to relax and let the die swell attain the equilibrium value[19].

c) Improved method for polymer melts.

The polymer is extruded into a silicon oil bath whose temperature is close to the extrusion temperature. The silicon oil must have the same density as the polymer melt at that temperature to prevent the polymer from floating or sagging in the oil. Experimentally it is convenient to have the oil density a little lower than that of the polymer to avoid problems of a large resistance to the flow of the polymer through the oil[20]. After the polymer has relaxed in the oil bath, photographs are taken and from them the die swell is obtained.

This last method is the one used in the present work.

CHAPTER 5. DIE SWELL - EXPERIMENTAL STUDIES.

5.1) Experimental Apparatus[20].

The apparatus used for measuring the die swell of three LDPE resins was the Instron Capillary Rheometer (ICR) with a thermostatting chamber to collect the polymer extrudates. The experimental set-up is shown schematically in Figure 22.

The thermostatting bath was connected to the thermostatting chamber in such a way that the heating medium could circulate continuosly. The outlet pipe from the thermostatting chamber has a larger diameter than the inlet pipe. This set-up prevents overflow in the thermostatting chamber and the liquid level can be controlled with a valve.

The thermostatting chamber was made of a piece of stainless steel pipe, ID = 6in, length = 10in, to which the bottom plate inlet and outlet connectors and the central shaft were welded. One side of the pipe has been cut off and in this space a flange was welded on which a double window was mounted. The double window is a sandwich of a Viton ring, Vycor glass, asbestos plate, Pyrex glass and asbestos plate. The cover, rotating on the central shaft has 6 holes, ID = ½in. In these holes, six glass tubes are suspended. Each of the holes is provided with dual action

Fig. 22
Die Swell Experimental Set-up

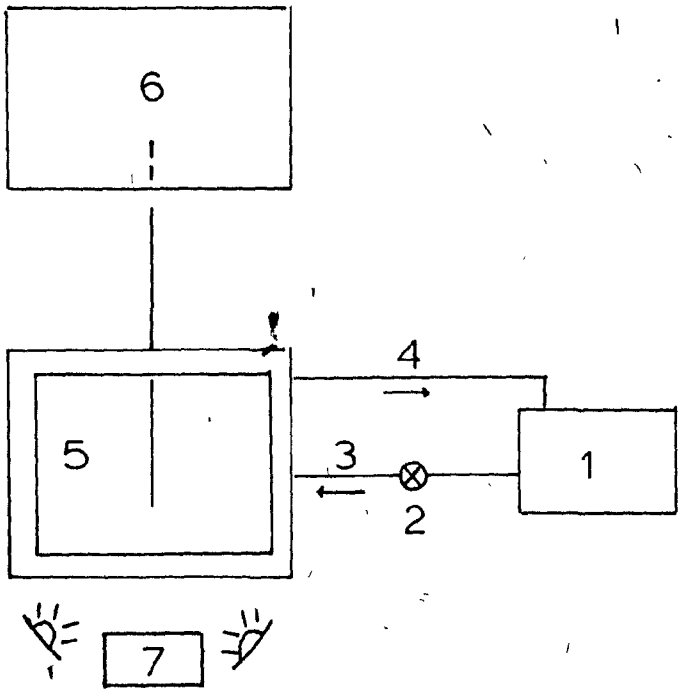

1: Circulating bath
2: Valve
3: Inlet pipe
4: Outlet pipe
5: Thermostting Chamber
6: Capillary Rheometer
7: Camera

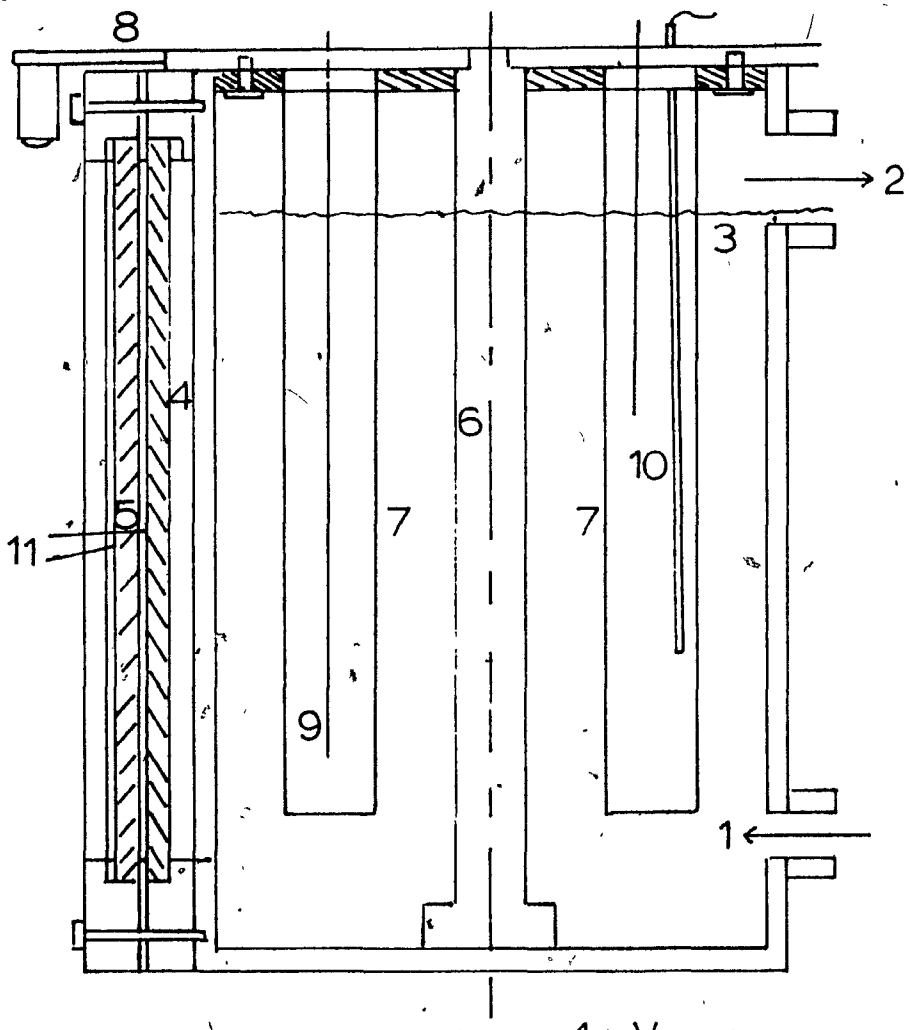

Fig. 23
Cross sectional view
Thermostatting Chamber

1: Liquid inlet
2: Liquid outlet
3: Liquid level
4: Vycor
5: Pyrex plates
6: Central shaft
7: Pyrex tubes
8: Shears
9: Extrudate
10: Thermocouple
11: Asbestos

shears which cut the extrudate and hold it in a fixed position. Details of the thermostatting chamber and the cover plate are shown in Figure 23.

The heating medium is silicone oil (Dow Corning, Fluid 200, 100cs.). This oil fills the chamber but is outside the glass tubes. Inside the tubes where the extrudates are collected the oil used depends on the melt density of the particular polymer that is going to be tested.

5.2) Experimental Technique.

The oil in the thermostatting bath is preheated to the desired temperature. This takes about one hour. After that, the valve is opened to let the oil flow from the thermostatting bath to the thermostatting chamber. The liquid level is also controlled by this valve. Once the appropiate level is reached, the oil circulates in the chamber continuosly. The desired temperature in the chamber (inside the glass tubes) is reached after about two hours. The oil in the chamber and inside the glass tubes must be stirred to obtain a homogeneous temperature throughout. In the meantime the ICR is heated to the desired extrusion temperature and the load cell calibrated. The temperature in the chamber is monitored by means of a thermocouple placed in one of the glass tubes. The ICR is filled with the polymer and the equipment

is ready to start with the experiments. Since the thermostatting chamber has six tubes but one contains the thermocouple and one contains a standard it is possible to make experimental runs of four extrusion speeds without opening the chamber.

A certain crosshead speed is chosen and the polymer extruded until a steady force is recorded. At this point the thermostatting chamber is aligned with the ICR in such a way that the polymer extrudate flows into one of the glass tubes. When a specified amount of polymer is in the glass tube the crosshead of the ICR is stopped and the sample cut using the shears. The same procedure is repeated for another three cross head speeds. The samples in the tubes are allowed to relax for about 5-10 min and after that a photograph of each sample is taken. Then the ICR is charged again, the glass tubes emptied and the equipment is ready for another experimental run.

The photographs were taken with a Nikon camera. The camera is mounted on a tripod and two 500W tungsten bulbs were used for lighting the samples. All the photographs were taken from the same distance and height and with the same lens aperture and exposure time to prevent variations in the photo graphs. At the beginning and at the end of each roll of film the standard was photographed. The standard is a metal strip with a thin slit in the middle section. The width of the slit is known.

The developed film was analized using a Nikon Shadow graph Model 2. This equipment allows the measurement of the

polymer extrudates in a relative scale. The real dimensions of the standard are known and also the reading of the standard from the Shadowgraph. In this way we can make a scale that relates the reading from the Shadowgraph with the real dimensions of the polymer extrudate.

5.3) Experimental Results.

The capillary used has an L/D = 40; it has a diameter of 0.052in and is 2.0in in length. This L/D ratio was chosen based on the fact that for LDPE die swell is not only a function of shear rate and temperature, but also of L/D at low L/D ratios. This dependence of L/D on die swell disappears for L/D ratios above 30.[33] The temperature of the oil in the glass tubes in the thermostatting chamber was 140°C. The temperature was limited by the boiling point of the oil.

The shear rate and the shear stress at the wall were calculated by means of the following equations valid for simple shear flow in a capillary viscometer.

$$\dot{\gamma}_{ap} = \frac{4Q}{\pi R^3} \qquad (38)$$

$$\tau_w = \frac{\Delta P R}{2L} \qquad (39)$$

The true shear rate is calculated from the Rabinowitsch equation

$$\dot{\gamma} = \frac{3}{4}\dot{\gamma}_{ap} + \frac{1}{4}\dot{\gamma}_{ap}\left(\frac{d\log \dot{\gamma}_{ap}}{d\log \tau_w}\right) \qquad (40)$$

The proper value of the diameter of the extruded polymer is calculated as follows:

$$D(\text{extrudate, real}) = \left(\frac{\text{sample reading from SG}}{\text{std. reading from SG}}\right) \times \text{(physical dimensions of the std.)} \qquad (41)$$

The die swell is obtained using the definition

$$B_o = \frac{D}{D_o} \qquad (42)$$

The die swell values obtained by using equation (42) are values measured at the thermostatting temperature. So, in order to obtain the values of die swell corresponding to a certain extrusion temperature, a density correction has to be made. The die swell at the extrusion temperature is given by

$$B = B_o\left(\frac{\rho_o}{\rho}\right)^{1/3} \qquad (43)$$

where ρ_o is the density of the polymer melt at the thermostatting temperature and ρ is the density of the polymer melt at the extrusion temperature.

Figures 24 to 26 show the curves of the die swell as a function of shear rate for resins 1, 9 and 10 at temperatures of 160, 180 and 200^{0}C.

5.4) Discussion.

The three LDPE resins studied followed the expected relation between die swell and shear rate and die swell and temperature. Die swell increased with shear rate and decreased (for the same resin) with temperature.

The range of crosshead speeds used was from 0.05cm/min to 10cm/min. The shear rate range for the particular capillary used was from 3 to 1300sec^{-1}. At high crosshead speeds (5cm/min and higher) melt fracture was observed. At 5cm/min melt fracture is incipient and at 10cm/min the surface of the polymer melt was very irregular, making the measurement of the die swell meaningless. This phenomenon was more pronounced with resin 10. Also, from the experimental point of view it was difficult to collect the extrudate in the oil bath without having problems of the polymer sticking at the tube walls or hitting the bottom of the tube. At low crosshead speeds it takes a long time for the polymer extrudate to flow into the oil bath. Since there is a small gap between the exit of the capillary and the entrance of the glass tube in the thermostatting chamber the polymer

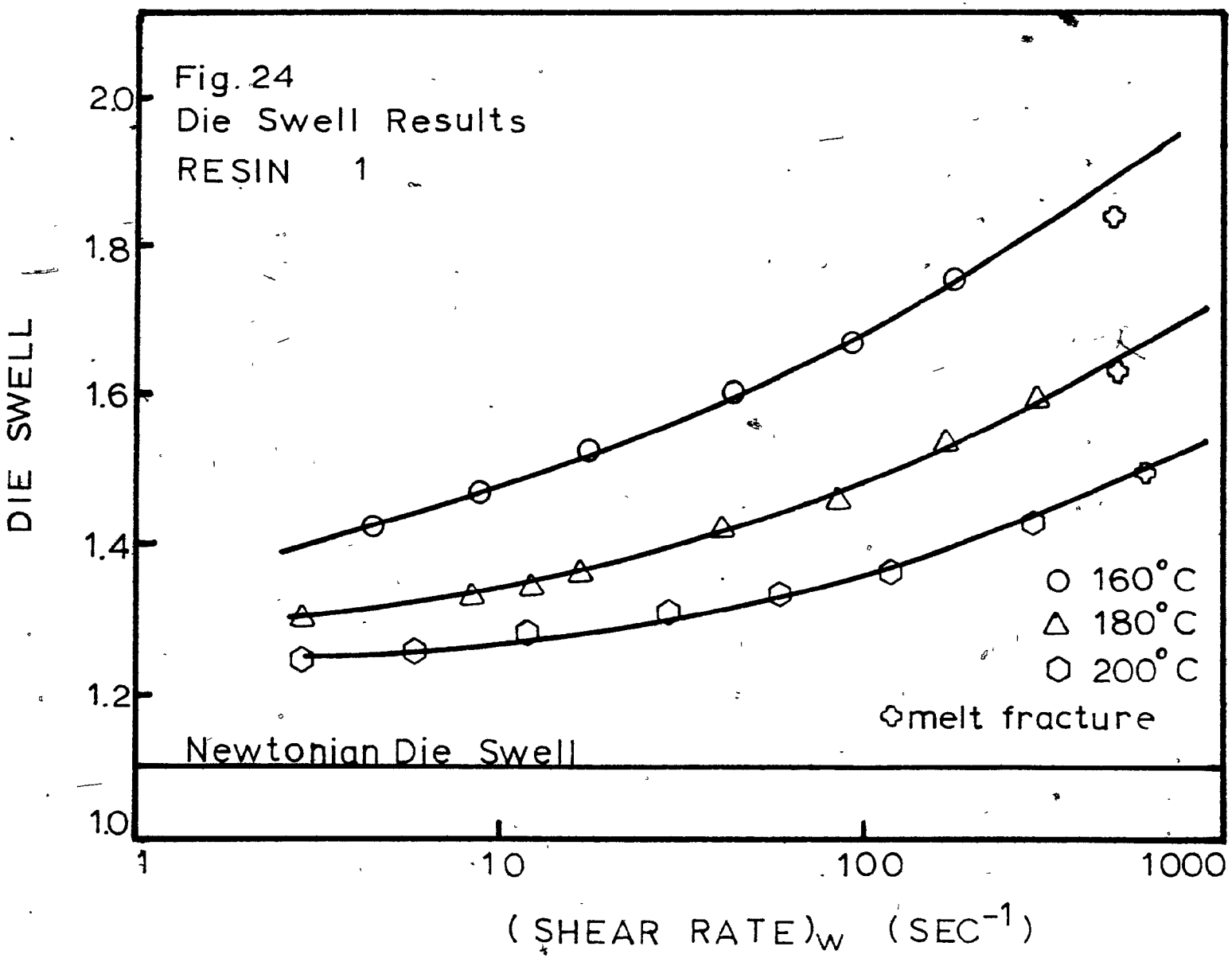
Fig. 24
Die Swell Results
RESIN 1
DIE SWELL
2.0
1.8
1.6
1.4
1.2
1.0
1
10
100
1000
(SHEAR RATE)$_w$ (SEC^{-1})
○ 160°C
△ 180°C
⬡ 200°C
✿ melt fracture
Newtonian Die Swell

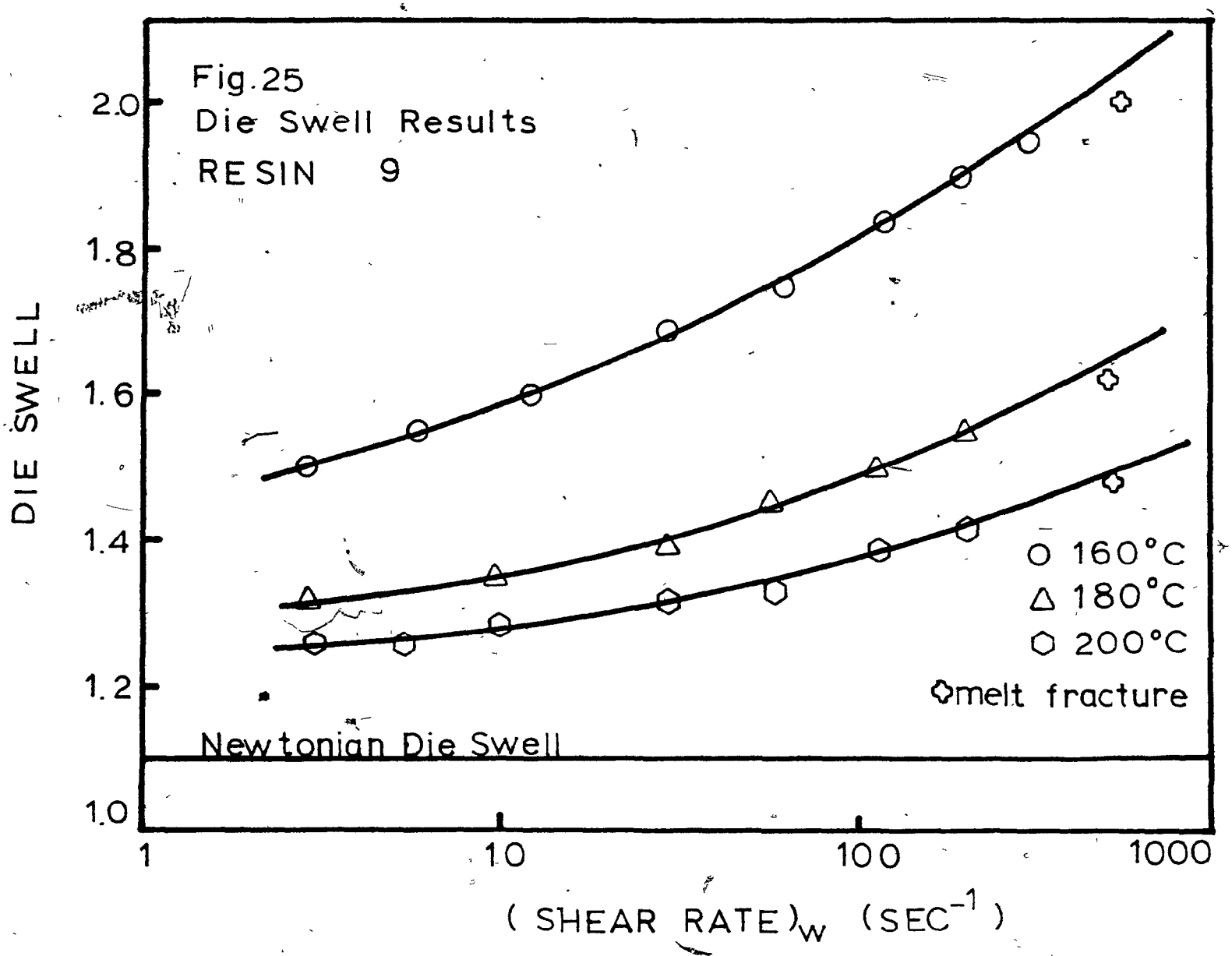
Fig.25
Die Swell Results
RESIN 9
DIE SWELL
2.0
1.8
1.6
1.4
1.2
1.0
1
10
100
1000
(SHEAR RATE)$_w$ (SEC^{-1})
O 160°C
Δ 180°C
O 200°C
melt fracture
Newtonian Die Swell

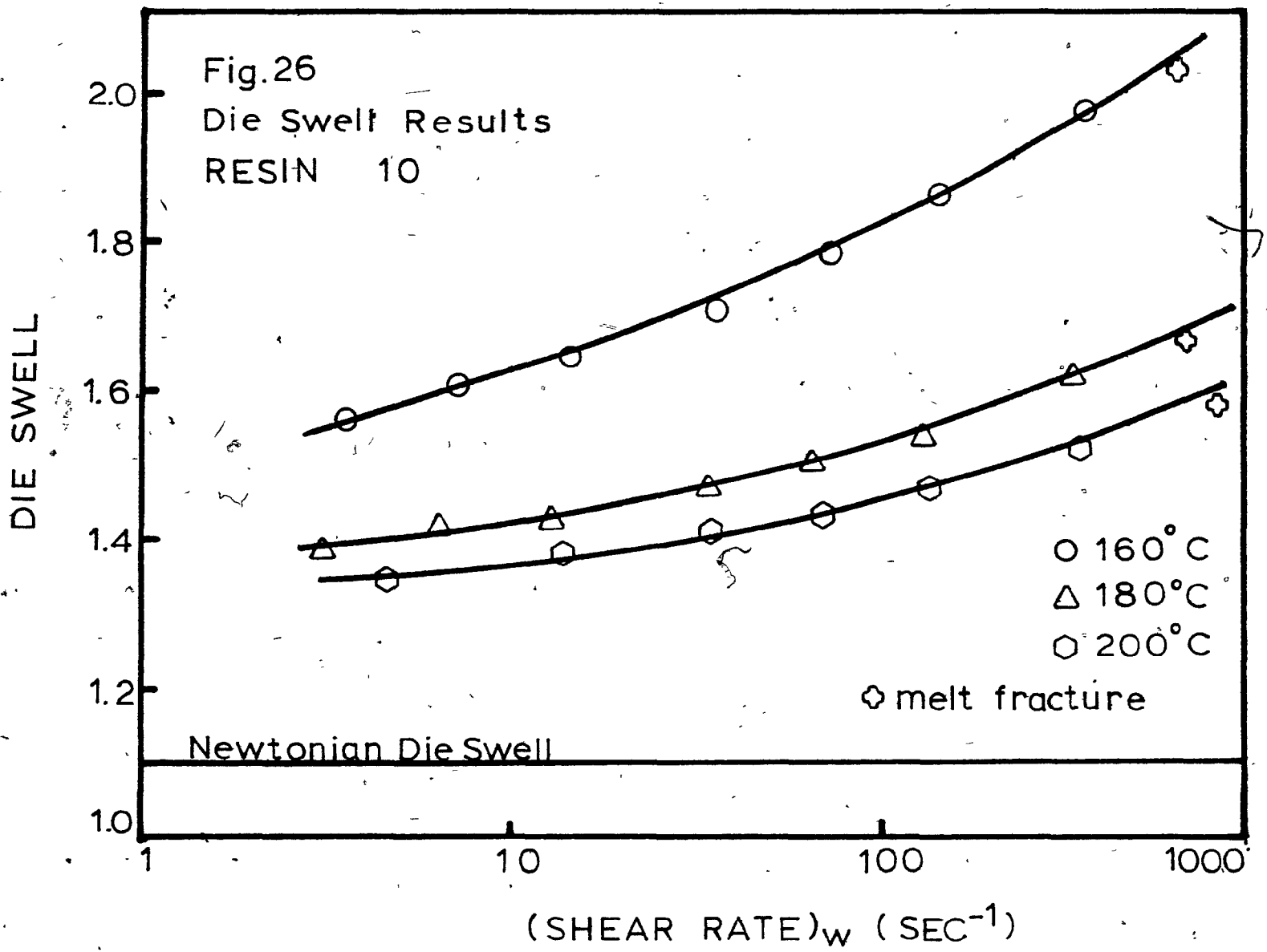
Fig.26
Die Swell Results
RESIN 10
DIE SWELL
2.0
1.8
1.6
1.4
1.2
1.0
Newtonian Die Swell
○ 160°C
△ 180°C
⬡ 200°C
✿ melt fracture
1
10
100
1000
(SHEAR RATE)w (SEC-1)

tends to crystallize when in contact with air before going into the chamber. Also at high temperatures this slow flow can cause the degradation of the polymer inside the ICR barrel.

Die swell data were used to test an equation proposed by Tanner[1,2]. This equation is

$$B = 0.1 + \{ 1 + (\frac{\theta^2 \dot{\gamma}^2}{8\eta^2}) \}^{1/6} \qquad (37)$$

Die swell data coupled with viscosity data were used in equation (37) to calculate the first normal stress coefficient. The results are presented in Figures 27 to 32 for resins 1, 9 and 10 at 160 and 180°C.

These figures show both the first normal stress coefficient calculated from the experimental normal stress data and the first normal stress coefficient calculated from the experimental die swell data using equation (37).

For all three resins the first normal stress coefficient calculated from die swell data was consistently higher than the values obtained from the cone and plate flow. Unfortunately just one or two points could be measured experimentally at the same shear rate in both experiments. This is due to the limitations of both the Rheometrics Mechanical Spectrometer and the Instron Capillary Rheometer. The Mechanical Spectrometer is good for low shear rates and the Instron Rheometer for high shear rates. The

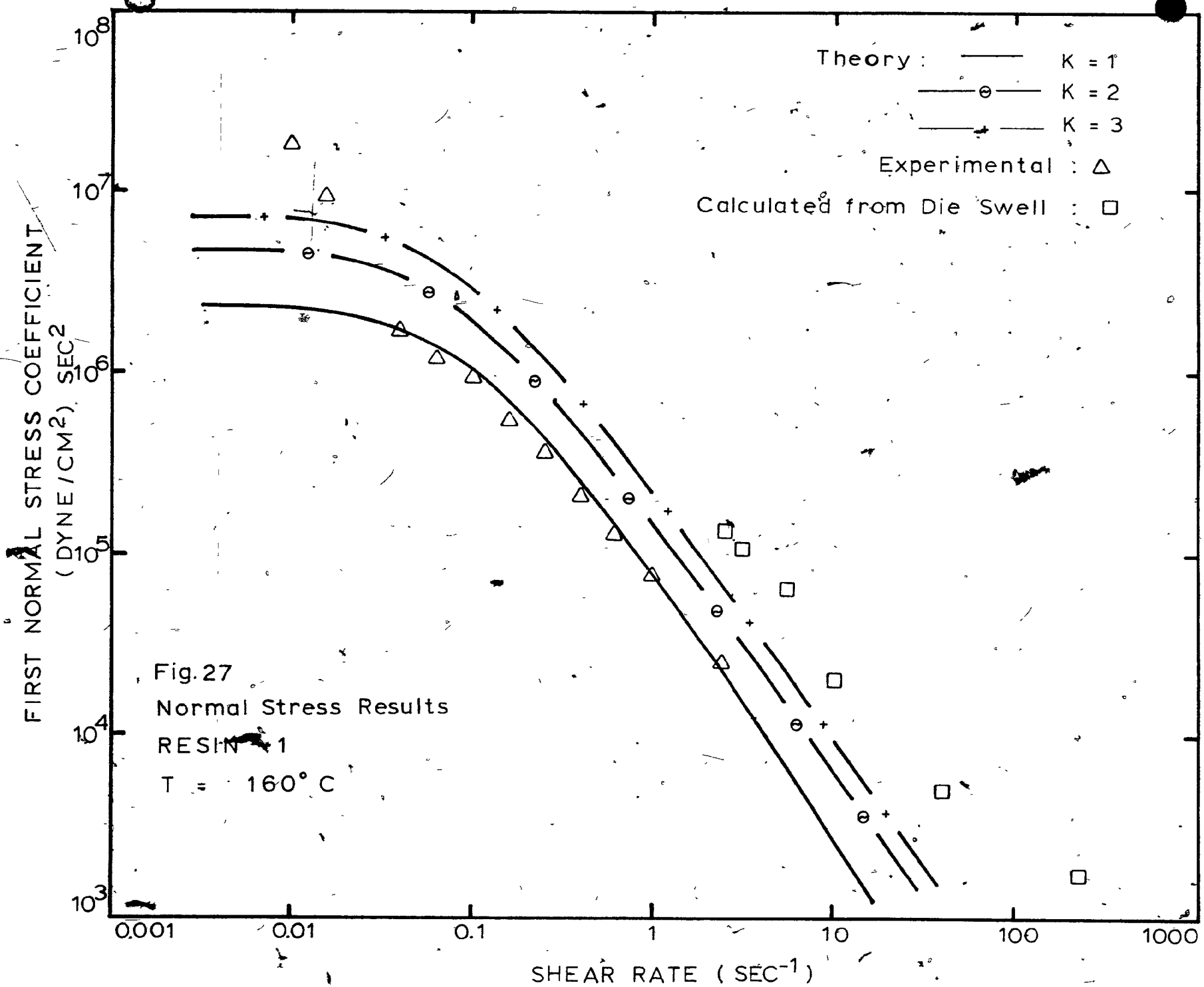

Fig. 27
Normal Stress Results
RESIN 1
T = 160° C

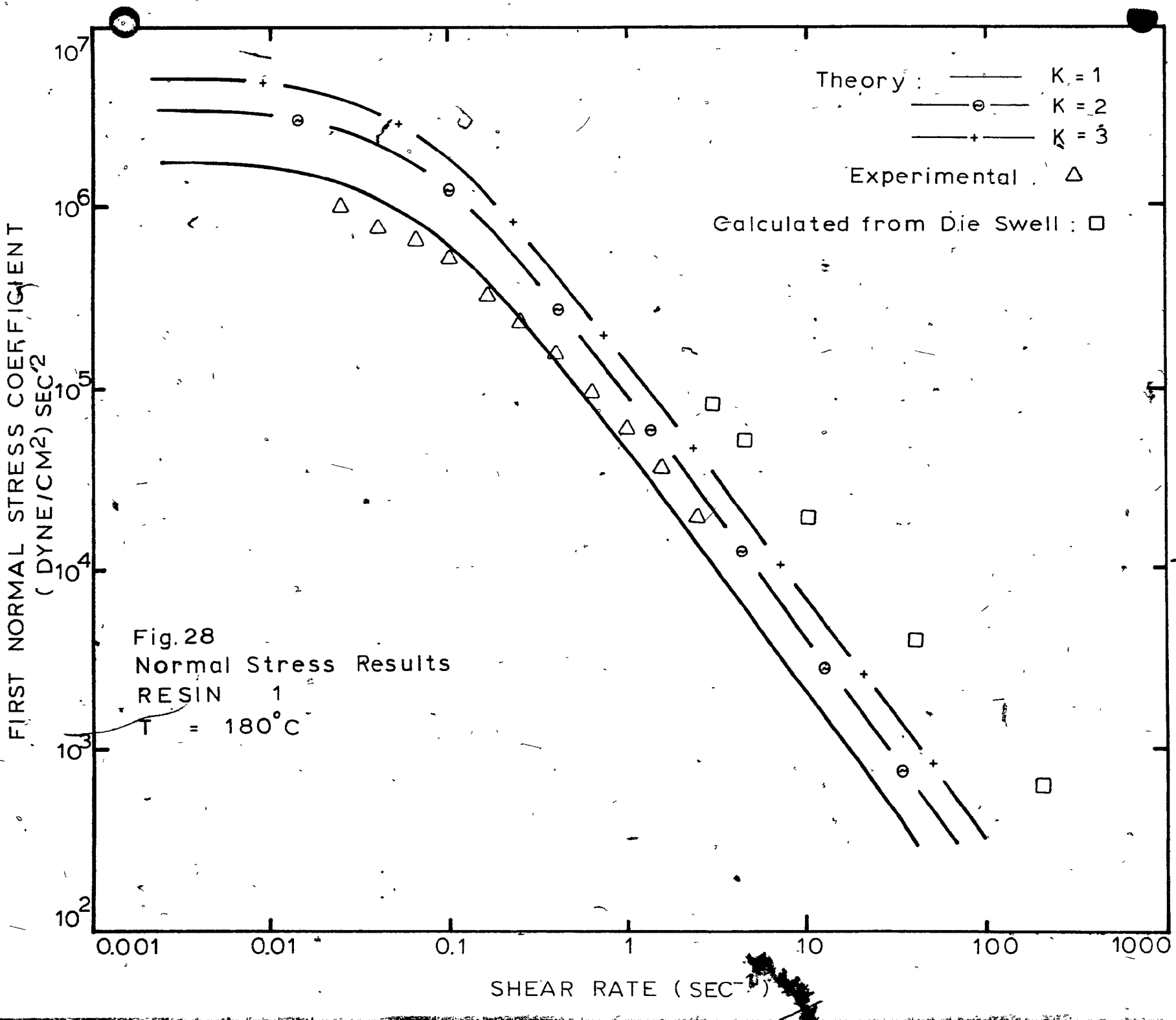

Fig. 28
Normal Stress Results
RESIN 1
T = 180°C

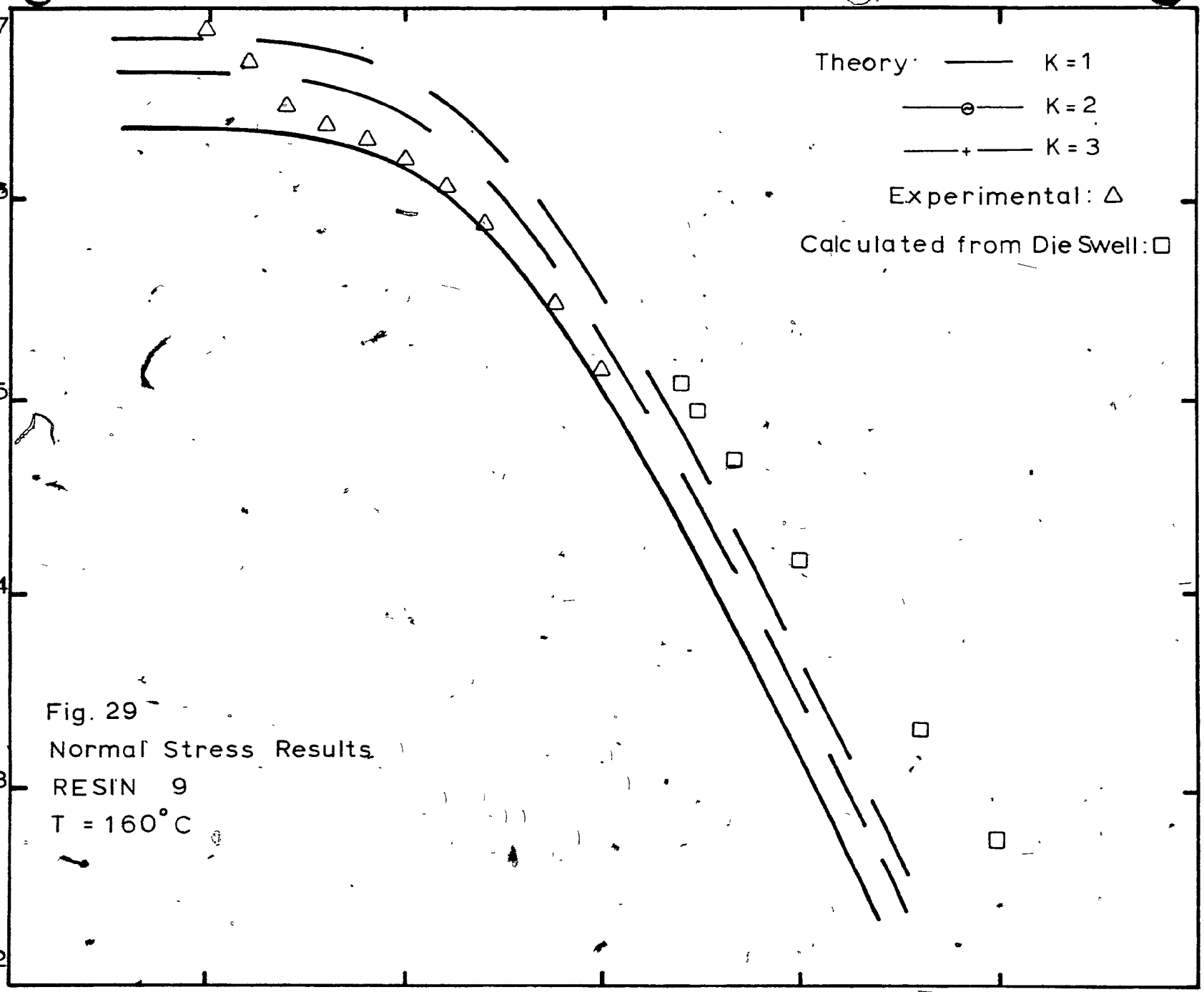

Fig. 29
Normal Stress Results
RESIN 9
T = 160°C

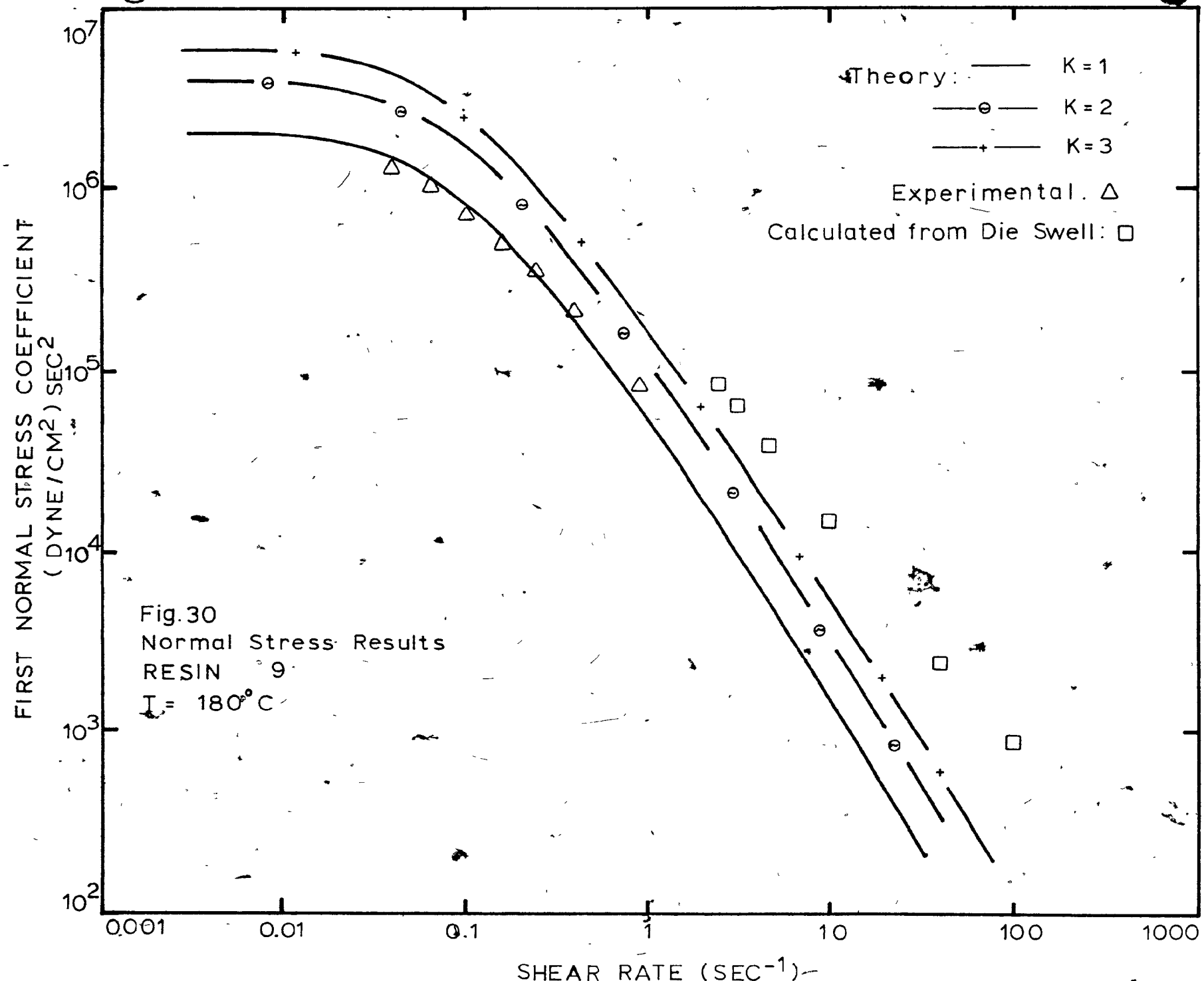

Fig. 30
Normal Stress Results
RESIN 9
T = 180°C

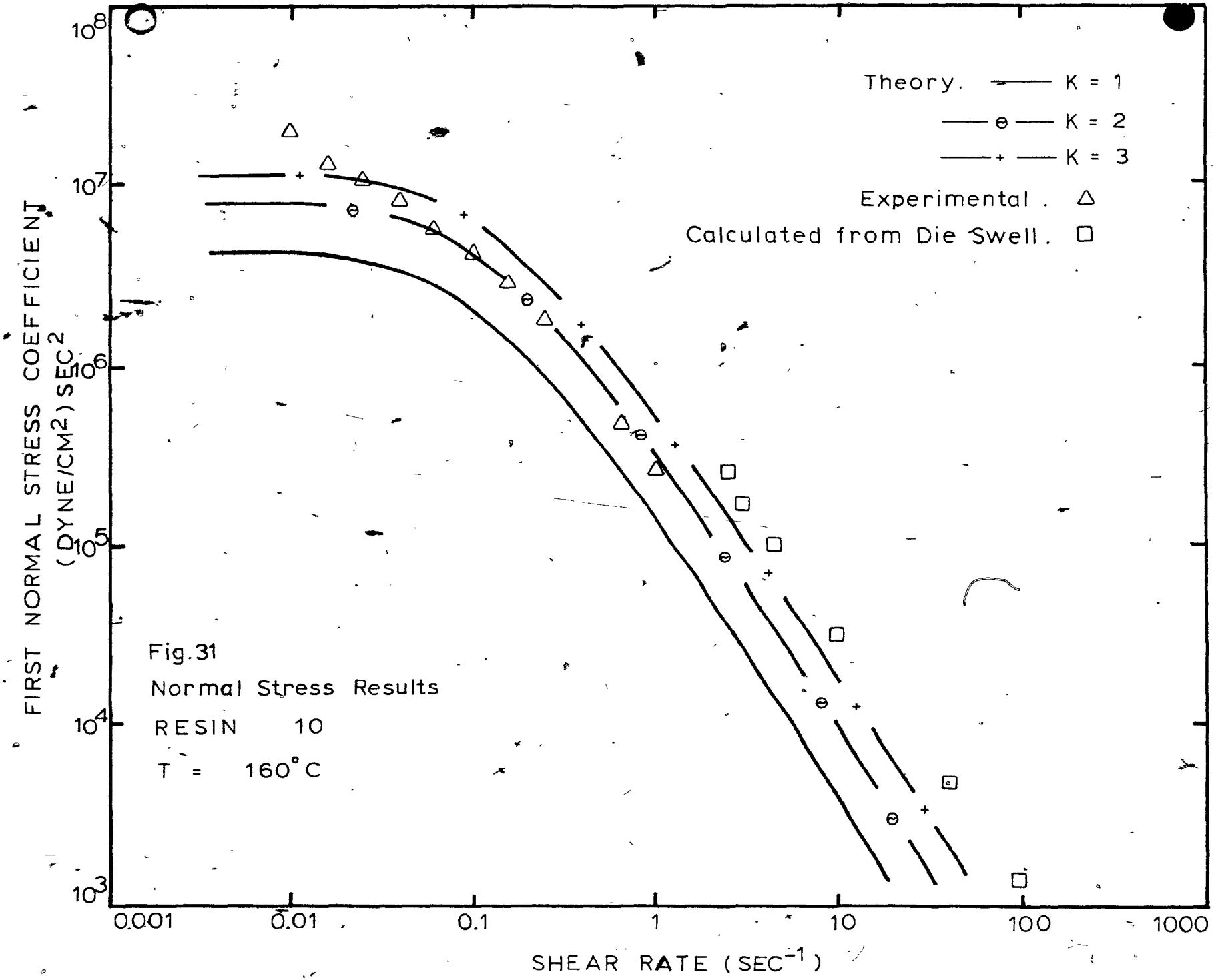

Fig.31
Normal Stress Results
RESIN 10
T = 160°C

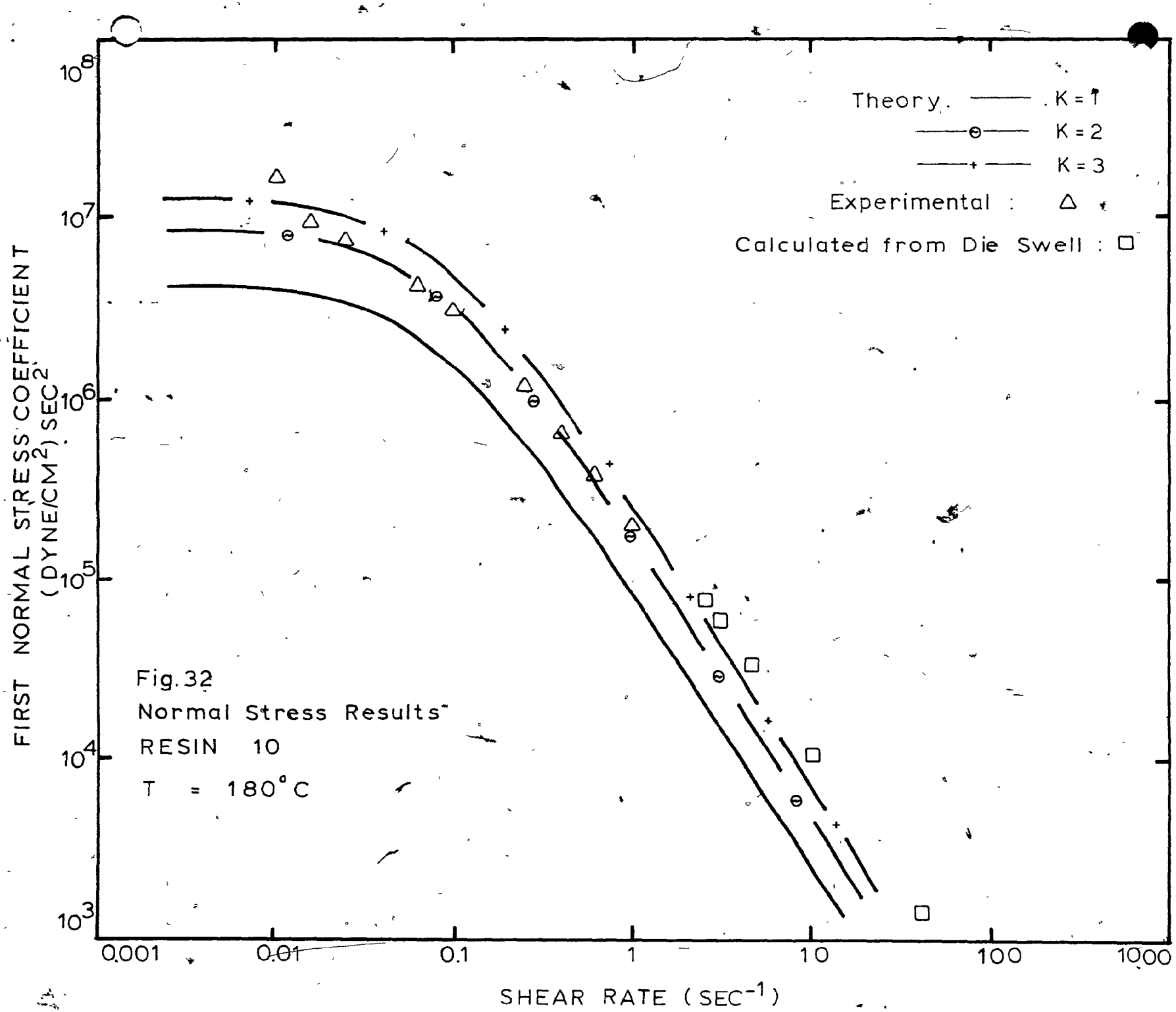

Fig. 32
Normal Stress Results
RESIN 10
T = 180°C

shear rates in which we could get data from both experiments represent in one case the upper limit (RMS) and on the other hand the lower limit (ICR) of the apparatus.

CHAPTER 6. METHODS FOR MEASURING EXTENSIONAL VISCOSITY.

6.1) Introduction.

Extensional flow in its three modes, planar, uniaxial and biaxial, received little attention until fairly recently although it was mentioned as early as 1906 by Trouton. Controlled, steady elongation is more difficult to achieve in the laboratory than the more traditional viscometric flows. In extensional flow, the only measurable material function, the extensional viscosity, is difficult to measure and the results of several investigators have been contradictory.

Extensional flows play an important part in several polymer processing operations. In particular it is important in the spinning of fibers (melt and dry), film casting, blow molding and film blowing.

An extensional flow is one in which the velocity field is given by

$$u_i = a_i x_i \tag{44}$$

in a cartesian coordinate system. In steady extension the a_i coefficients are constants. For an incompressible fluid

$$\frac{\partial u_1}{\partial x_1} + \frac{\partial u_2}{\partial x_2} + \frac{\partial u_3}{\partial x_3} = 0 \tag{45}$$

and thus

$$a_1 + a_2 + a_3 = 0$$

In uniaxial extension the constants in equation (44) are

$$a_1 = \dot{\varepsilon} \qquad (46)$$
$$a_2 = a_3 = -\tfrac{1}{2}\dot{\varepsilon}$$

where $\dot{\varepsilon}$ is the rate of extension or strain rate. The elongational strain as a function of time for steady uniaxial extension can be found considering a rod shaped sample clamped at one end and stretched in the positive X direction. From equation (44) we have

$$u_x = \frac{dX}{dt} = \dot{\varepsilon}x \qquad (47)$$

The distance, X, from the clamped end to a material point initially at X_o will be

$$X = X_o e^{\dot{\varepsilon}t} \qquad (48)$$

The elongational strain, called also Hencky strain is

$$\ln(X/X_o) = \ln(L/L_o) = \dot{\varepsilon}t \qquad (49)$$

For steady uniaxial extension there is only one measurable material function, called the uniaxial extensional viscosity. This material property is defined as

$$\eta_t = \frac{\sigma_{11}-\sigma_{22}}{\dot{\varepsilon}} \qquad (50)$$

Experimentally, extension is done by exerting an external force, F, over some area of the sample. Therefore,

it is of interest to relate these measurable quantities to the normal stress difference $\sigma_{11} - \sigma_{22}$.

In the case of steady uniaxial extension, if inertia and surface tension can be neglected, we can say that

$$F/A = P_A + \sigma_{11} \tag{51}$$

where P_A is the ambient pressure. Considering that inertia has been neglected, any stress in a direction normal to the direction of elongation will be the negative of the ambient pressure P_A, therefore

$$\sigma_{22} = \sigma_{33} = -P_A$$

$$\sigma_{11} - \sigma_{22} = \tau_{11} - \tau_{22} = F/A \tag{52}$$

Finally the expression for the extensional viscosity is

$$\eta_T = \frac{F/A}{\dot{\varepsilon}} \tag{53}$$

There are two ways of doing uniaxial extension experiments. We can maintain either F/A or $\dot{\varepsilon}$ constant at different values and make measurements at different time intervals on the other one. This has given rise to two types of experiments; these are Creep experiments (stress maintained constant), and Stress Growth experiments (strain rate maintained constant).

6.2) Creep Experiments.

Apparatus operating in this mode have been developed by Cogswell[21], Vinogradov[22] and Münstedt[23].

The Cogswell apparatus[21], shown in Figure 33, stretches a sample clamped at both ends and immersed in an oil bath at a controlled temperature. One clamp is fixed and the other is free running. Both clamps are water cooled to avoid necking at the clamp where stress concentration exists. A dead weight load is applied to the running clamp by means of a specially-shaped cam. This cam is programmed to vary the load with the uniformly decreasing cross sectional area of the extending sample. This gives a constant uniaxial stress.

The forces related to the length by the expression

$$F = \frac{F_o L_o}{L} \qquad (54)$$

where F_o and L_o are the force and length at time 0 respectively and L and F are the length and the force at time t. The length of the sample is measured by clamp separation using a scale on the drive wheel of the cam. The samples used are cylinders with a length to diameter ratio of five.

Vinogradov's apparatus[22], shown in Figure 33, is similar to the one used by Cogswell. The difference lies in the use of a disc with two spiral grooves with weights suspended from them to apply the load to the moving clamp.

Each groove on the disc corresponds to a cam. The system to record the velocity of the moving clamp is more sophisticated and uses an electric circuit with a photo cell, an amplifier and a reversible motor. Attached to the motor is a variable resistor, that inserted in the balance circuit, gives a reading of the velocity at different times. A mechanism is built in the disc to prevent the acceleration of the weight. By measuring the velocity of the moving clamp the rate of extension can be calculated. No mention is made of the dimensions of the samples.

Münstedt's apparatus[23], shown in Figure 33, is an improvement of the apparatus described above. In the construction of this equipment care was taken to avoid the difficulties of maintaining constancy of stress over a wide range of deformation, homogeneity of sample deformation during the measurements, clamping of the sample and friction of the loading system. In this equipment the sample is mounted vertically and inside an oil bath which compensates the gravity effect by buoyancy and assures a good temperature distribution. The fact that the sample is mounted vertically is important as this allows the elimination of a bearing in the oil bath. The sample is loaded by a cam (mounted on an air bearing to reduce friction) which reduces the lever arm of the load as the sample elongates. Assuring that the volume of the sample is constant during elongation the cam can be shaped so that the stress is constant at all times. The elongation is mea-

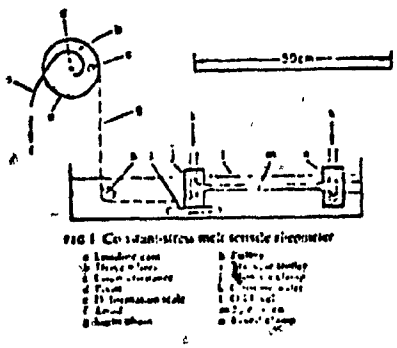

F.N. Cogswell.

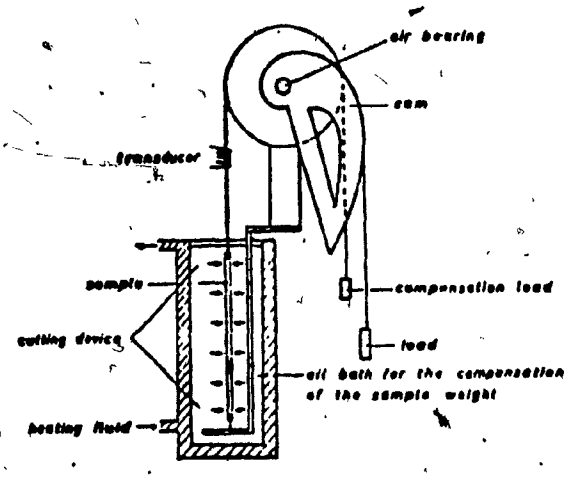

W. Munstedt.

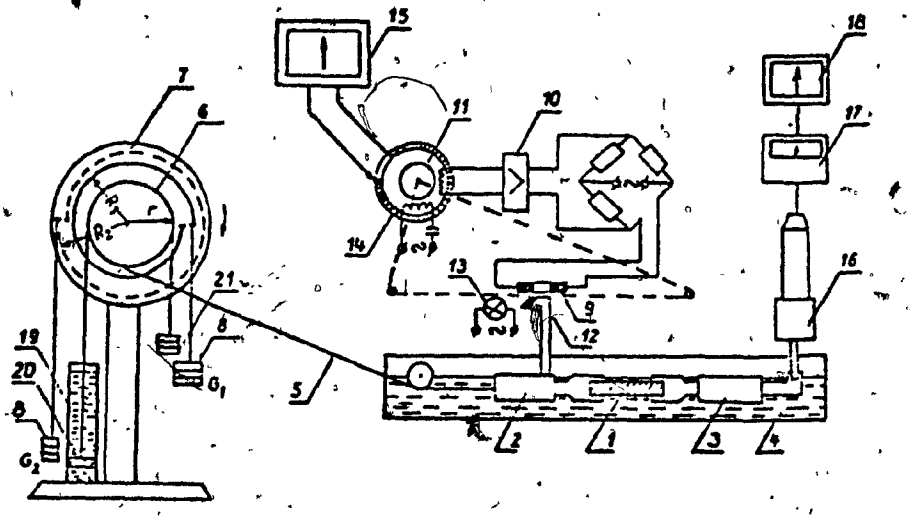

G.V. Vinogradov et al.

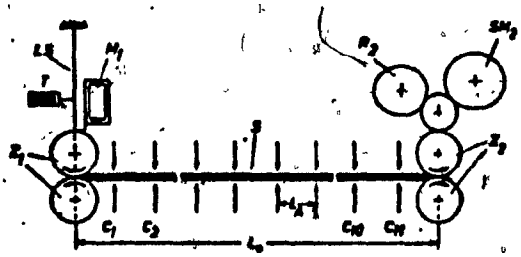

J. Meissner.

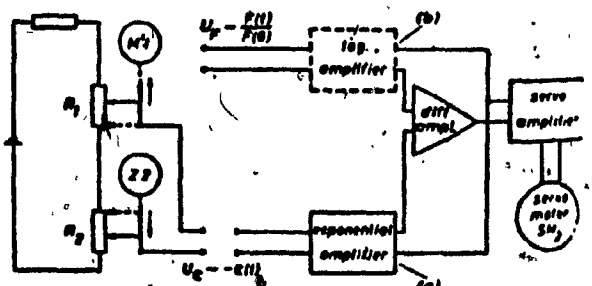

Figure 33. Experimental set-up of previous researchers. Creep Experiments.

sured by a transducer and recorded as a function of time. To obtain high resolution in the whole range of elongation the position of the transducer is changed automatically by a servo motor system.

The samples are fastened by glueing them into metal clamps. The samples used were 3 and 5 cm in length and 4mm in diameter and were prepared by extruding the polymer through a suitable die.

6.3) Stress Growth Experiments.

Apparatus designed to operate at constant strain rate have been developed by Vinogradov[24], Stevenson[25], Meissner[26], Ballman[27] and Shaw[28].

The apparatus used by Vinogradov is shown in Figure 34. The sample is immersed in a thermostatting bath and taped between one fixed and one moving clamp. Attached to the fixed clamp a force transducer is installed to record the force as a function of time. The moving clamp is driven by a mechanical drive. Attached to the drive is a measuring mechanism that permits the recording of the length of the sample as a function of time. From these measurements the strain rate can be computed. The driving mechanism is programmed in such a way that the velocity varies according to the equation

$$u = L_o \dot{\varepsilon} e^{\dot{\varepsilon} t} \qquad (55)$$

to maintain a constant strain rate. The samples were cylindrical in shape and their dimensions were 8mm in diameter and 30mm long.

Stevenson used a modified tensile testing machine as shown in Figure 34. The sample was placed inside a constant temperature chamber filled with silicone oil of the same density as the polymer and mounted on a variable speed testing machine. The machine was programmed by means of an analog computer to work at constant strain rate. A chain connected the specimen to the load cell which recorded the force necessary to elongate the specimen. During an experiment the length of the sample was recorded with a camera. The force and sample length data as functions of time were analyzed to give the stress as a function of time. The sample was held in position by two hard rubber faucet washers. The strain in the sample was recorded photographically by measuring the distance between 5mm wide grid marks placed 5mm apart in the central portion of the sample. The samples used were 9cm in length and 1.75cm diameter on the ends and 1.33cm diameter in the central portion. For high elongation rate experiments shorter samples, 6cm in length, were used.

Shaw[28] used equipment similar to the one used by Stevenson. The apparatus is shown in Figure 34. It consists

of a servohydraulic tensile testing machine made by Instron Corp. with a programmable signal generator and an oil bath. The difference from Stevenson's technique is that the samples used were different. The samples were rings made by compression molding. This shape seems to help eliminate erroneous stresses at low deformations. The dimensions of the rings were:

Inner radius: 0.22 and 0.37cm

Outer radius: 0.32 and 0.48cm.

The most extensive work on extensional viscosity has been done by Meissner[26]. A representation of his apparatus is given in Figure 34. It consists of two rotational clamps at a fixed separation from each other that pull the sample out in opposite direction and constant rotational speeds with the result that the sample is stretched with constant extensional strain rate. The latest version of this equipment has only one set of rotary clamps and one end of the sample is glued to a fixed part. The force measuring device is a linear displacement transducer. The sample under test is a rod of molten polymer immersed in silicone oil. The oil provides the heating, compensates for gravity by buoyancy and centers the fluid rod along the clamp separation by means of slow convective currents. This equipment although primarilly designed for stress growth experiments can also be operated in the creep mode if the synchronous motor M_2 is replaced by a servo motor of fast response

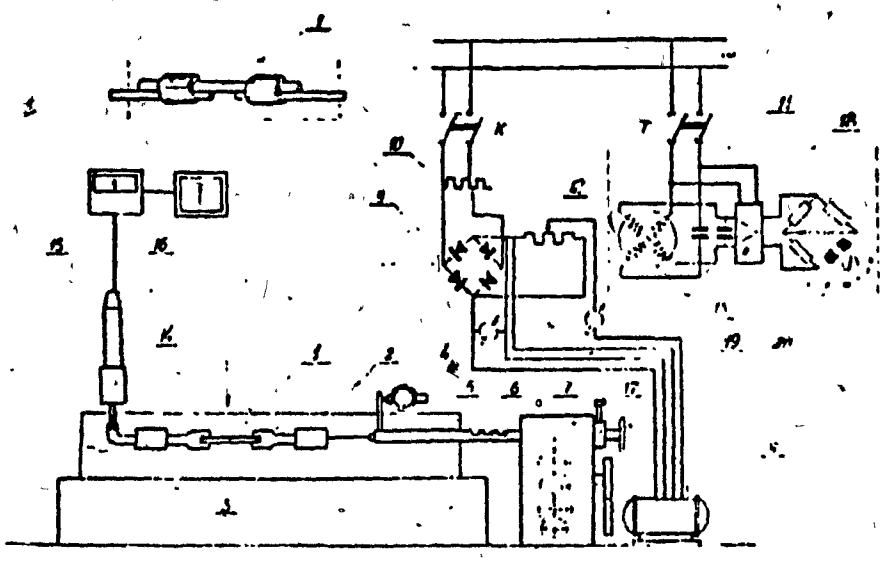

G.V. Vinogradov et al.

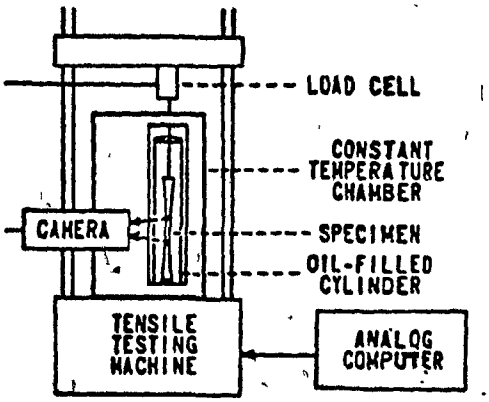

J.F. Stevenson.

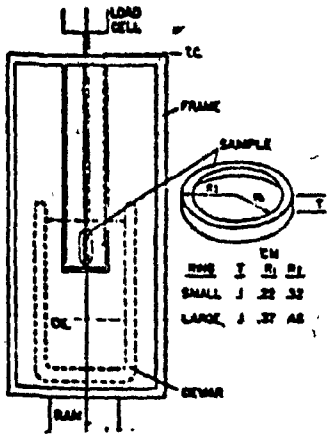

M.T. Shaw.

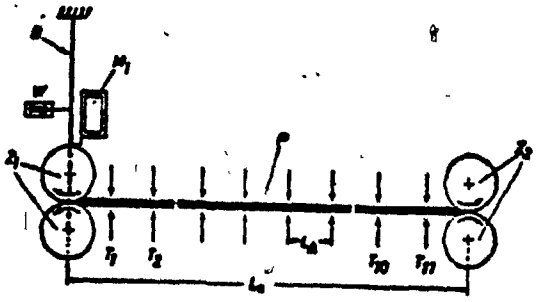

J. Meissner.

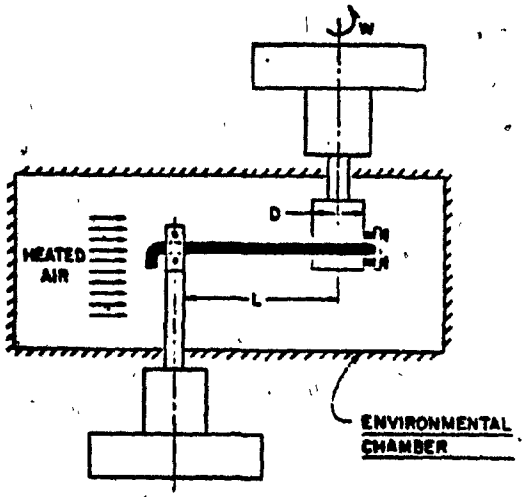

Ballman & Everage.

Figure 34.
Experimental set-up of previous researchers.
Stress Growth Experiments.

and the rotational speed of the synchronous motor M_1 is so slow that clamp Z_1 performes only a fraction of a full rotation within the duration of the test.

Ballman and Everage[27] used an apparatus that is similar to the rotating clamp device of Meissner described above. The apparatus is shown in Figure 34. The test material was held in a stationary clamp at one end and wrapped around a winder rod at the other end. The stationary clamp was mounted on the Rheometrics Mechanical Spectrometer transducer which detected the tensile force in the sample. The winder rod was connected to the drive mechanism and could be rotated over a wide range of speeds.

Table 2 and Figure 35 gives a summary of the researchers, the mode used, the materials tested, the operating conditions and some of the results obtained for extensional viscosity.

Table 2.

Summary of Previous Studies on Extensional Viscosity.

Researcher	Mode	Material	Conditions
F.N. Cogswell	Creep	LDPE	150^{0}C
G.V. Vinogradov	Creep Stress Growth	Polystyrene	130^{0}C
J.F. Stevenson	Stress Growth	Poly Isobutylene Isoprene Copolymer	100^{0}C
J. Meissner	Stress Growth	LDPE	150^{0}C
W. Munstedt	Creep	Polystyrene	140^{0}C
Ballman & Everage	Stress Growth	Polystyrene	155^{0}C

F.N. Cogswell

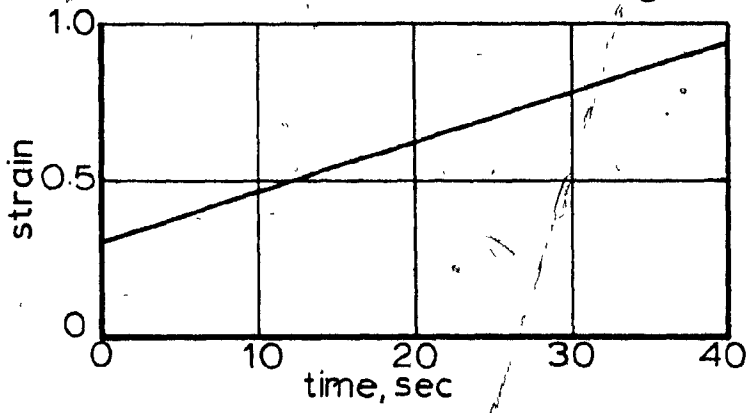

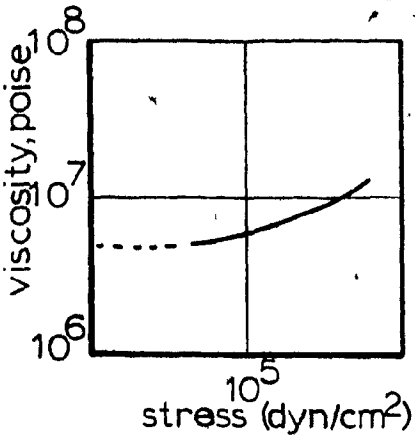

G.V. Vinogradov et al

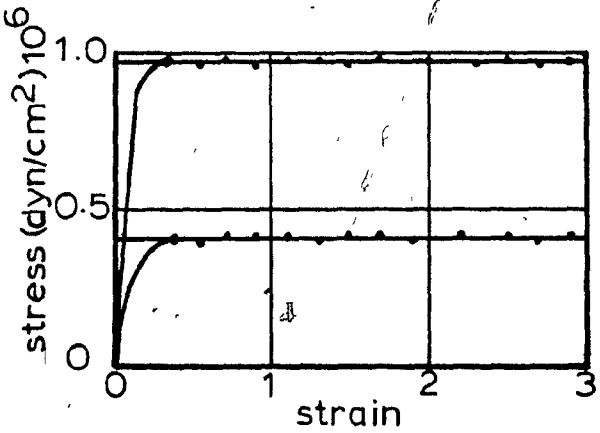

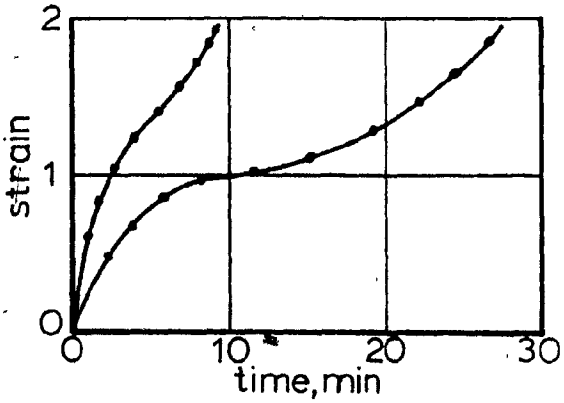

J.F. Stevenson

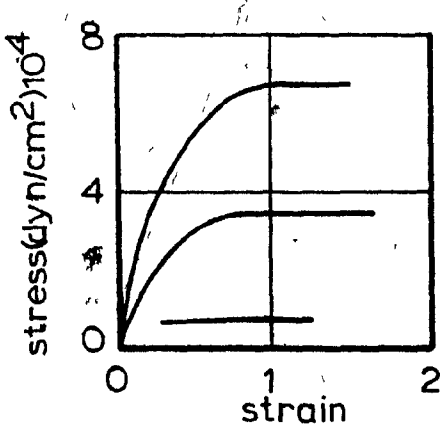

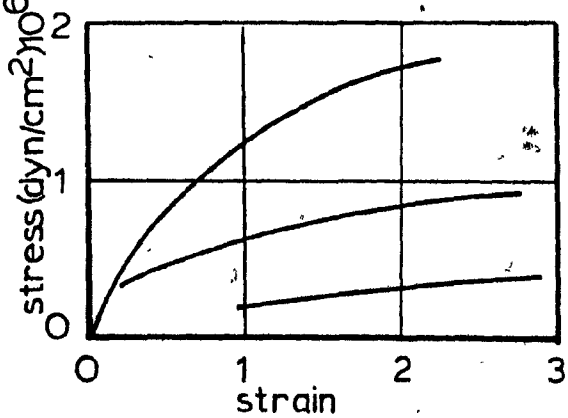

Fig.35 Typical results of previous researchers.

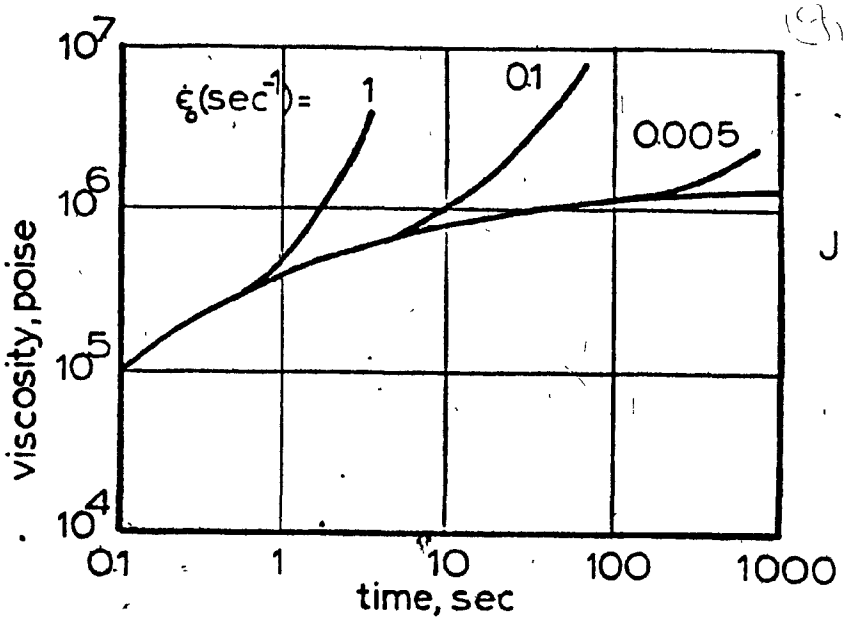

J. Meissner

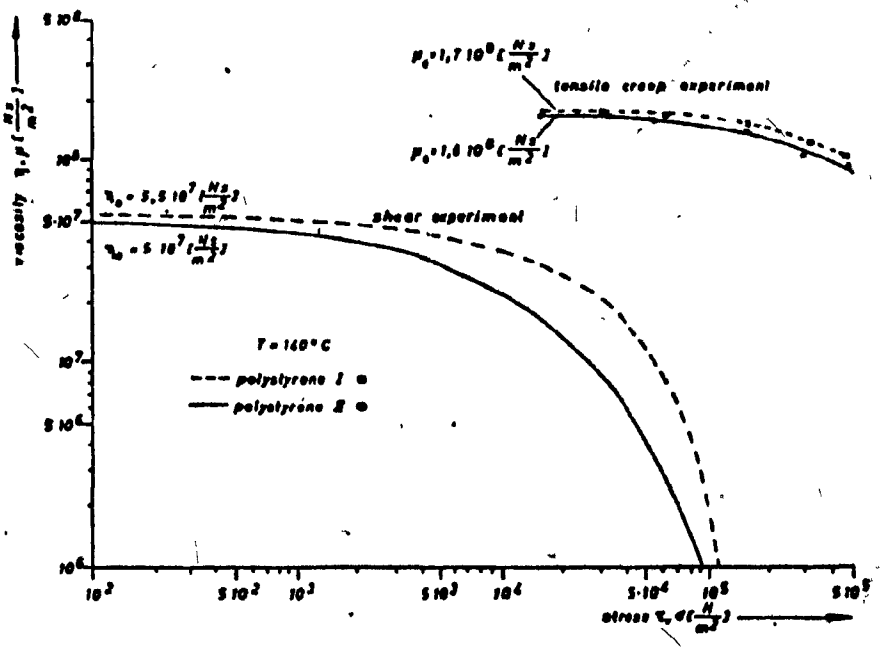

W. Münstedt

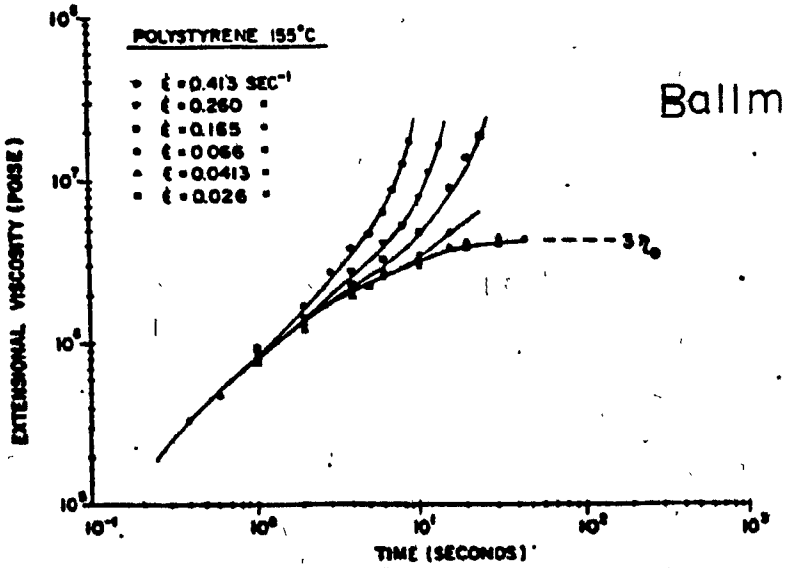

Ballman & Everage

Fig. 35
Cont.

CHAPTER 7. EXTENSIONAL VISCOSITY - EXPERIMENTAL RESULTS.

7.1) Experimental Equipment.

The equipment used to measure the extensional viscosity of polymer melts is described in detail by Rhi-Sausi[29] and Dealy and Rhi-Sausi[30]. A schematic view of the apparatus is presented in Figure 36. The equipment can operate in constant strain rate and constant stress modes. In the present work the constant strain rate mode was used. Modifications of the equipment were made to extend the range of strain rate and minimize some other problems.

A gear box with a bigger reduction ratio (15:1) was used to extend the lower end of the strian rate range to $0.005 sec^{-1}$. The contol system was modified to work at low strain rates. An analysis of the original control system established that the time constant of the control system was inversely proportional to the strain rate. This implied that the lower the strain rate the larger the time it takes to the control system to respond to obtain the desired strain rate. This transient time represented 55% of the total time of the experiment for the strain rate of $.005 sec^{-1}$. This further implied that an experiment carried out at this rate would be meaningless since the assupmtion of constant strain rate would not be valid throughout.

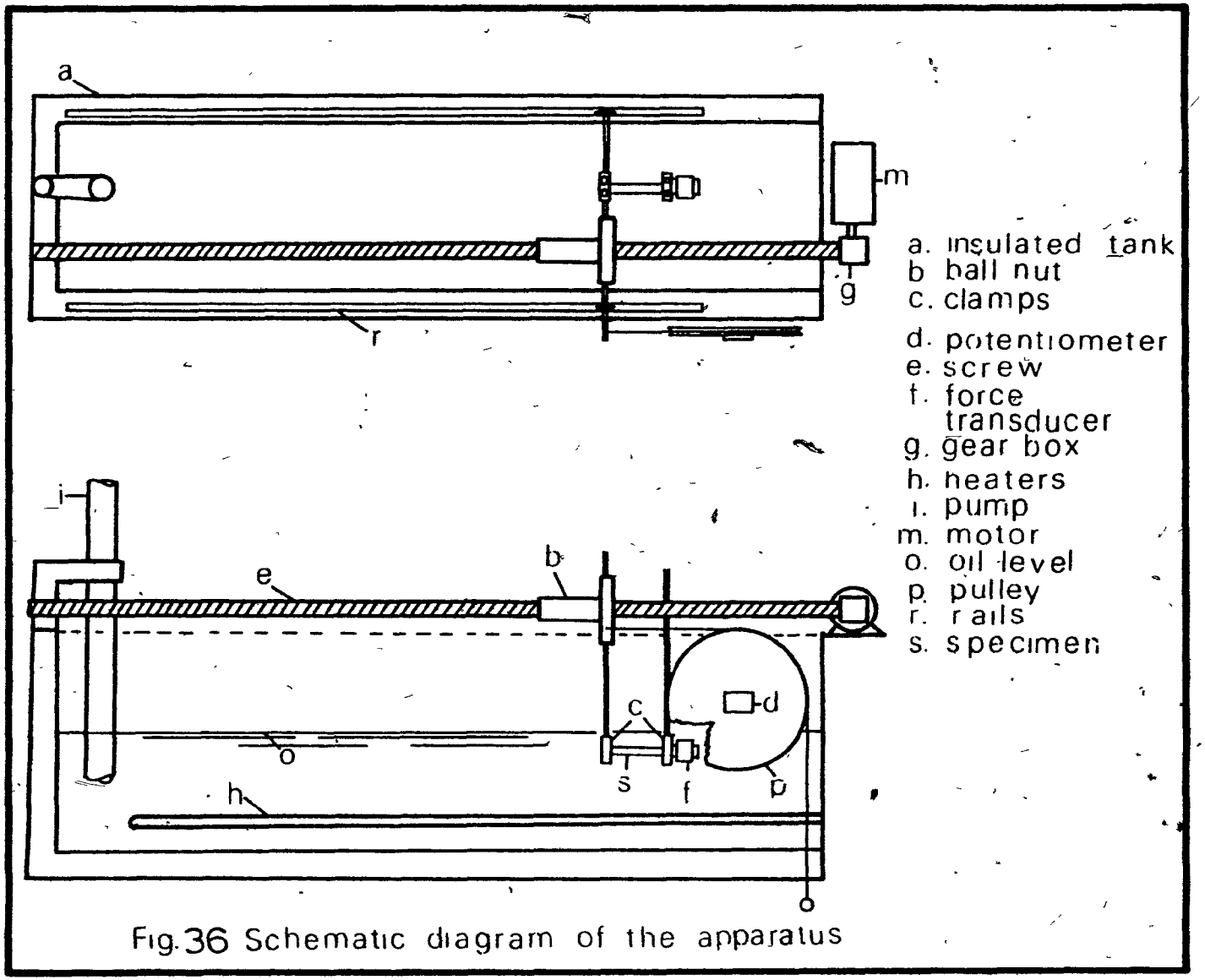

Fig. 36 Schematic diagram of the apparatus

The modified control system, shown in Figure 37, consists basically of the same components as the original one, but a feedback signal from the tachometer of the motor was supplied to the controller. In this way the voltage that is fed to the motor to drive the extension mechanism was controlled at the value it should have, by means of a voltage comparison (input and output) in the controller. In this way the necessary condition to have an uniaxial extensional flow

$$u = \dot{\epsilon}L \qquad (56)$$

will hold at all times.

It was found that the transient with this control system was reduced to 12% of the total time of the experiment for the lowest strain rate, $0.005 sec^{-1}$. Further elimination of this transient seems difficult to attain because of the mechanical set-up of the equipment, mainly due to the motor response.

The holding clamps are oil cooled (silicon oil Fluid 200, 5cs., Dow Corning). A careful control of the amount of cooling is necessary. A large cooling rate results in a section of unmelted polymer in the test sample near the clamps and a small one will allow the sample to flow out of the clamps. The cooling oil is circulated through the clamps by means of a circulating bath provided with an immersion pump (Neslab, Model TE9). The optimum temperature for the cooling oil in the clamps was found to be between

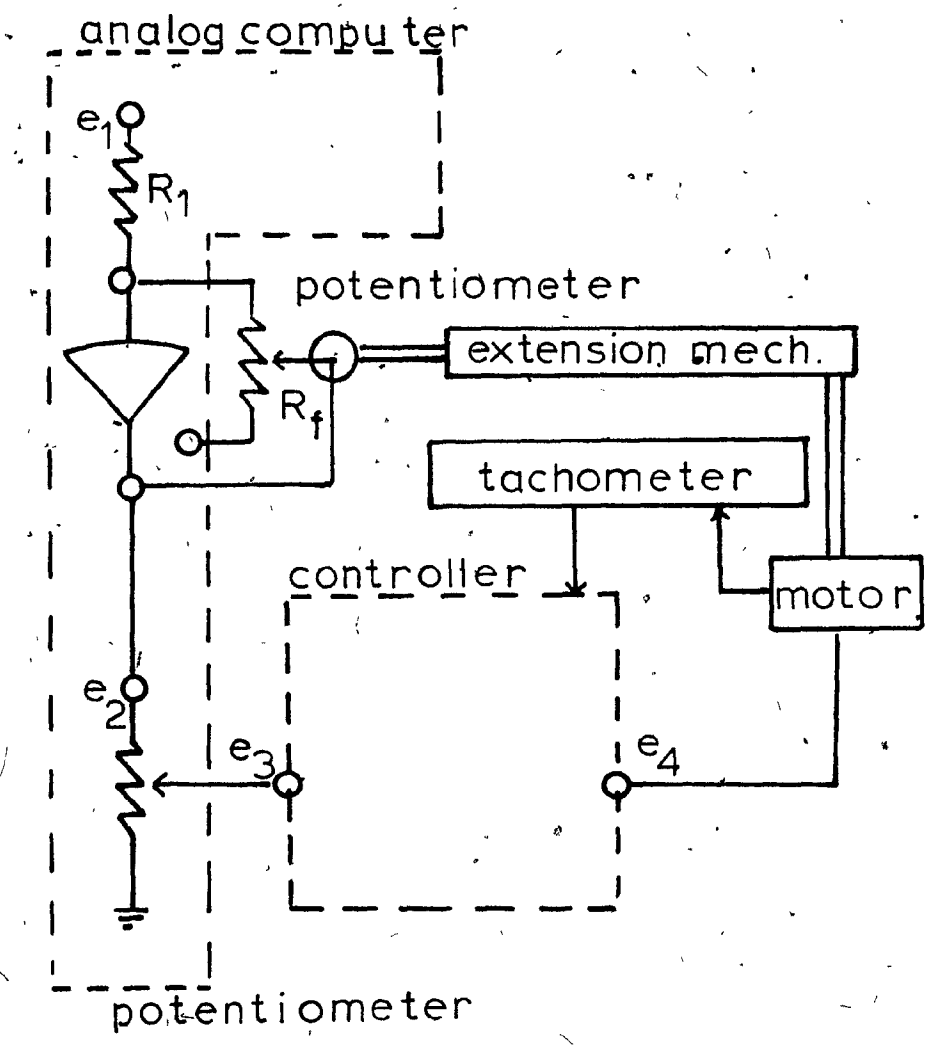

Fig. 37
Schematic diagram of the control system

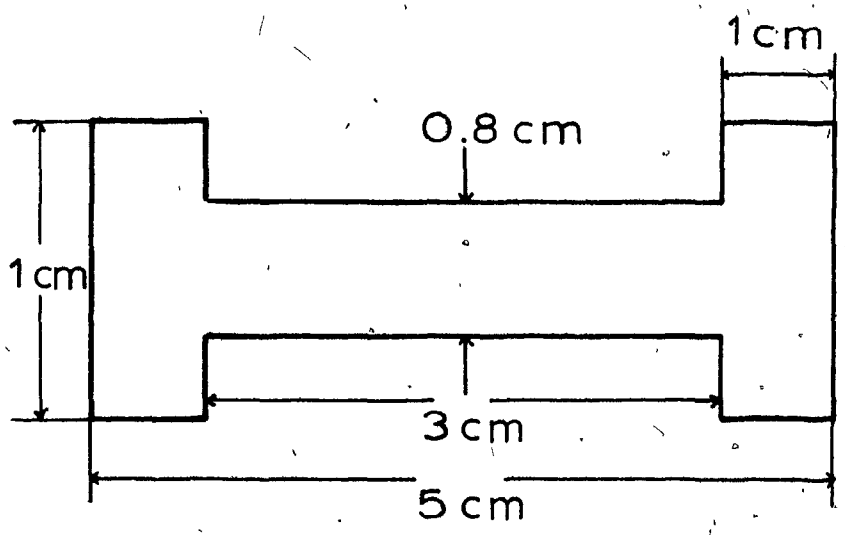

Fig. 38
Sample Dimensions.

115 and 120°C.

Cylindrical samples are prepared by transfer molding (180°C and 10-15 tons), annealing at 1 atm and machining to the final size and shape. The sample dimensions are shown in Figure 38.

7.2) Experimental Technique.

The oil bath is heated to the desired temperature. The immersion pump must be in operation during this time to assure homogeneity of the temperature throughout the bath. When the oil reaches the test temperature the cooling of the clamps is started. The clamps are brought to their initial position which is measured on the chart recorder. The length is measured by knowing that a certain voltage corresponds to a certain length. The initial position gives a measure of the initial length of the sample. The test sample is put between the clamps and allowed to melt completely. Care must be taken that the sample does not swell. This phenomenon can be caused by stresses frozen in the molding process or from an uneven cooling at the clamps. The strain rate is set to the desired value by means of a potentiometer in the analog computer. When the sample is completely melted the driving mechanism is turned on and the extension starts. The force is measured by means of an LVDT force transducer

connected to the fixed clamp. The length and the force are recorded as functions of time on a strip chart recorder. The extension is stopped near the end of the bath, the sample taken out and the moving clamp returned to its initial position. Another sample is clamped and another strain rate can be chosen to continue the experiments.

7.3) Experimental Results.

Figures 39 to 45 show the curves of Hencky strain vs. time for the different strain rate values that can be obtained from the extensiometer. The slope of these curves gives the strain rate.

It can be seen that the response of the control system of the driving mechanism is very good from the very beginning of the experiment. Theoretically the straight line obtained in the Hencky strain vs. time curves should pass through the origin. This is true at the high strain rates. At the low strain rates the deviation of the line from the origin is very small and is reasonably inside the experimental error.

Figures 46 to 52 show the curves of stress vs. time for Resins 1 and 9 for different strain rates at 180°C.

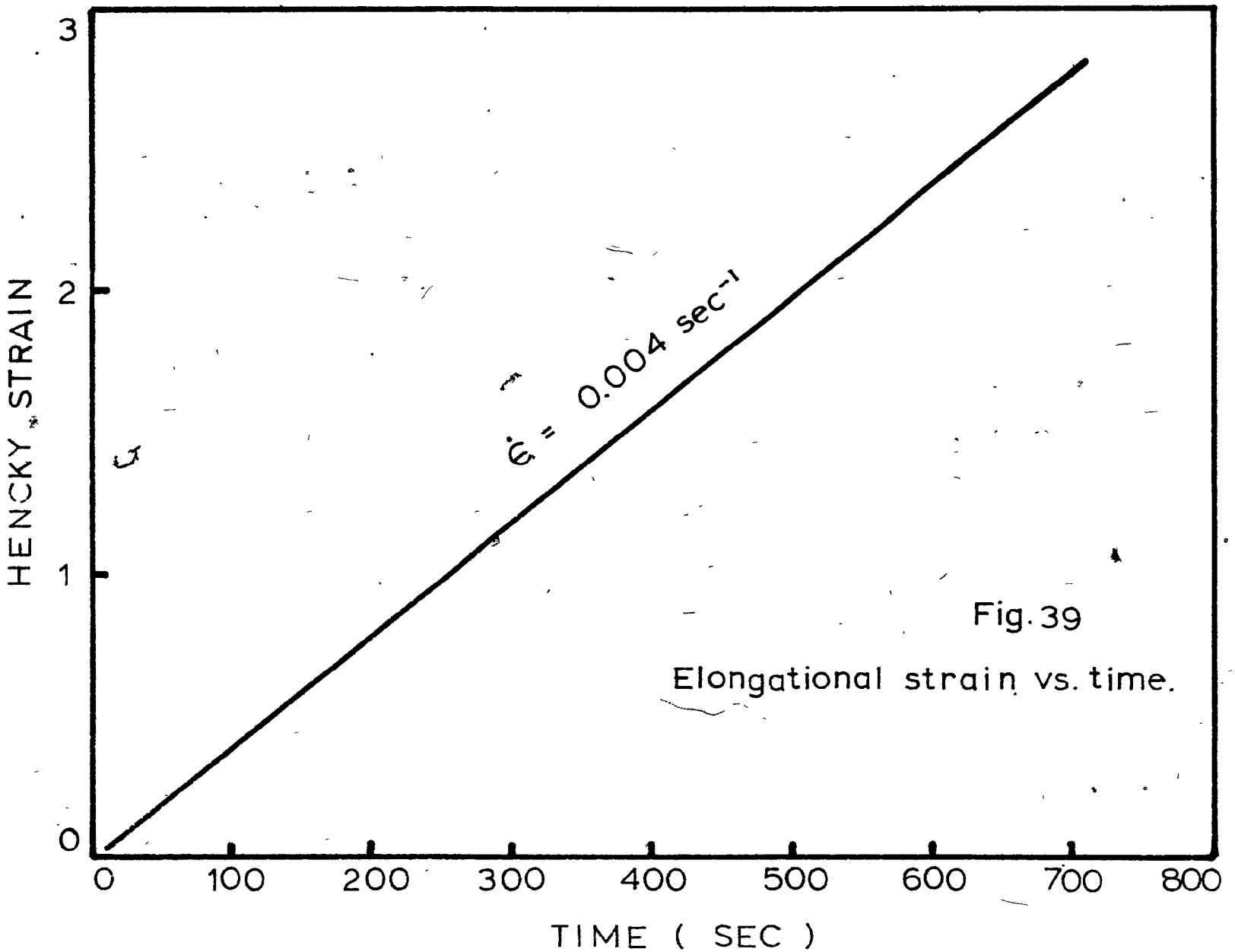

Fig. 39

Elongational strain vs. time.

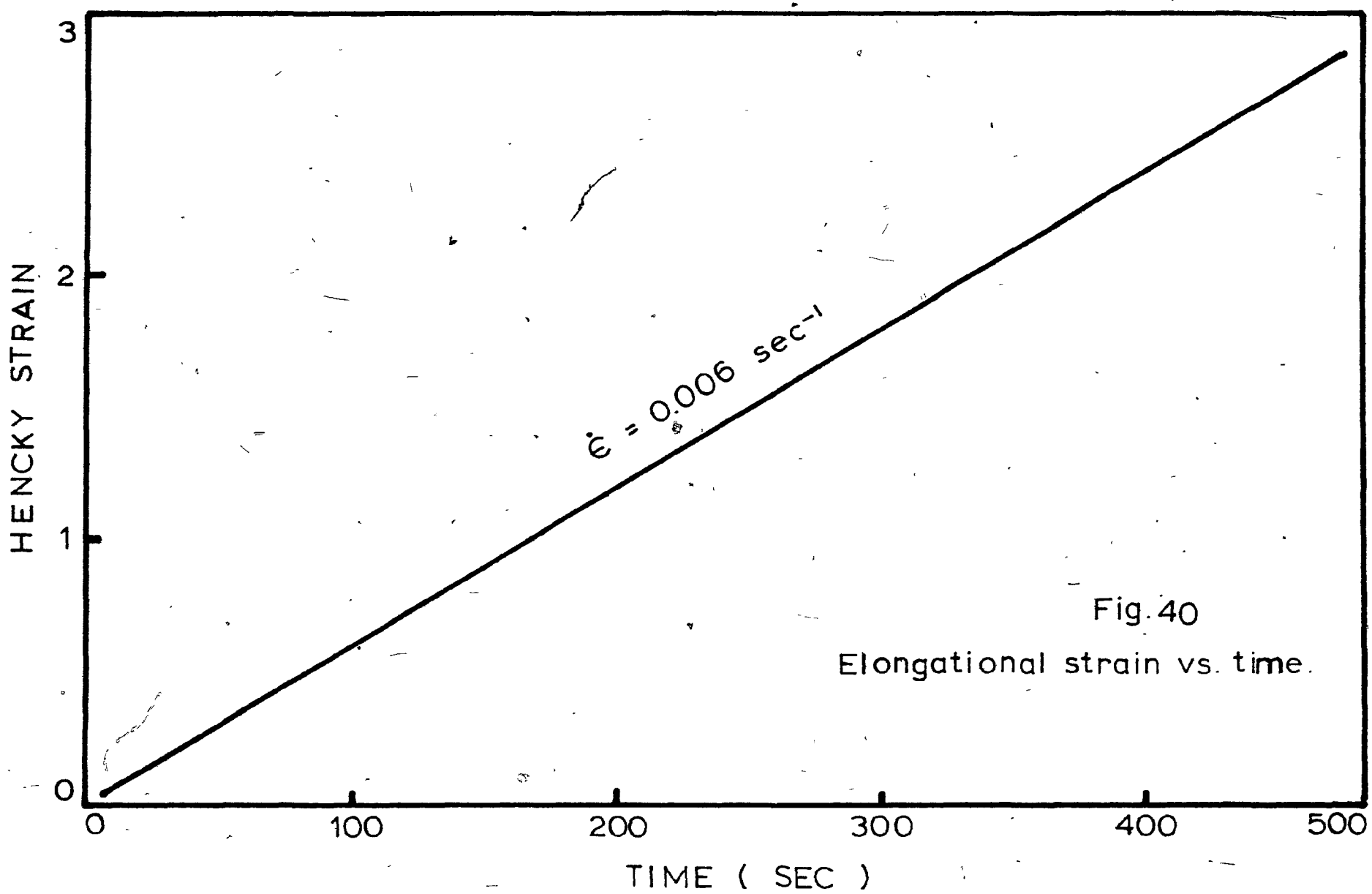

Fig. 40

Elongational strain vs. time.

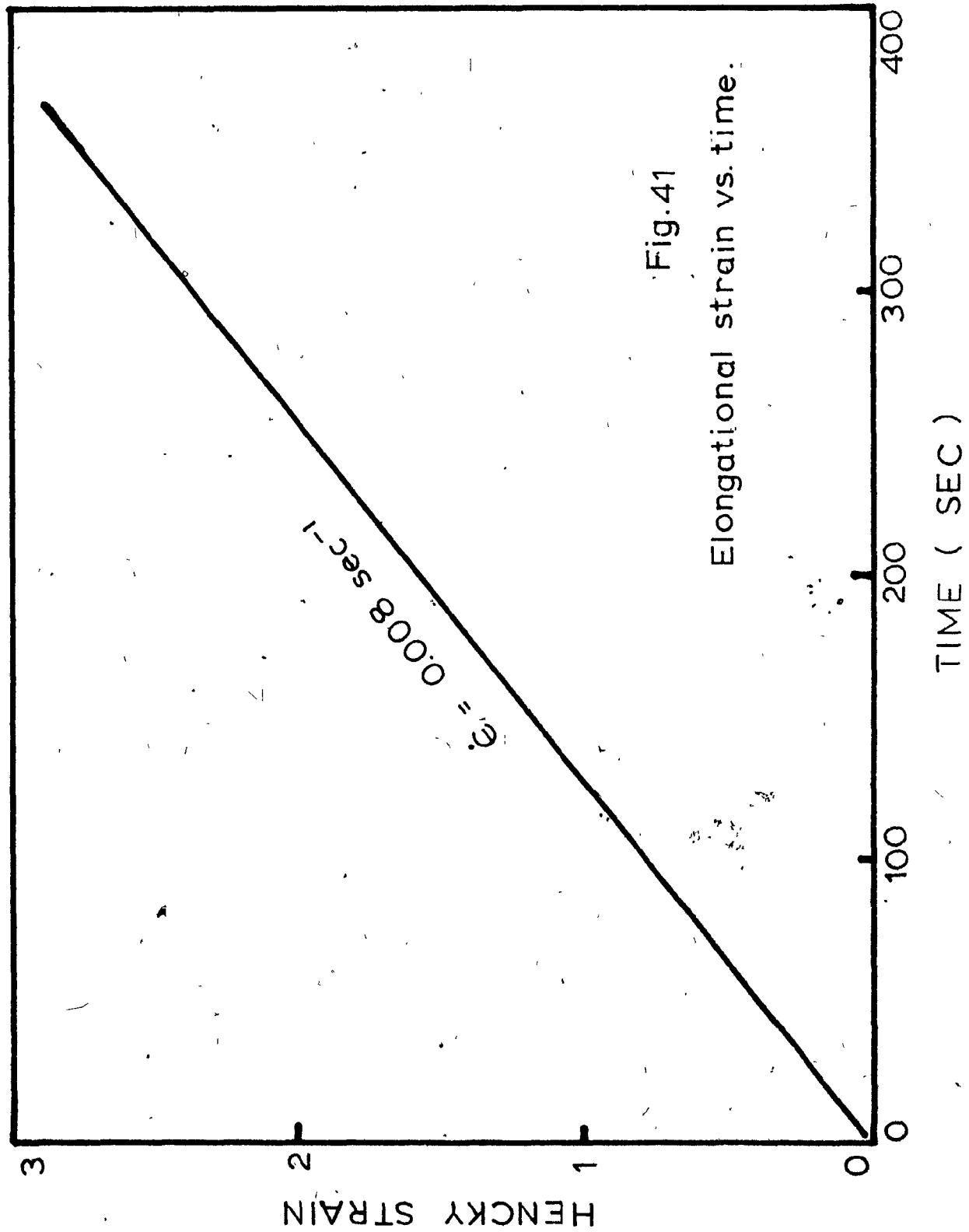

Fig.41
Elongational strain vs. time.

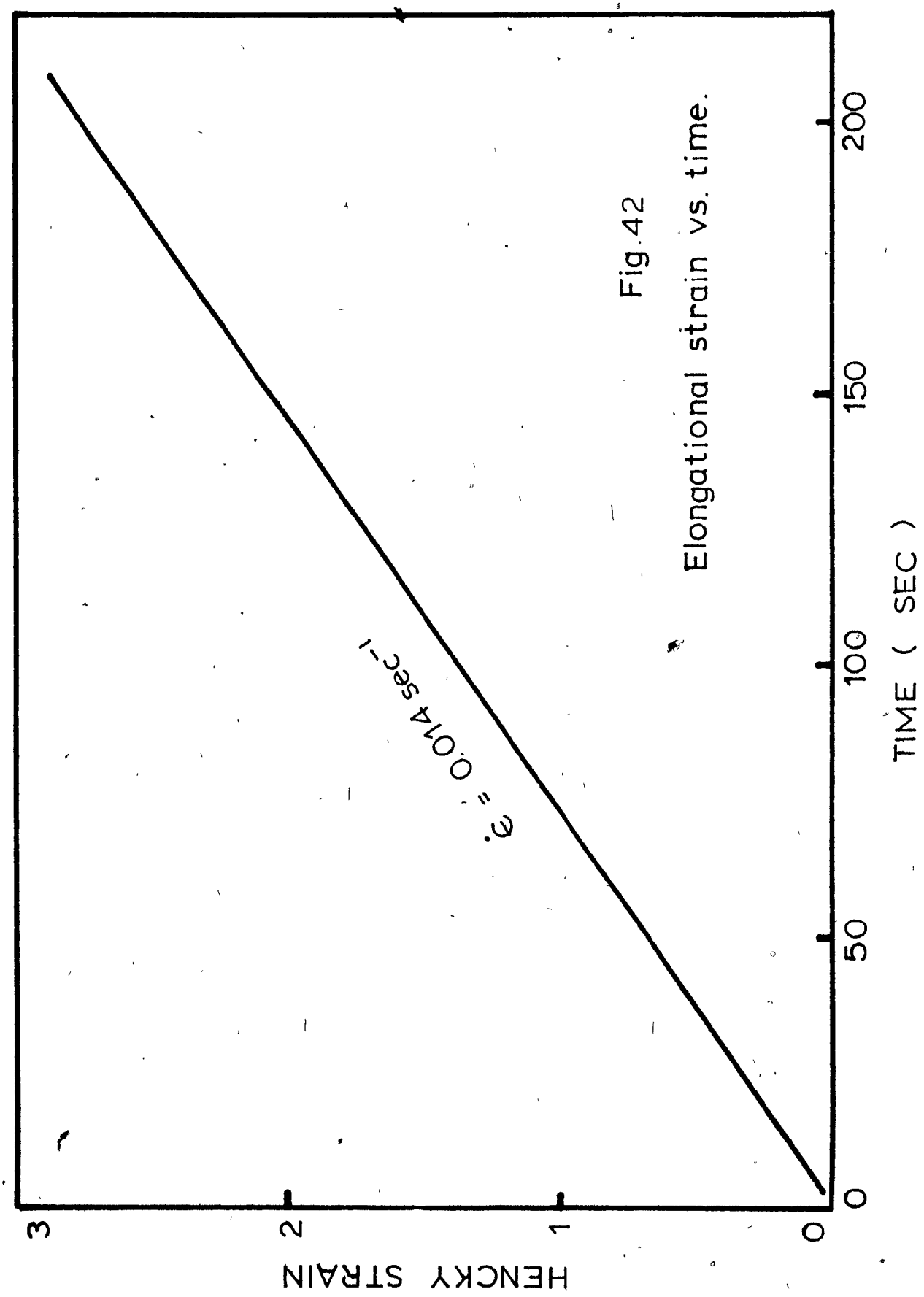

Fig.42
Elongational strain vs. time.

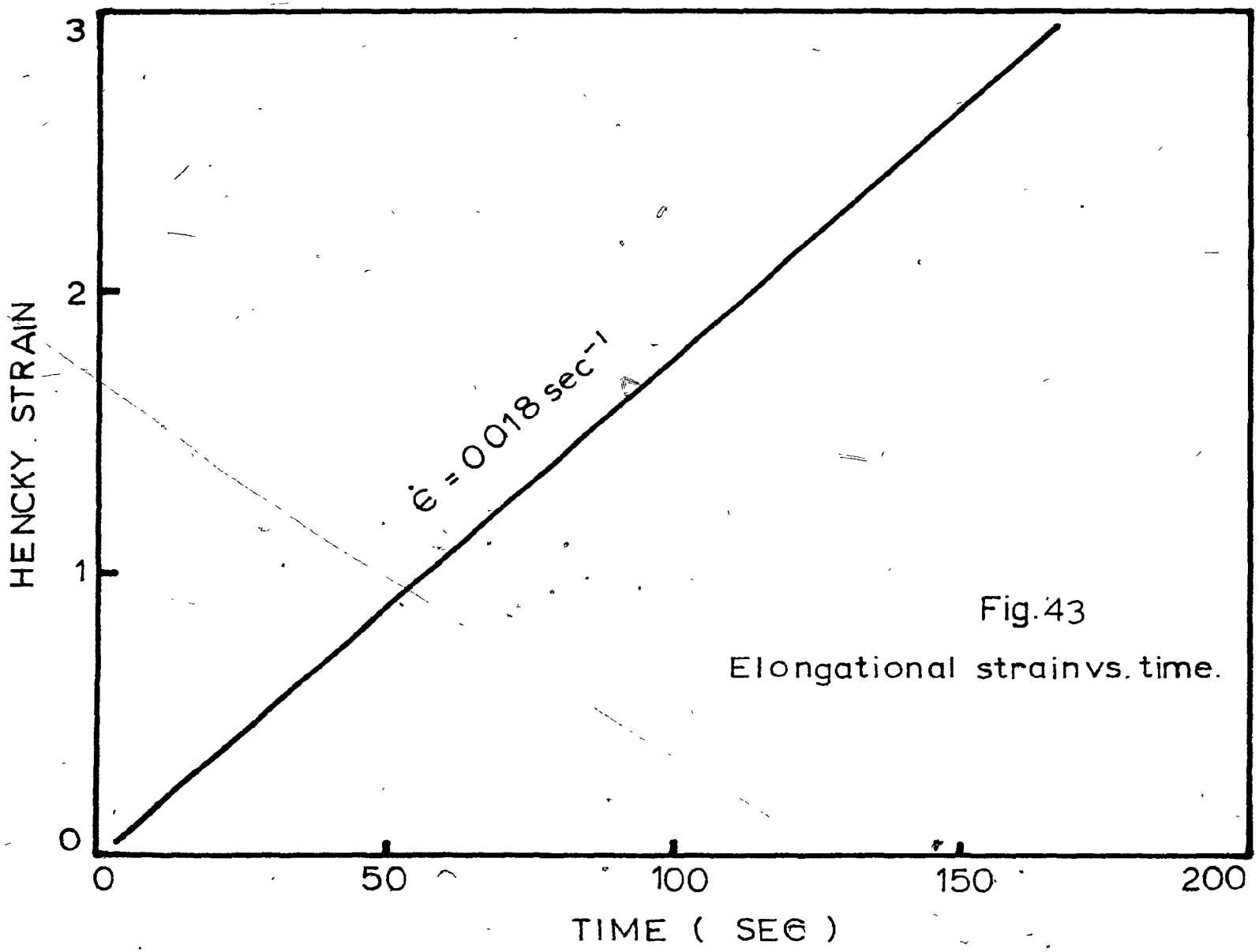

Fig. 43

Elongational strain vs. time.

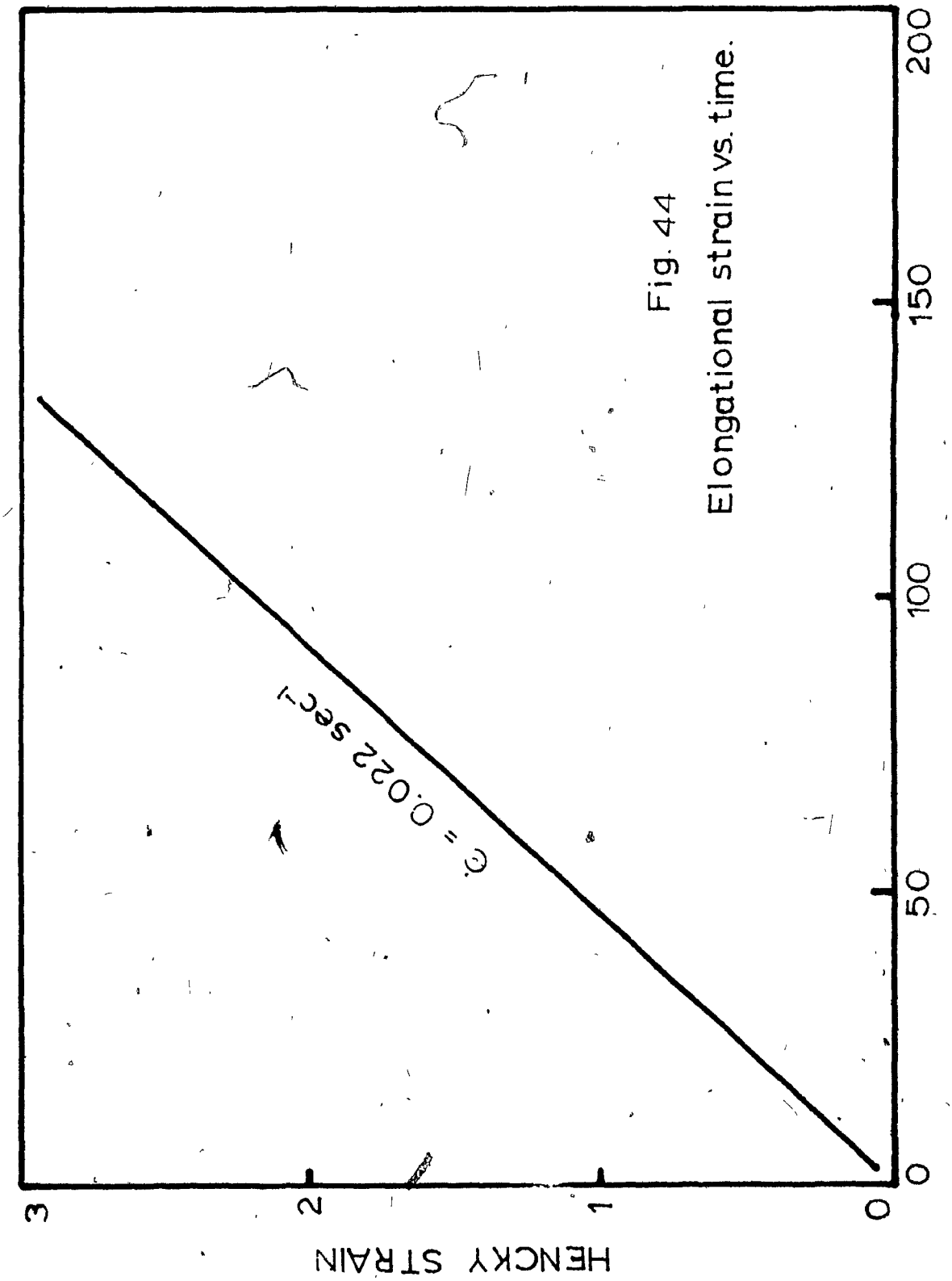

Fig. 44
Elongational strain vs. time.

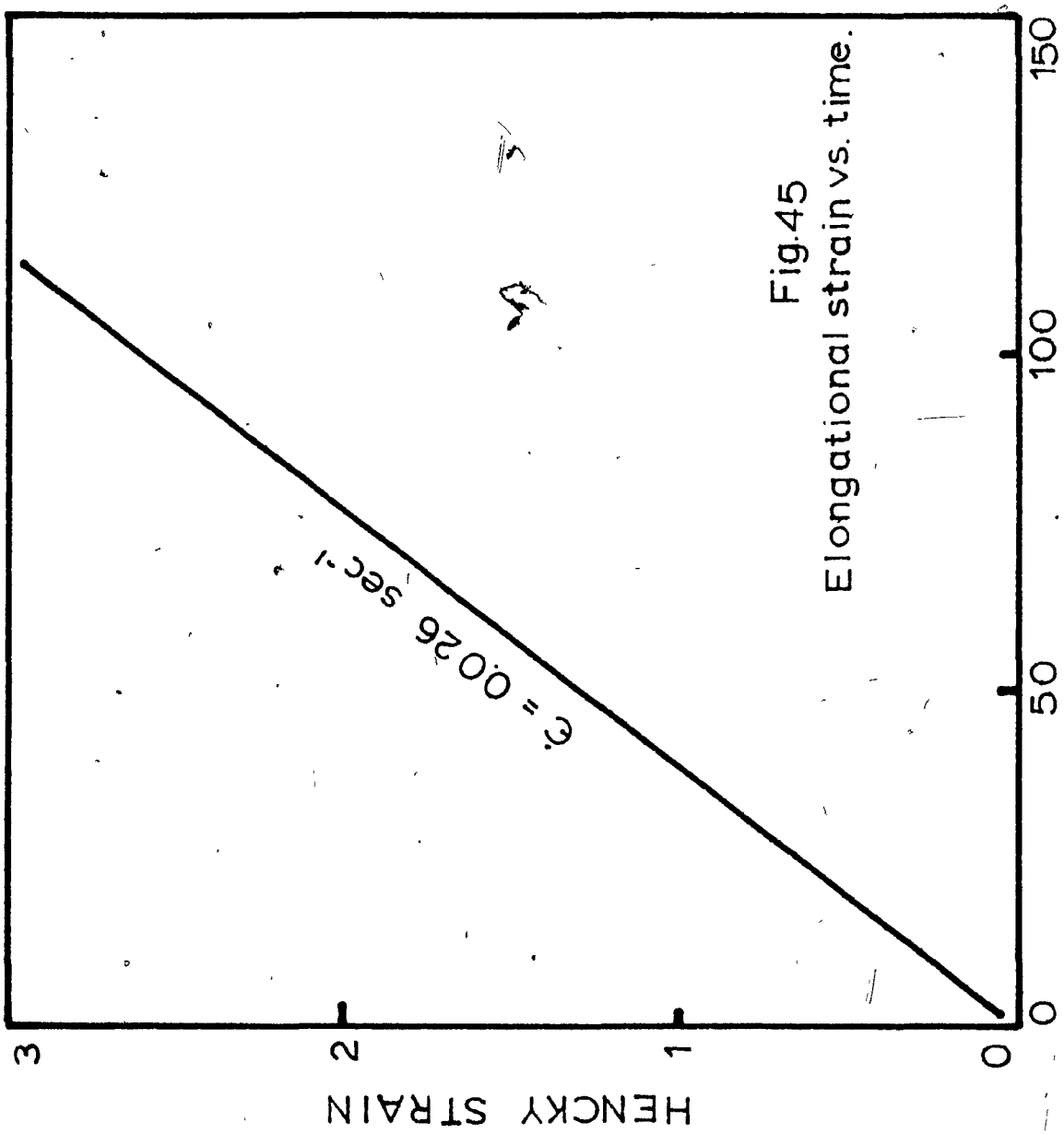

Fig.45
Elongational strain vs. time.

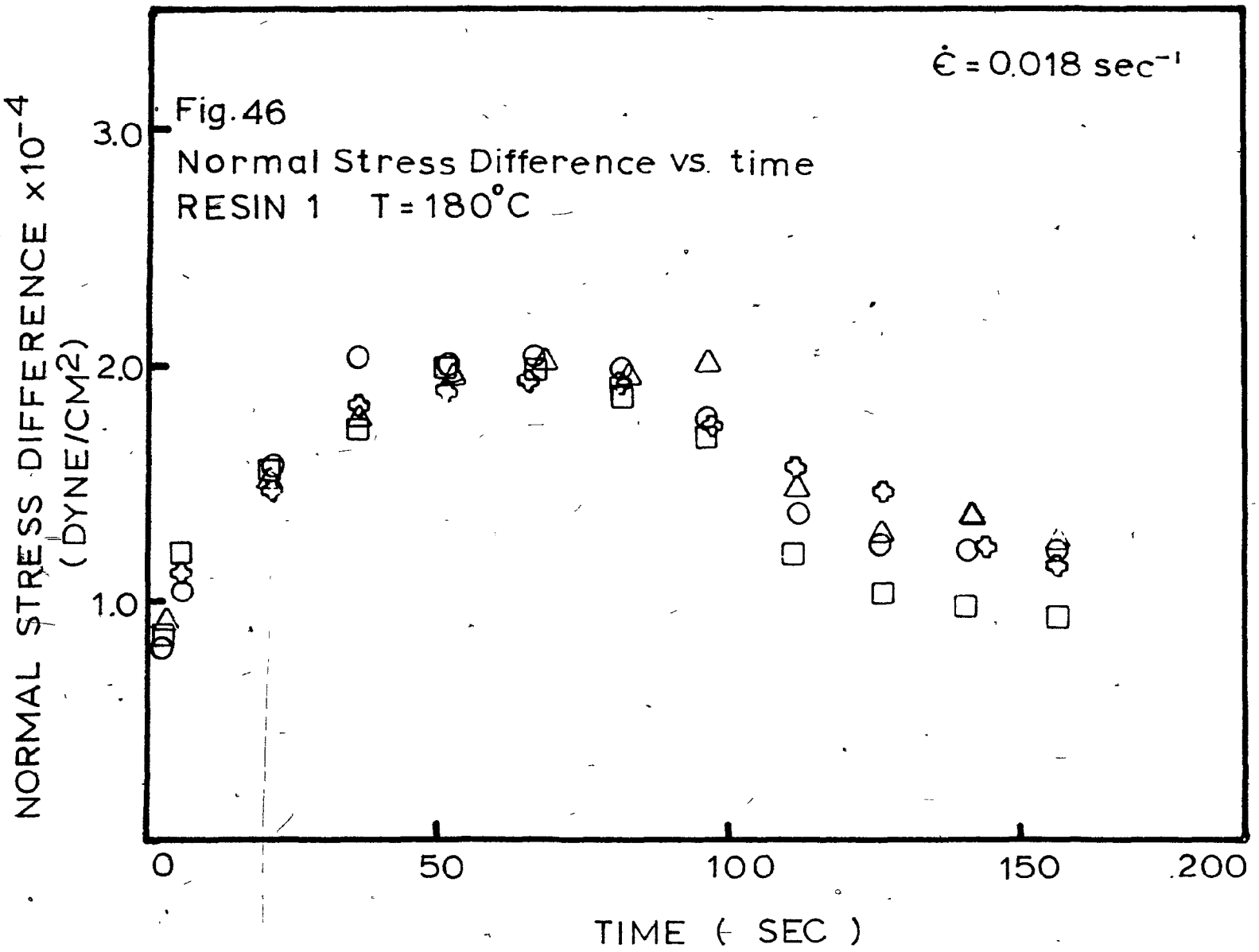

Fig. 46
Normal Stress Difference vs. time
RESIN 1 T = 180°C

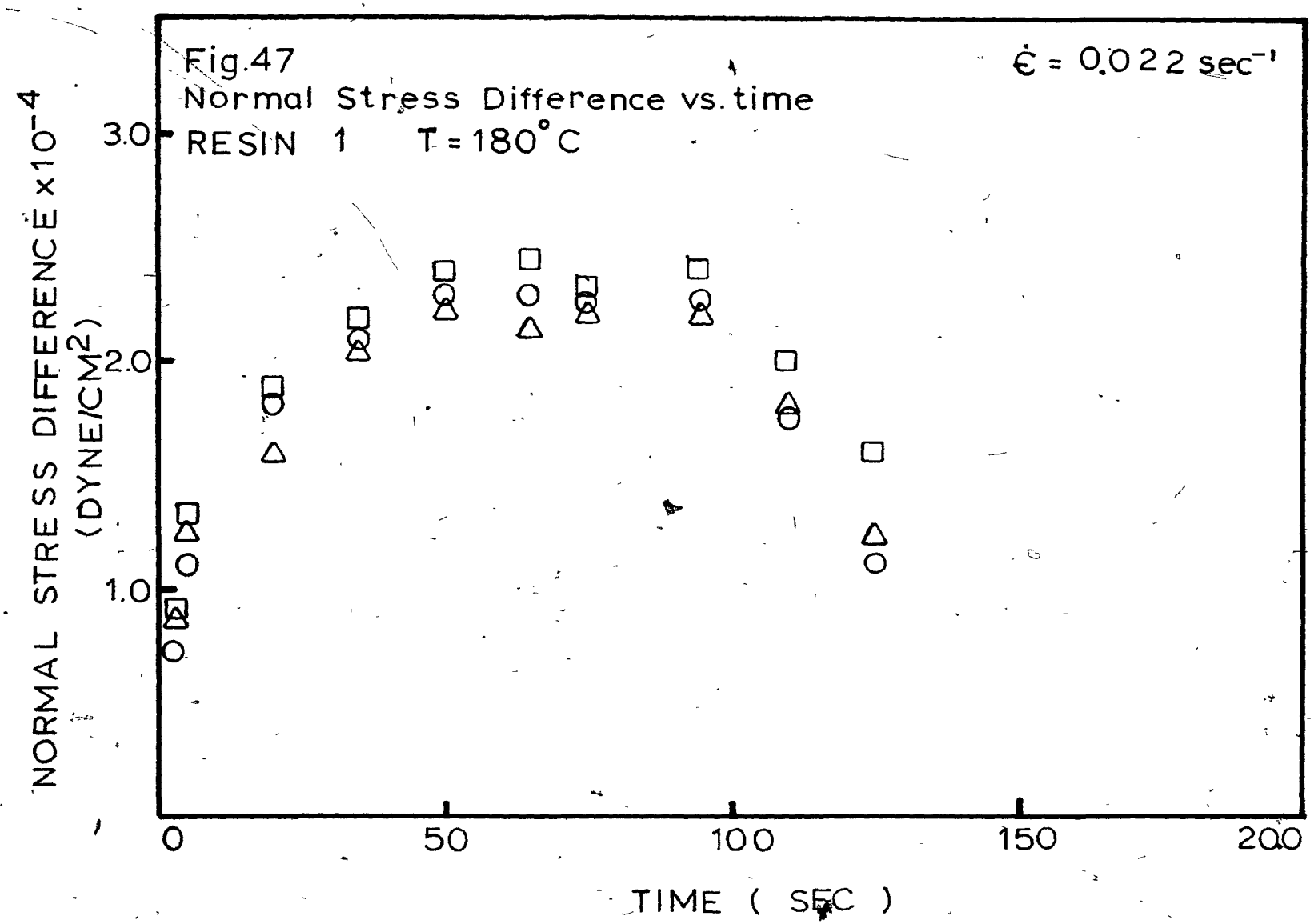
Fig.47
Normal Stress Difference vs. time
RESIN 1 T = 180°C
$\dot{\epsilon}$ = 0.022 sec^{-1}
NORMAL STRESS DIFFERENCE x10^{-4}
(DYNE/CM^2)
3.0
2.0
1.0
0
50
100
150
200
TIME (SEC)

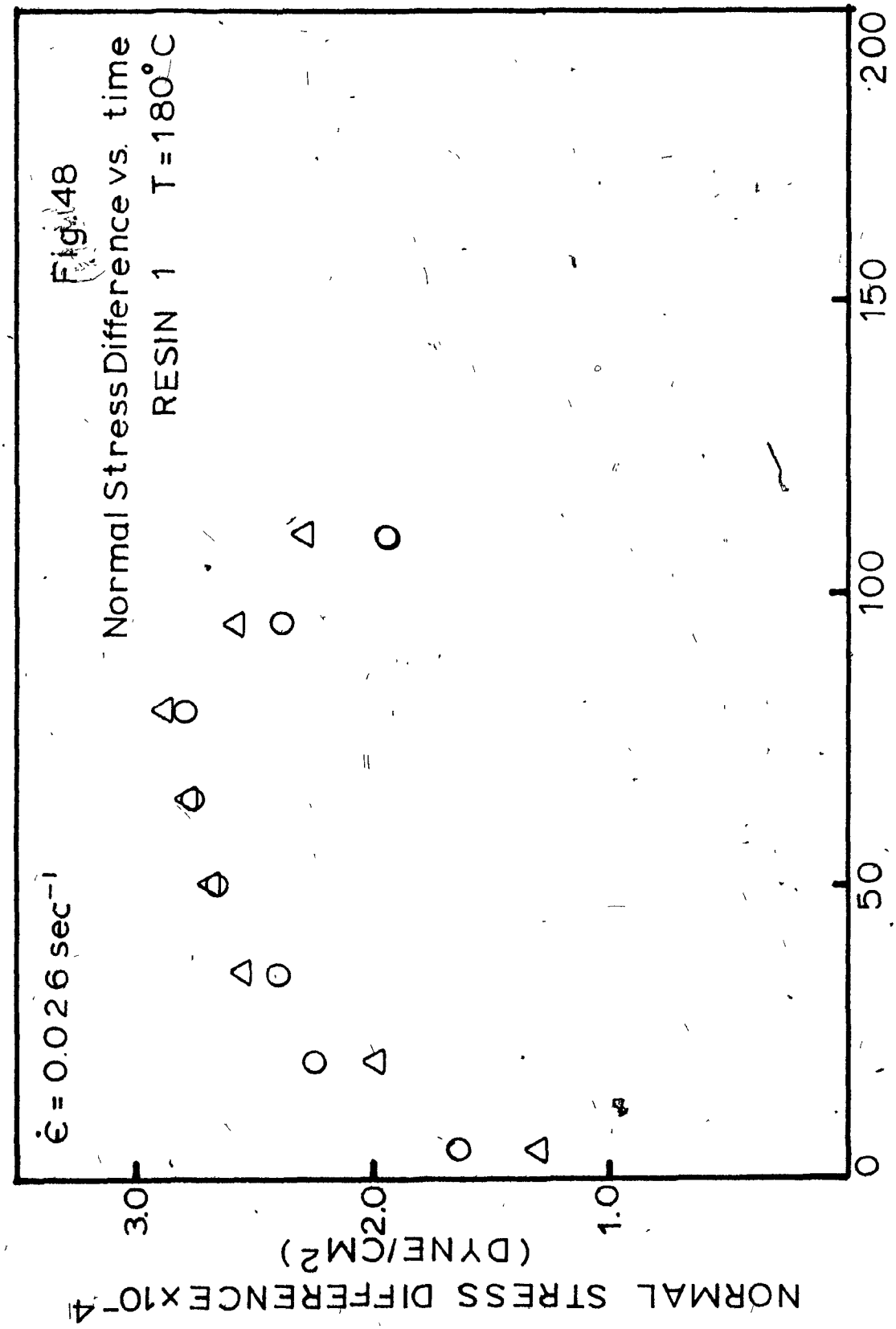
Fig. 48
Normal Stress Difference vs. time
RESIN 1 T = 180°C
$\dot{\epsilon} = 0.026\ sec^{-1}$
NORMAL STRESS DIFFERENCE $\times 10^{-4}$
(DYNE/CM²)
3.0
2.0
1.0
0
50
100
150
200
TIME (SEC.)

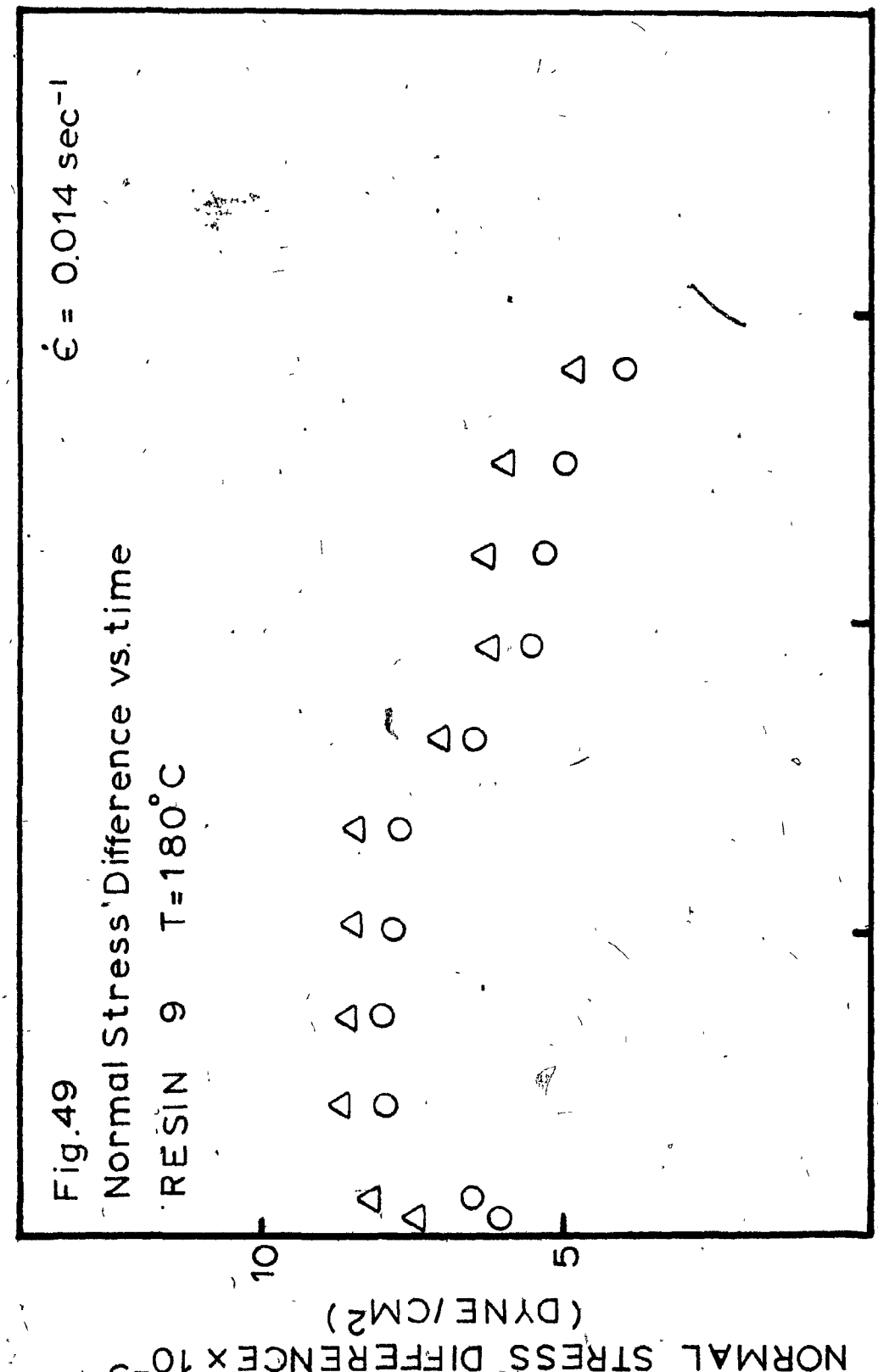
Fig.49
Normal Stress Difference vs. time
RESIN 9 T=180°C
$\dot{\epsilon}$ = 0.014 sec^{-1}
NORMAL STRESS DIFFERENCE x 10^{-3}
(DYNE/CM2)
10
5
0
50
100
150
200
TIME (SEC)

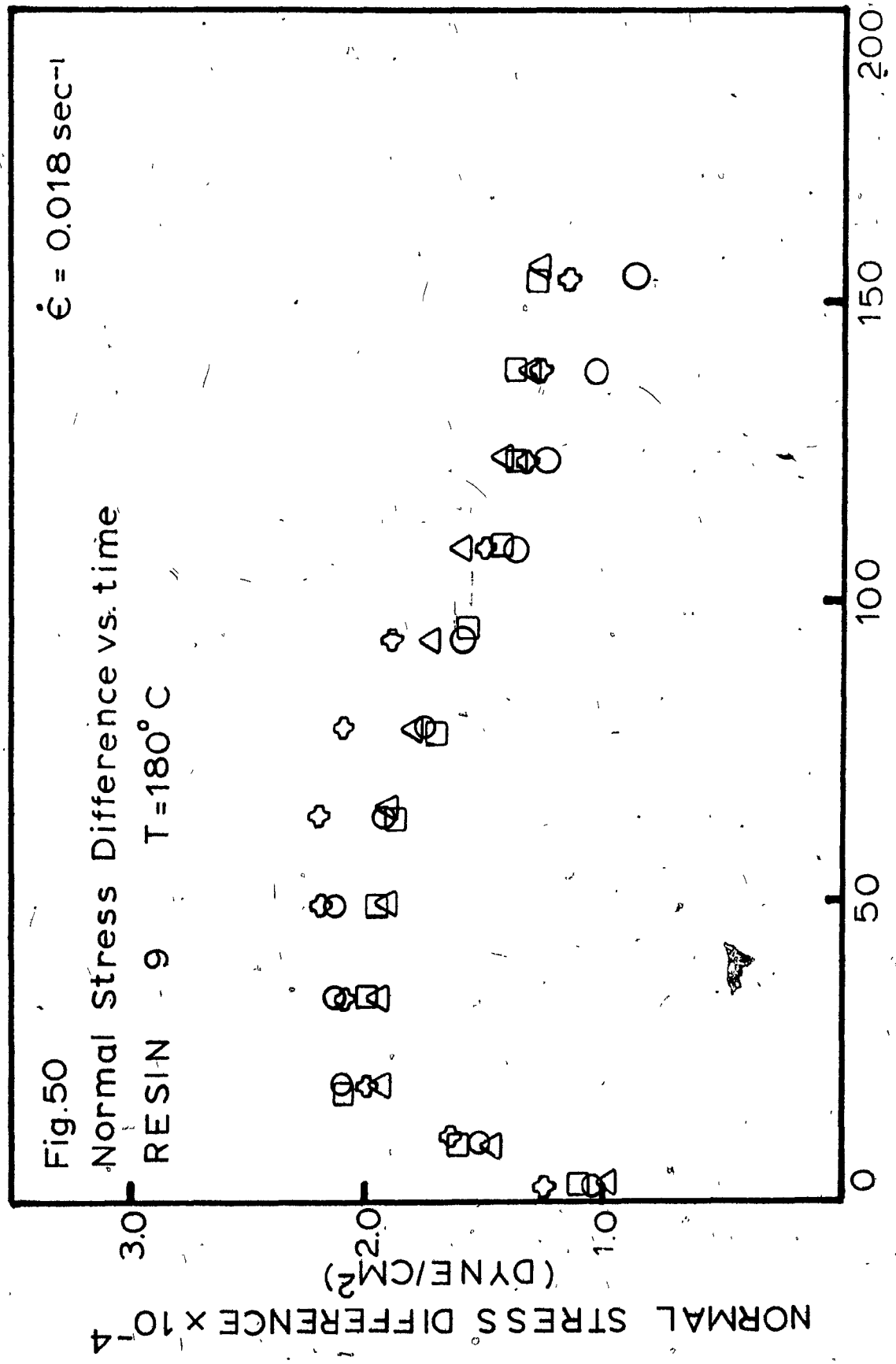
Fig.50
Normal Stress Difference vs. time
RESIN - 9 T=180°C
$\dot{\epsilon}$ = 0.018 sec⁻¹
NORMAL STRESS DIFFERENCE × 10⁻⁴ (DYNE/CM²)
3.0
2.0
1.0
0
50
100
150
200
TIME (SEC)

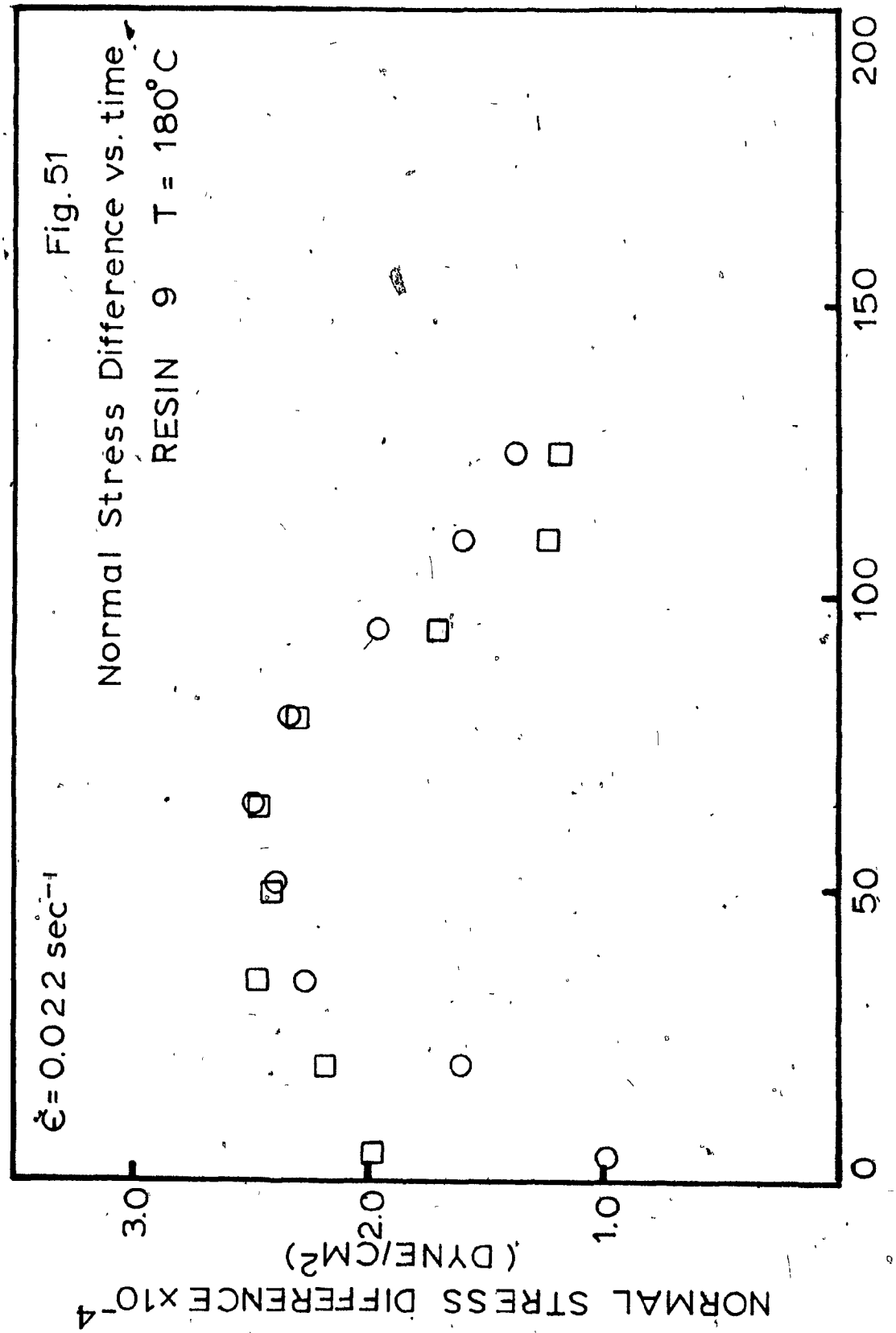
Fig. 51
Normal Stress Difference vs. time
RESIN 9 T = 180°C
$\dot{\epsilon}$ = 0.022 sec^{-1}
NORMAL STRESS DIFFERENCE x10^{-4}
(DYNE/CM2)
3.0
2.0
1.0
0
50
100
150
200
TIME (SEC)

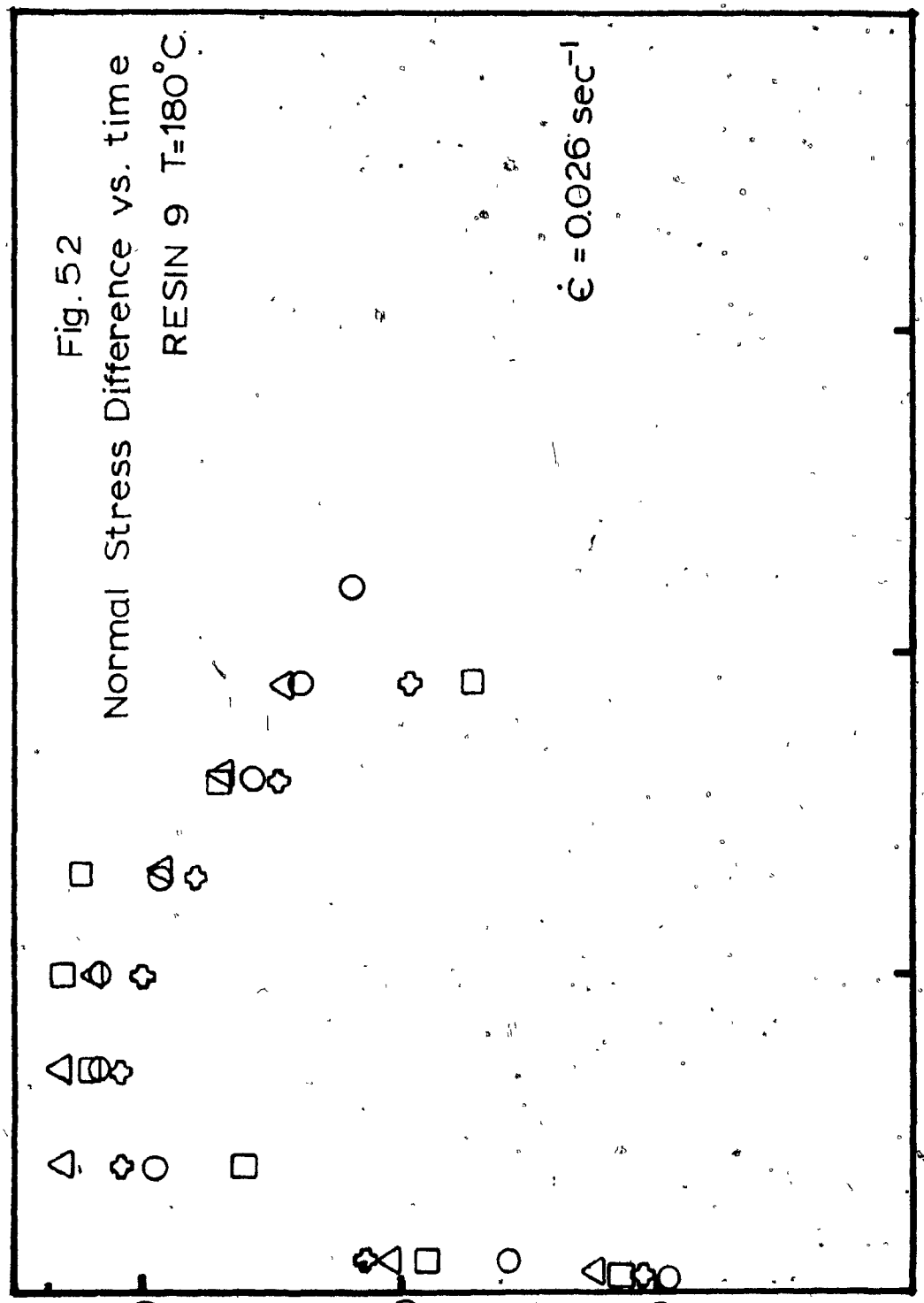
Fig. 52
Normal Stress Difference vs. time
RESIN 9 T=180°C
$\dot{\epsilon}$ = 0.026 sec^{-1}
NORMAL STRESS DIFFERENCE x10^{-4}
(DYNE/CM^2)
3.0
2.0
1.0
0
50
100
150
200
TIME (SEC)

7.4) Discussion.

The Hencky strain-time curves shown in the previous section were obtained without a polymer sample between the clamps. The actual experiment with the sample between the clamps showed no significant difference (of the order of 2%) in the strain rate values. This proves that the control system is reliable. Although the control system of the driving mechanism allows to obtain a strain rate of .004sec^{-1} without load, with the sample between the clamps the lowest strain rate obtained was 0.014sec^{-1}. This behavior caused by the load introduced by the sample, is due to the innability of the motor to respond properly at the start of the experiment. At the start the voltage supplied by the controller to the motor is so small that the load prevents the motor shaft from rotating. This causes a current overload that can damage the circuits in the controller. This situation could be improved by using a gear box with a higher gear ratio.

The stress was calculated using the ralations

$$\sigma_{11} - \sigma_{22} = F/A$$
$$A = \frac{A_o L_o}{L} \qquad (57)$$

The length, L, was corrected to take into account

the portions of the samples near the clamps that did not flow evenly. An attempt was made to reduce this problem by using a sample that was larger at the ends and smaller in the central portion and by cooling the clamps with hot oil (115-120^{0}C). The effect was not eliminated completely. Further improvement is possible if the dimensions of the central portion are reduced further. This would cause the ends of the sample, which are in contact with the cooling surface, to act as insulators to the rest of the sample so that the flow would be uniform from the very ends of the sample.

To obtain a value of the steady elongational viscosity the stress should reach a steady value. It is known that for LDPE the stress increases with time and after a certain elongation it levels off. This behavior has been reported by Laun[31]. It can be seen from the stress-time curves that the stress increases with time, tends to level off and then decreases. The increase of the stress with time and the tendency to level off is in agreement with previous experimental results. The decrease, on the other side, is never observed.

It is suspected that the decrease of the stress with time after a tendency to level off is caused by imperfections in the system used to measure the force exerted to elongate the samples. As was mentioned before an LVDT force transducer was used to measure the force. The range of this force transducer is from 0 to 500g. The forces that were measured in all the experiments in this work have a maximum value of 10-15g., with most values below 5g. The transducer is

working very close to its lower limit of operation and therefore the linearity of the response is questionable.

Another factor that can cause the stress to decrease is the actual length of the sample when a certain elongation is reached. At this point the sample tends to float in the oil bath. The length that is recorded is in fact the length between the two clamps. When the extension is not large, the sample length and the length recorded are the same. But if the sample floats the real length is larger that the one recorded, and the area is smaller than the one used in the calculations. It is not believed that the error in the length is an important one.

Summarizing, it can be said that the control system of the driving mechanism is working well inside the range of experimental error. This can be seen from the graphs of Hencky strain vs. time and from the uniformity of the extended samples.

Several modifications are proposed so that the equipment is capable of producing improved results. First of all, a more suitable force transducer should be selected. A transducer with a range of 0 to 50g. should be adequate. The set-up of the force transducer should be revised in order to minimize as much as possible undesired movements of the transducer when the clamps are put in position or taken out.

Secondly, the size of the samples should be modified. The sample should be made shorter, to obtain higher extensions or strains. This would allow to check the results ob

tained by Laun[31], that after a certain strain (approximately a value of 4) the stress levels off to a constant value. The highest strain rate obtained in the present equipment is 2.8 and it would be convenient to go to a strain rate of 4 or more for the reasons cited above. Of course this is also limited by the size of the tank.

The diameter of the central portion of the sample should be reduced. This would reduce the portions of the sample, near the clamps, that do not flow evenly. Both reductions, in length and diameter have to be studied with care. If the sample becomes shorter and thinner the force required to stretch the sample (at a particular strain rate) will decrease and also there is the possiblity that the sample will break before the experiment is completed. Therefore, the dimensions of the sample have to be optimized so that the force can be measured accurately and the uneven flow at the clamps is minimized.

APPENDIX I .

CONE AND PLATE FLOW [32] .

Consider the flow between a rotating cone and a flat plate as shown in Figure A-1.

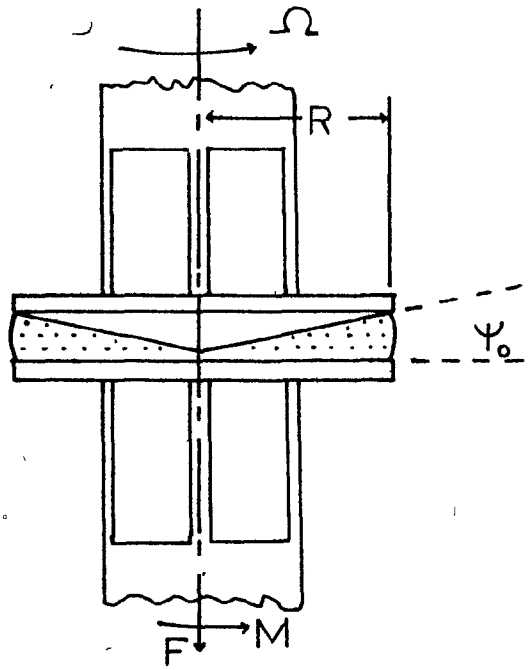

The following assumptions are made about the flow field:

i) Inertial effects are negligible.

ii) The cone angle is very small. This enables us to assume that the shear rate is constant throughout the gap.

iii) The cone and plate have infinite dimensions.

iv) Steady simple shear flow continues up to the free surface.

v) Surface tension forces are negligible.

If inertial forces are neglected and edge effects at the periphery of the cone are ignored, the dynamic equation in spherical coordinates (ϕ, θ, r) is

$$\frac{1}{r}\left(\frac{\partial}{\partial r}\left(r^2\tau_{r\phi}\right)\right) + \frac{\partial\tau_{\theta\phi}}{\partial\theta} + \tau_{r\phi} + 2\tau_{\theta\phi}\cot\theta = 0 \qquad (I.1)$$

With the above assuptions, the only non zero velocity component is u_ϕ and by symmetry of the flow in the ϕ direction the only non zero components of the rate of deformation tensor are

$$\Delta_{\phi r} = r\frac{\partial}{\partial r}\left(\frac{u_\phi}{\sin\theta}\right) \qquad (I.2)$$

$$\Delta_{\phi\theta} = \frac{\sin\theta}{r}\frac{\partial}{\partial\theta}\left(\frac{u_\phi}{\sin\theta}\right)$$

The boundary conditions are:

$$u_\phi = \Omega r(\sin\tfrac{\pi}{2} - \Psi_o) \qquad \Psi = \Psi_o$$

$$u_\phi = 0 \qquad \Psi = 0 \qquad (I.3)$$

$$u_\phi = 0 \qquad r = 0$$

Since the velocity is related to the rotational speed and this to the angle and from the form of the boundary conditions a solution of the form

$$u_\phi = rg(\Psi) \tag{I.4}$$

is proposed.

Expression (I.4) substituted in (I.2) shows that

$$\Delta_{\phi r} = 0$$

$$\tau_{r\phi} = \tau_{\phi r} = 0$$

Then the dynamic equation (I.1) becomes

$$-\frac{\partial \tau_{\theta\phi}}{\partial\theta} + 2\tau_{\theta\phi}\cot\theta = 0$$

and

$$\tau_{\theta\phi} = \frac{C}{\sin^2\theta} \tag{I.5}$$

To evaluate the constant C in equation (I.5) we notice that the measured torque M arises from the shear stress exerted on the surface of the cone.

$$M = \int_o^R \tau_{\theta\phi}\Big|_{\pi/2 - \Psi_o} 2\pi \{ r \sin(\pi/2 - \Psi_o) \}^2 \, dr \tag{I.6}$$

Evaluation of the integral in equation (I.6) with the expression given in (I.5) for $\tau_{\theta\phi}$ gives

$$C = \frac{3M}{2\pi R^3}$$

and

$$\tau_{\theta\phi} = \frac{3M}{2\pi R^3 \sin^2\theta} \tag{I.7}$$

Since $\theta = \pi/2 - \Psi$ and we assume that Ψ_o is very small, $\sin\theta = \sin(\pi/2 - \Psi_o) \simeq 1$. Then, expression (I.7) becomes

$$\tau_{\theta\phi} = \frac{3M}{2\pi R^3} \qquad (I.8)$$

Using expression (I.2), the boundary conditions (I.3) and from the fact that the angle is small we get the expression for the shear rate in the cone and plate flow.

$$-\Delta_{\theta\phi} = \dot{\gamma} = \frac{\Omega}{\Psi_o} \qquad (I.9)$$

To calculate the normal stress differences we start with the r component of the equation of motion

$$-\rho\frac{u_\phi^2}{r} = -\frac{\partial P}{\partial r} + \frac{\partial \tau_{rr}}{\partial r} - \frac{\tau_{\theta\theta} + \tau_{\phi\phi} - 2\tau_{rr}}{r} \qquad (I.10)$$

Since shear rate is independent of r and τ_{rr} depends only on shear rate, $\partial\tau_{rr}/\partial r = 0$

$$-\rho\frac{u_\phi^2}{r} = -\frac{\partial P}{\partial r} - \frac{\tau_{\theta\theta} + \tau_{\phi\phi} - 2\tau_{rr}}{r} \qquad (I.11)$$

The stress measured at the surface of the plate ($\Psi = 0$) is given by

$$\sigma_{\phi\phi}(r,0) = -P(r,0) + \tau_{\theta\theta} \qquad (I.12)$$

Substitution of equation (I.12) in equation (I.10) gives

$$-\rho\frac{u_\phi^2}{r} = \frac{\partial\sigma_{\theta\theta}}{\partial r} - \frac{\tau_{\theta\theta}+\tau_{\phi\phi}-2\tau_{rr}}{r} \qquad (I.13)$$

But also at $\Psi = 0$, $u_\phi = 0$, therefore

$$\frac{\partial\sigma_{\theta\theta}}{\partial r} = \frac{\tau_{\theta\theta}+\tau_{\phi\phi}-2\tau_{rr}}{r} \qquad (I.14)$$

The first normal stress is defined as $N_1 = \tau_{\phi\phi} - \tau_{\theta\theta}$ and the second as $N_2 = \tau_{\theta\theta} - \tau_{rr}$. Therefore,

$$\tau_{\theta\theta} + \tau_{\phi\phi} - 2\tau_{rr} = N_1 + 2N_2 \qquad (I.15)$$

so equation (I.14) becomes

$$\frac{\partial\sigma_{\theta\theta}}{\partial r} = \frac{N_1 + 2N_2}{r}$$

$$\frac{\partial\sigma_{\theta\theta}}{d\ln r} = \{ N_1(\dot\gamma) + 2N_2(\dot\gamma) \} \qquad (I.16)$$

If the total vertical force exerted against the cone is measured, it is possible to determine the first normal stress difference $\tau_{\phi\phi} - \tau_{\theta\theta}$ directly, without a measurement of the stress distribution in the system. For the small cone angles usually employed the force may be calculated from

$$F = -\pi R^2 \{ (-P(R) + \tau_{rr}) + \tfrac{1}{2}(\tau_{\theta\theta} - \tau_{\phi\phi}) \} \qquad (I.17)$$

If the system is in equilibrium with the atmosphere on its outer boundary

$$-P(R) + \tau_{rr} = \sigma_{rr}(R) = 0$$

then equation (I.17) reduces to

$$\tau_{\phi\phi} - \tau_{\theta\theta} = \frac{2F}{\pi R^2} \qquad \text{(I.18)}$$

APPENDIX II.

Parameters of the Carreau Viscosity Equation.

(It is common and accepted practice to assume η_∞ to be zero for polymer melts.)

Resin 1.

T ^{0}C	λ	N	η_0 (poise)
160	21	0.175	2×10^5
180	30	0.1288	1.4×10^5

Resin 9.

T ^{0}C	λ	N	η_0 (poise)
160	10	0.312	2.7×10^5
180	20	0.1863	1.6×10^5

Resin 10.

T ^{0}C	λ	N	η_0 (poise)
160	13	0.2674	3.8×10^5
180	22	0.267	2.5×10^5

REFERENCES.

1) Abdel - Khalik S.I., Hassager O., Bird R.B., Pol. Eng. & Sci., 14, 859, (1974).

2) Tanner R.I., J.Pol.Sci., A-2, 8, 1067, (1970).

3) Vu T.K.P., Rod Climbing in molten polymers.M.Eng. Thesis, Chem. Eng. Dept. Mc Gill University, (1976).

4) Tee T.T., Large Amplitude Oscillatory Shearing of Polymer melts, Ph.D. Thesis, Chem. Eng. Dept. Mc Gill University, (1974).

5) Oldroyd J.G., Proc. Roy. Soc. (London), A-200,523, (1950).

6) Goddard J.D., Miller C., Rheol. Acta, 5, 177, (1966).

7) Goddard J.D., Trans. Soc. Rheol., 11, 381, (1967).

8) Bird R.B., Hassager O., Abdel-Khalik S.I., AICHEJ, 20, 1041, (1974).

9) Walters K., Rheometry, Chapman & Hall, London (1975).

10) Lodge A.S., Adams N., Phil. Trans. Roy. Soc. London, 256A, 149, (1964).

11) Hutton J.F., Proc. Roy. Soc. (London), A287, 222,(1965).

12) Gleissle W., Paper presented at the meeting of the German Society of Rheology, (1974).

13) Ginn R.F., Metzner A.B., Trans. Soc. Rheol., 13, 429,1969

14) Metzner A.B., Houghton W.T., Sailor R.A., White J.L. Trans. Soc. Rheol., 5, 133, (1961).

15) Mendelson R.A., Finger F.L., Bagley E.B., J.Pol.Sci., Part C, 35, 177, (1971).

16) Vlachopoulos J., Horie M., Lidorikis S., Trans. Soc. Rheol., 16, 669, (1972).

17) Metzner A.B., Houghton W.T., Sailor R.A., White J.L., Paper presented at the Int. Symp. on Second Order Effects in Elasticity, Plasticity & Fluid Dynamics,Haifa,Israel, April, (1962).

18) Bagley E.B., Storey S.H., West D.C., J.Appl.Pol.Sci., 7, 1661, (1963).

19) Kowalski R., Ph.D. Dissertation, Pol. Inst. Brooklyn, (1963).

20) Utracki L.A., Bakerdjian Z., Kamal M.R., J.Appl.Pol.Sci., 19, 481, (1975).

21) Cogswell F.N., Plastic and Polymers, 36 , 109, (1968).

22) Vinogradov G.V.,Fikham V.D., Radushkevick B.V., Rheol. Acta, 11, 286, (1972).

23) Munstedt W., Rheol. Acta, 14, 1077, (1975).

24) Vinogradov G.V., Radushkevick B.V., Fikham V.D., J.Pol.Sci., A-2, 8, 1, (1970).

25) Stevenson J.F., AICHEJ, 18, 540, (1972).

26) Meissner J., Trans. Soc. Rheol. 16, 407, (1972).

27) Everage A.E., Ballman R.L., J.Appl.Pol.Sci., 20, 1137, (1976).

28) Shaw M.T., Paper presented at the Int. Rheol. Cong., Gottenburgh, Sweden, 1976.

29) Rhi-Sausi J., Extensiometer for Polymer Melts. M.Eng. Thesis,Dept. Chem. Eng., Mc Gill University, 1975.

30) Dealy J.M., Rhi-Sausi J., Pol.Eng. Sci. (1976) (in press).

31) Laun H.M., Munstedt H., Paper presented at the Int. Rheol. Cong.,Gottenburgh,Sweden, 1976.

32) Middleman S., Flow of High Polymers, Interscience,(1968).

33) C.D. Han, Rheology in Polymer Processing, Academic Press, (1976).

NOMENCLATURE.

A : Cross sectional area of the specimen at $t = t$.

A_o: Cross sectional area of the specimen at $t = 0$.

a_i: Coefficients in equation (44).

a_n: Constant in equation (3).

b_n: Constant in equation (3).

B : Die swell at extrusion temperature.

B_o: Die swell at thermostatting temperature.

D : Diameter of the extrudate.

D_o: Diameter of the capillary.

F : Total normal force.

K : Empirical constant.

L : Sample length at time $t = t$.

L_o: Sample length at time $t = 0$.

M : Torque.

N_1: First normal stress difference.

N_2: Second normal stress difference.

N : Parameter in the Carreau viscosity equation.

P_A: Ambient pressure.

ΔP: Pressure drop in the capillary.

Q : Volumetric flow rate.

R : Radius of the cone.

Re_{cp} : Reynolds number for the cone and plate flow.

s : Time interval $(t - t')$.

S_w : Recoverable shear strain at the wall.

t : Time.

$\underline{u}$: Velocity vector.

$\underline{x}$: Position vector.

Greek letters:

$\dot{\gamma}$: Shear rate.

$\dot{\gamma}_{ap}$: Apparent shear rate.

$\dot{\varepsilon}$: Elongational strain rate.

η : Shear viscosity.

η_o: Zero shear viscosity.

η_∞: Shear viscosity ($\dot{\gamma}\to\infty$)

η_T: Elongational viscosity.

θ, θ_1: First normal stress coefficient.

θ_2: Second normal stress coefficient.

λ: Parameter in the Carreau viscosity equation.

λ_0: Time constant.

ν : Kinematic viscosity.

ρ : Polymer density at extrusion temperature.

ρ_o: Polymer density at thermostatting temperature.

$\underline{\underline{\sigma}}$: Total stress tensor.

$\underline{\underline{\tau}}$: Deviatoric stress tensor.

τ_{12} : Shear stress.

τ_R: Stress at the rim.

Ψ_o: Cone angle.

Ω : Rotational speed.

$\nabla\underline{u}$: Velocity gradient.